PhD degree in Molecular Medicine (curriculum in Molecular Oncology)

European School of Molecular Medicine (SEMM),

University of Milan and University of Naples “Federico II”

Settore disciplinare: MED/04

Contact sites between the endoplasmic reticulum and the plasma membrane control EGFR endocytosis

Elisa Barbieri

IFOM, Milan

Matricola n. R10334

Supervisor: Prof. Pier Paolo Di FIore

IFOM, Milan

Added Supervisor: Dr. Sara Sigismund

IFOM, Milan

Anno accademico 2015-2016

TABLE OF CONTENTS

FIGURE INDEX

TABLE INDEX

LIST OF ABBREVIATIONS

AP2	Adaptor protein 2
ARF	ADP-ribosylation factor
Cam	Calmodulin
Cav	Caveolin
CBR	Cannabinoid receptor
CCP	Clathrin-coated pits
CCV	Clathrin-coated vesicles
CHC	Clathrin heavy chain
CLC	Clathrin light chain
CLIC	Clathrin-independent carriers
CME	Clathrin-mediated endocytosis
CTxB	Cholera toxin B
DKK	Dickkopf
DRM	Detergent resistant membrane
DUB	Deubiquitinating enzymes
Dyn	Dynamin
Dvl	Dishevelled
ECM	Extracellular matrix
EGF	Epidermal growth factor
EGFR	Epidermal growth factor receptor
EM	Electron microscopy
EndoA	Endophilin A
EPS15	Epidermal growth factor receptor substrate 15
ER	Endoplasmic reticulum
ERK	Extracellular signal regulated kinase
ESCRT	Endosomal sorting complex required for transport
FEME	Fast endophilin mediated endocytosis
Fz	Frizzled

GEEC	GPI-AP enriched early endosomal compartment
GPCR	G protein-coupled receptor
GPI	Glycosylphosphatidylinositol
Grb2	Growth factor receptor-bound protein 2
HGFR	Hepatocyte growth factor receptor
IL2R	Interleukin 2 receptor type
IP3	Inositol-1,2,3-trisphosphate
IP3R	Inositol-1,2,3-trisphosphate receptor
KD	Knock down
LRP6	Low density lipoprotein receptor-related protein 6
MAPK	Mitogen-activated protein kinase
MCS	Multiple cloning site
MHC	Major histocompatibility complex
MVB	Multivesicular body
NCE	Non-clathrin endocytosis
NGFR	Nerve growth factor receptor
ORD	Oxysterol-binding related domain
ORP	Oxysterol-binding protein
Pak1	P21-activated-kinase
PI3K	Phosphoinositide 3-kinase
PI3P	Phosphatidylinositol-3-phosphate
PI(3,4,5)P3	Phosphatidylinositol 3,4,5-trisphosphate
PI(4)P	Phosphatidylinositol 4-phosphate
PI(4,5)P2	Phosphatidylinositol 4,5-bisphosphate
PKC	Protein kinase C
PLC	Phospholipase C
PM	Plasma membrane
PPMP	DL-threo-1-Phenyl-2-palmitoylamino-3-morpholino-1-propanol
PTB	PhosphoTyr-binding
PTRF	Polymerase I and transcript release factor
RHD	Reticulon homology domain
RTK	Receptor tyrosine kinase
SARA	Smad anchor for receptor activation
SH2	Src homology 2
SILAC	Stable isotope labelling with amino acids in cell culture
siRNA	small interfering RNA
SV40	Simian virus 40
TCR	T-cell receptor
TKB	Tyrosibe kinase-binding domain
TFR	Transferrin receptor
TGFβR	Tumor growth factor β receptor
Ub	Ubiquitin
UBA	Ubiquitin associated domain
UIM	Ubiquitin-interacting motif
VAP	Vamp-associated protein

ABSTRACT

The epidermal growth factor receptor (EGFR) can be internalized through different routes. While clathrin-mediated endocytosis destines EGFR for recycling and signaling, internalization through non-clathrin endocytosis (NCE) targets the receptor for degradation. Since NCE appears to be a major negative regulator of EGFR levels, a more complete picture of this pathway would likely reveal new insights into aberrant EGFR signaling observed in many types of cancer.

By combining a candidate gene approach with an unbiased proteomic approach, we have defined EGFR-NCE as molecularly distinct from other NCE pathways, relying on functional regulators not previously implicated in endocytosis. We found that reticulon 3 (RTN3), an endoplasmic reticulum (ER)-resident protein, is fundamental for NCE-mediated EGFR internalization, and that its ablation delays EGFR degradation, demonstrating that the NCE pathway is a critical regulator of the EGF-dependent cellular response. We show that, upon stimulation with high dose of EGF, RTN3 is localized in close proximity to EGFR and that it is crucial for the formation of contact sites between the ER and the plasma membrane (PM), which are needed for NCE to proceed efficiently. We also show that ER contact sites are involved in local Ca^{2+} release: high EGF doses induce a release of Ca^{2+} from the ER to the PM, which is strongly inhibited upon knockdown of RTN3. This calcium release depends on the inositol trisphosphate (IP3) cascade and is essential for the internalization of EGFR via NCE.

In conclusion, we have discovered a new clathrin-independent endocytic pathway that relies on the action of RTN3. RTN3 is necessary for the formation of contact sites between the ER and EGFR-NCE sites at the PM, which are required for IP3R-dependent local calcium release and the completion of EGFR internalization through NCE.

INTRODUCTION

1. Endocytosis: cells orchestrate multiple entry routes

The plasma membrane (PM) defines the space of a single cell and is a dynamic structure, essential in capturing and decoding signals coming from the extracellular space. Endocytosis is a fundamental process that allows the cell to communicate with the extracellular environment and to regulate membrane composition. In the cell, various types of endocytic routes coexist and operate in parallel to precisely regulate PM composition and signaling.

Diverse types of endocytosis are classified based on the size of endocytic structures: phagocytosis and macropinocytosis are responsible for great rearrangements of the PM caused by the uptake of large particles and the extracellular milieu, respectively. Micropinocytosis, instead, is characterized by small membrane invaginations involved in different types of internalization processes, including the well-characterized clathrin-mediated endocytosis (CME) and a vast number of non-clathrin endocytic (NCE) processes (Figure 1 and Table 1).

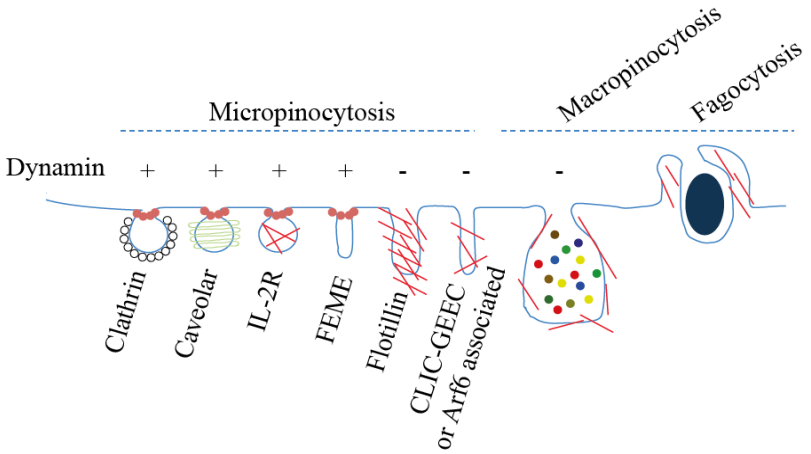

Adapted from Mayor, *Cold Spring Harb Perspect Biol*, 2014 (1)

Figure 1. Endocytic pathways.

Endocytic pathways are represented: on the left, micropinocytic pathways, characterized by dynamin (pink circles) dependence (+) or independence (-); on the right, macropinocytosis

and fagocytosis that are dynamin independent. All dynamin-independent pathways appear to require the actin machinery (red bars).

Pathway	Morphology and size	Coat	Dynamin dependence	Small GTPase involved	Internalized cargoes	Associated/ regulatory proteins
Phagocytosis	Cargo shaped > 500 nm	None	No	Rac1, RhoA, Cdc42	Pathogens, apoptotic cells, FcRs	Actin, ARP2/3, formins, PI3K, WASP, WAVE2, amphiphysin, coronin, others
Macro-pinocytosis	Ruffled 0.2-10 μm	None	In some cases	Rac1, Cdc42, Arf6, Rab5	RTKs, fluids, some bacteria	Actin, ARP2/3, cortactin, PI3K, SRC, PAK1, RAS, CTBP1/BARS, others
Clathrin-mediated	Vesicular 100-200 nm	Clathrin	Yes	Rab5	RTKs, GPCR, TfR, some toxins, bacteria, viruses	AP-2, EPSINS,EPS15,intersectin, amphiphysin (plus many others, >50)
Caveolae-mediated	Flask-shaped 50-120 nm	Caveolin 1 and 2	Yes	Not clear	GPI-linked proteins, CTxB, SV40	PTRF/cavin, SRC, SDPR, SRBC
CLIC/GEEC	Tubular	No	No	Cdc42, Arf1	Fluids, bulk membrane, GPI-linked proteins	Actin, GRAF1, ARHGAP10
IL2Rβ	Vesicular 50-100 nm	Yes	Yes	RhoA, Rac1	IL2Rβ, γc-cytokine receptor	PAK1 and 2, cortactin, N-WASP
Arf6-dependent	Tubular	None as yet	None as yet	Arf6	MHCI, MHCII, CD59, CD55, GLUT1	None as yet
Flotillin-dependent	Vesicular	No	No	None	CTxB, CD59, proteoglycans	None as yet
FEME	Tubular	No	Yes	RhoA, Rac1	IL2-R, iota toxin, CTxB, STxB	PAK1, PAK2, Endophilin-A's

Table 1. **Internalization pathways**.

The table summarizes internalization pathways described in the literature. Morphology and size of the internalizing structures, the presence or not of a coating protein, the dependence on dynamin, the kind of GTPases involved, the type of internalized cargo, and known associated proteins are listed for each internalization pathway.

CLIC, clathrin-independent carriers; GEEC, GPI-AP enriched early endosomal compartment; RTK, receptor tyrosine kinase; GPCR, G protein-coupled receptor; TfR, transferrin receptor; CTxB, cholera toxin B; SV40, simian virus 40; GPI, glycosylphosphatidylinositol; MHC, major histocompatibility complex; PTRF, polymerase I and transcript release factor; SDPR, serum deprivation response; SRBC, SDR-related gene product that binds to c-kinase; CtBP1, C-terminal binding protein 1.

1.1 Phagocytosis

Phagocytosis is defined as the process used by specific cells to engulf particles, cellular debris and microorganisms with diameters greater than 500 nm (2). The first step of this process is the recognition of the particle by specific receptors; the phagocytic cup is then formed thanks to the polymerization of F-actin. The actin reorganization process is strictly regulated by different GTPases, among which Rac1, whose activation, according to recent evidence, can be regulated directly by mechanical signaling coming from changes in membrane tension (3). The internalization of engulfed particles then proceeds through the formation of the phagosome and, through acidification, leads to the degradation of the content (for a recent review see (4)).

1.2 Macropinocytosis

Macropinocytosis is an actin-based endocytic process used by cells to engulf extracellular fluid (5). The initial step is membrane ruffling, which is driven by actin polymerization; Rac1 is the main GTPase involved in this process and the system is regulated by Pak1 (p21-activated-kinase) (6). Recent data suggests that the deactivation of Rac1 is fundamental for the completion of macropinosome formation, while the dependence on dynamin for the scission is not yet clarified, although it may be required in some types of macropinocytosis (7).

Growth factors are known to be able to stimulate macropinocytosis (8). More in detail, a macropynoctic-like pathway has been shown to be involved in the internalization of a vast percentage of activated EGFRs (epidermal growth factor receptor). This pathway is characterized by the involvement of circular dorsal ruffles/waves that, for their action, require, among others, actin, cortactin, dynamin 2 and EGFR kinases. How the entrance into this route is regulated is not defined. Indeed, one of the possibilities is that, considering that the

activation mode of this pathway leads to the internalization of a large portion of the PM, EGFR can be internalized because of this massive rearrangement (9).

1.3 Clathrin-mediated endocytosis

Since their first purification in 1975, clathrin-coated vesicles have been extensively studied. Clathrin-coated vesicles contain the internalized cargo, surrounded by different clathrin-adaptor proteins. Adaptor proteins are required for the formation of the outer clathrin layer and have a regulatory function in the formation of the pit.

1.3.1 Clathrin-coated pits

Clathrin can assemble into a lattice of hexagons and pentagons (Figure 2a), while in the non-assembled form it exists as a three-legged structure called triskelion. Each triskelion is made of three copies of a 180 kDa protein, the clathrin heavy chain (CHC), that form the structural basis of the lattice; and three copies of the clathrin light chain (CLC, 25 kDa) that regulate the formation of the lattice. During recent years, imaging techniques have drastically evolved, leading to an extremely high resolution of clathrin-coated pits. Thanks to cryo-electron microscopy (cryo-EM), all connections between each single triskelion can be visualized (Figure 2b). The domains of the CHC have been identified and their specific function and structure has been characterized. The terminal domain of clathrin heavy chain has binding sites for adaptor proteins and is connected through a linker, an ankle and a distal segment to the proximal segment. The latter is the binding site for the CLC (Figure 2c, (10-13)).

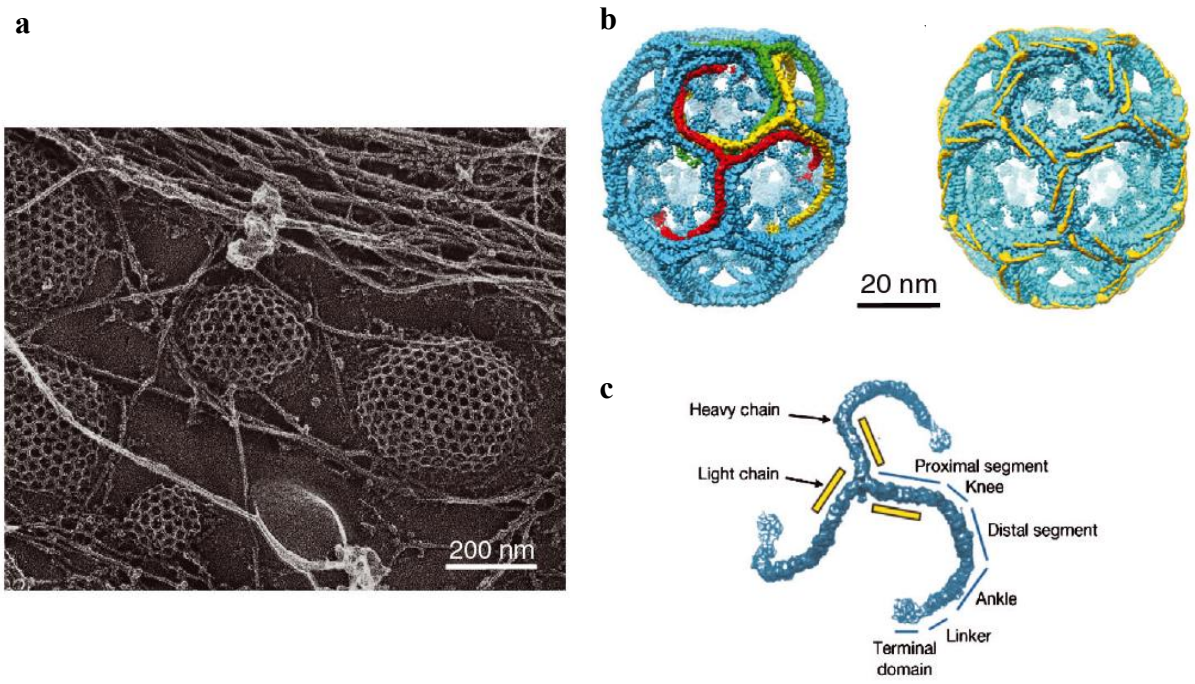

Adapted from Robinson, *Traffic*, 2015 (10)

Figure 2. Clathrin structure.

a) Electron micrograph of clathrin-coated pits budding from the plasma membrane.

b) Hexagonal barrel showing the positions of the clathrin heavy chain (left, red and yellow); and of the light chains (right, yellow).

c) Clathrin triskelion, showing the various domains as reported.

Purified clathrin can *per se*, as well as in the presence of adaptor proteins, assemble *in vitro*. In the cell, the formation of the clathrin-coated vesicles is a tightly regulated process. Concomitantly with the initial membrane invagination, started by the concerted action of clathrin and adaptor proteins, the recognition of the cargo is necessary, empty vesicles are aborted otherwise. After stabilization, clathrin polymerization facilitates the formation of a 'neck' where membranes are in close apposition. At this level, the GTPase dynamin plays a fundamental role, acting at the pinching-off step (Figure 3).

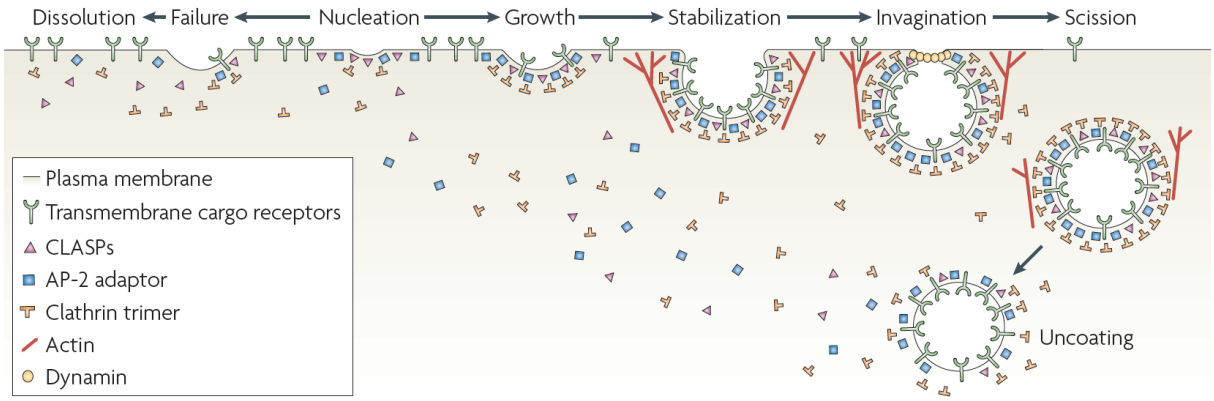

Adapted from Traub, *Nat Rev Mol Cell Biol*, 2009 (14)

Figure 3. Clathrin coat assembly.

The figure describes the different steps of clathrin-coated vesicle formation. The formation of a clathrin-coated pit start from nucleation of AP2 and adaptor proteins at the PM. During the growing phase, the clathrin coat protein is recruited by AP2 and other accessory proteins that facilitate the formation of a polymerized coat. The structure is stabilized by actin filaments and finally detached from the PM by the action of dynamin.

1.3.2 Adaptor proteins

Since the first purification of clathrin-coated vesicles, the presence of other proteins, linked to clathrin, was evident. These proteins have been purified through the years. The first two isolated proteins were adaptor protein-1 (AP1), involved in the transport between trans Golgi network and endosomes, and adaptor protein-2 (AP2), involved in endocytosis; followed by many others. AP2 is the principal component of CCPs and is the best characterized adaptor proteins. AP2 has two large subunits of 100 kDa, named α and β; a medium subunit of 50 kDa, μ; and a small subunit of 20 kDa, σ. The two large subunits, α and β, possess a globular C-terminal region that is linked to the N-terminal 'head'. The α subunit, also called 'ear', interacts with phosphoinositides at the level of the PM and with proteins containing the DPF and DPW motifs (Figure 4). The interaction with clathrin occurs through the β domain, while the μ and σ domains are involved in cargo recognition. Many studies also led to the identification of the consensus YXXϕ (where ϕ represents any bulky hydrophobic residue)

that, together with the dileucine motif (possessed by EGFR and TfR), is characteristic of CME.

Adapted from Robinson, *Traffic*, 2015 (10)

Figure 4. The AP complex.
Schematic diagram of an AP complex, showing the four subunits β, μ σ and γ or α, and the clathrin box.

All stages of clathrin pit formation have been dissected (15) and many other clathrin-associated proteins have been identified, many of which are associated to coated pits at a specific stage of pit formation or vesicle maturation. An example of this specific recruitment is auxilin, which arrives immediately after vesicle scission and recruits Hsc70 to direct uncoating of the pit (15-17). Another example is Hip1R, which binds to the clathrin light chains and is involved in actin recruitment, a process that in some cases is needed for the maturation and budding of coated vesicles (18-20).

Other accessory proteins with a specific cargo-recognition motif are epsins and Eps15 (epidermal growth factor receptor substrate 15), which recognize ubiquitinated cargos. Epsins

are able to bind clathrin and associate with Eps15 thanks to the binding of epsin NPF motifs with the Eps15 homology (EH) domain of Eps15 (21). Moreover, both epsins and Eps15 have a DPF/DPW motif and bind AP2 (21). Epsins and Eps15 are redundantly necessary for CME of EGFR (22). Moreover, the function of epsin and Eps15 is not unique for CME, indeed, our laboratory has showed that they are also involved in EGFR-NCE (22).

1.4 Non-clathrin endocytosis (NCE)

CME is a well-characterized pathway. Historically, CME has been considered the major endocytic route and was recently described as the principal pathway contributing to the endocytic flux in basal conditions in some cellular context (23). However, parallel to CME, a number of non-clathrin endocytic pathways have evolved and are all un-affected by clathrin ablation but are dependent on raft domains (1,24). These rafts are cholesterol-enriched assemblies of lipids and proteins that can interact with each other to form larger and more stable domains (25). NCE pathways can be constitutive or triggered by a specific signal and are, more in general, categorized based on their dependence on (1):

i) dynamin

ii) coat proteins: like caveolins or flotillins

iii) small GTPases: like Arf6, RhoA, Cdc42

The classification of different NCE pathways is not always linked to stringent criteria, but some features lead to the identification of major endocytic routes.

1.4.1 Caveolae-mediated endocytosis

Caveolae are small membrane invaginations with a diameter of 60-80 nm, and their presence in cells depends on the tissue; for example, caveolae are almost undetectable in kidney cells, but represent 50% of the PM in adipocytes (26). There are three types of caveolin (Cav) in

mammalian cells: Cav1, Cav2 and Cav3, the first two are usually co-expressed in different cell types, while Cav3 is mainly expressed in striated muscle cells. Cav1 is fundamental for the formation of caveolae: loss of Cav1 causes the disappearance of caveolae and the exogenous expression of Cav1 is sufficient to trigger caveolae formation in cells lacking endogenous caveolins (27).

All caveolins are integral membrane proteins characterized by both N- and C-termini that face the cytoplasm, and a putative hairpin domain embedded into the PM (Figure 5). Cav1 is the more studied caveolin, it is palmitoylated, oligomeric and is able to bind cholesterol and fatty acids (28,29).

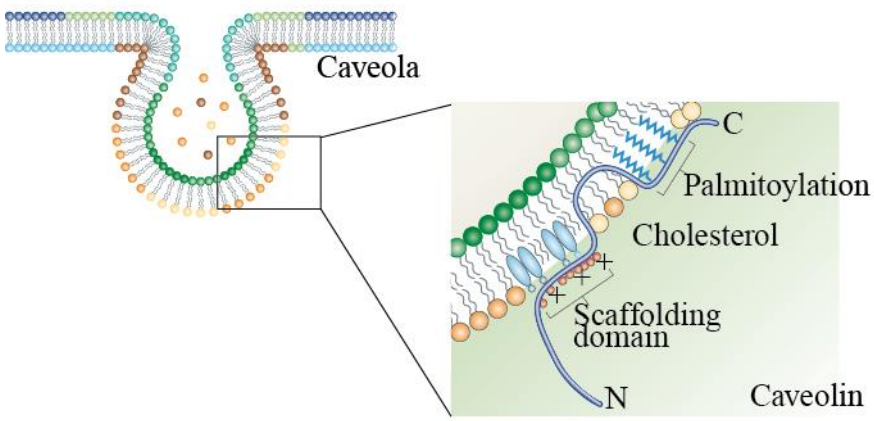

Adapted from Parton and Simons, *Nature reviews*, 2007

Figure 5. Caveolin topology.
Membrane topology of caveolin, the N- and C-termini face the cytoplasm and the hairpin domain is embedded into the PM.

The formation of caveolae is strictly regulated by cavins, which are cytoplasmic proteins recruited to caveolae that are needed for the stabilization of caveolin oligomers. Among the cavin proteins: cavin1 (also known as PTRF) and cavin-2 and -3 have been described as substrates for protein kinase C (PKC) (reviewed in (30)). Once formed, the budding of caveolae from the PM requires dynamin.

The formation of higher-order structures named rosettes or caveolar clusters is characteristic of caveolae (Figure 6a). These structures are peculiar for specific tissues like white adipose tissue and endothelia. In the first case, caveolae ere involved in lipid regulation, while in the second case, caveolae are used as membrane reservoirs in response to mechanical stress of the cell (31,32). In particular, considering the great membrane-capacity of rosettes, disassembly of these structures can buffer membrane tension in response to mechanical stress (31). Through exocytosis, the same type of protection can occur to provide physical protection against lysis. Opposite to exocytosis, endocytosis of caveolar clusters has been associated with wound repair (33). For the regulation of all these functions, the interaction of caveolae with actin, in particular with stress fibers, is fundamental (32). Stress fibers are in turn fundamental for focal adhesions. Several studies suggest a role for Cav1 also in the regulation of focal adhesions, especially through endocytosis of integrins, indicating an association between caveolae and the extracellular matrix (ECM) (Figure 6b).

The emerging picture for caveolae is dynamic; their role in endocytosis is still debated but it is known that their dynamics are differently regulated depending on cell type and along the cell cycle. During mitosis, there is an increased localization of Cav1 into vesicles, possibly important for the equal redistribution of Cav1 into the two daughter cells (34).

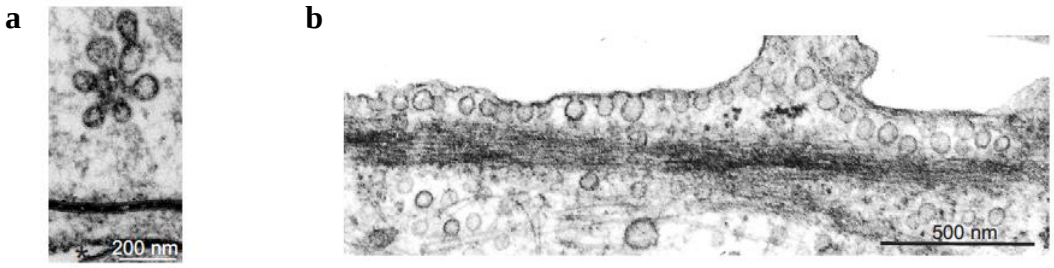

Adapted from Echarri and Del Pozo, *Journal of Cell Science*, 2015 (32)

Figure 6. Association of caveolae with stress fibers.

a) Electron microscopy image of a caveolar rosette. Ruthenium Red labeling (dark signal) shows the connection of the rosette with the outside of the cell (*).

b) Electron microscopy showing caveolae co-aligned with stress fibers (black).

1.4.2 Flotillin-mediated endocytosis

Flotillin-1 and -2 (reggie-2 and reggie-1, respectively) acquired their names because they were found associated with the so-called floating fraction of lipid rafts after solubilization of membranes in Triton X-100 (35). These membrane-associated proteins are expressed in mammals, bacteria, plants, fungi and metazonas but not in budding yeast and *C. elegans*, and have a conserved sequence (36).

Flotillins are ubiquitously expressed in different cellular types and have a dynamic subcellular distribution. Originally, flotillins were defined as proteins associated with caveolae, but later studies changed this idea: depending on the cell context, flotillins can be found at the PM, the Golgi complex, endosomes, lysosomes and exosomes. In particular, flotillins can be found associated with endosomes when cells are stimulated with EGF, but no co-localization has been found prior to 15 minutes of cell stimulation. The ablation of flotillins does not have any effect on EGF internalization (37), thus suggesting that they are more likely a cargo in this internalization process rather than effectors/regulators. Moreover, flotillins-1 has not been found to co-localize with transferrin, while its ablation is reported to impair the internalization by fluid phase of the GPI-linked protein CD59 (38), even if this point is under debate (39).

Flotillins are thought to work in the localization of some cargoes at the PM, indeed, together with the prion protein (Prp), they are involved in the recruitment of the transporter Glut4, cadherin, and TCR to the PM in adipocytes, in embryonic and epithelial cells, and in lymphocytes, respectively (40).

1.4.3 CLIC-GEEC pathway

It has been reported that the major fluid phase endocytic pathway, at least in fibroblasts, is the so-called clathrin-independent carrier (CLIC)-GPI-anchored protein-enriched early endosomal compartments (GEEC) (41). Through this pathway, large amounts of extracellular

fluids, glycosylphosphatidylinositol (GPI)-anchored proteins, CD44, major histocompatibility complex class I (MHCI), and toxins like Shiga and cholera are internalized (42,43).

The morphology of CLIC-GEEC is tubulo-vesicular and the size of the structures is 40-80 nm. Membranes associated with this pathway are highly dynamic and connected with the activity of the small G-proteins Cdc42 and the BAR protein GRAF1 (GTPase regulator associated with focal adhesion Kinase-1), which exhibit a GAP activity for Cdc42. The GTPase activity of Cdc42 is necessary for the recruitment of the actin machinery required for the execution of the endocytic process. The BAR domain of GRAF1 is needed for membrane curvature and, together with the pleckstrin homology (PH) -domain, localizes GRAF1 to (phosphatidylinositol 4,5-bisphosphate) PI(4,5)P2 -enriched lipid structures. In addition, GRAF1 possess an SH3 domain through which it interacts with dynamin that, however, is not needed for the internalization step but is recruited later in the endocytic process.

Depletion of GRAF1 causes a 60% reduction in the internalization of dextran, a typical cargo for this pathway, but has no effect on transferrin internalization, which occurs only through CME. Recently, the same selective block of the pathway, following the CLIC cargo CD44, has been observed in cells treated with the inhibitor of glycosylceramide synthase (DL-threo-1-Phenyl-2-palmitoylamino-3-morpholino-1-propanol, PPMP). This effect has been related to the requirement of a fraction of CLICs on galectin-3 that drives the glycosphingolipid-dependent membrane bending at the initial steps of CLIC biogenesis (43).

1.4.4 ARF6-associated pathway

Another form of NCE is the highly conserved, dynamin independent, ADP-ribosylation factor 6 (ARF6)-associated pathway (44). Cargoes internalized trough this endocytic route are different and can be divided into proteins involved in: i) nutrient and ion transport (Glut1, CD98, Lat1); ii) matrix interaction (CD44, CD147); iii) immune response (MHC class I, CD1a); and iv) GPI-anchored proteins (CD55 and CD59) ((45) and reviewed in (46)).

Interestingly, after internalization, cargoes entering into this route undergo distinctive sorting. For example, CD55 and Glut1 follow MHCI internalization and can be found in EEA1-positive endosomes, where also transferrin is present, whereas CD44, CD98 and CD147 do not enter the EEA1-positive compartment; however, the fate of all cargoes internalized through this pathway is mainly recycling (45).

Some of the cargoes internalized through the Arf6-positive pathway are the same as the CLIC-GEEC, however, in cells where this pathway is active, Arf6 ablation has only a minor impact on internalization, suggesting that Arf6-positive and the CLIC-GEEC are distinct endocytic routes sharing some of the molecular players (1).

1.4.5 IL-2 receptor endocytic route

The Interleukin-2 receptor (IL-2R) is internalized through another class of NCE pathways that is characterized by small non-coated PM invaginations (50-100 nm). IL-2 receptors are associated predominantly with detergent-resistant membrane domains (DRMs). The association with DRMs is triggered by IL stimulation and maintained alongside early steps of endocytosis. Endocytosis of IL-2R specifically occurs at the level of membrane protrusion rather than at the level of 'flat' PM (reviewed in (47)).

The molecular machinery underlying the endocytosis of the IL-2R has been characterized (48,49), starting from the requirement of dynamin and RhoA to complete the internalization (50). Activated IL-2R triggers the PI(3)P (phosphatidylinositol 3-phosphate) signaling cascade, which then activates RhoA and Rac1, followed by the activation of p21-actiavted kinase 1 (Pak1) by Rac1. Pak1, in turn, phosphorylates cortactin that, together with neuronal Wiskott-Aldrich syndrome protein (N-WASP), promotes the formation of F-actin, which is needed for the completion of the endocytic process (49).

1.4.6 Fast endophilin-mediated endocytosis (FEME)

A new route belonging to the category of NCE pathways has recently been described. This pathway relies on the rapid formation of tubulo-vesicular endocytic structures that depend on endophlin A proteins (A1, A2, A3), hence the name: fast endophilin-mediated endocytosis (FEME). Endophilins were already known to be peripheral players involved in clathrin-mediated endocytosis, although the triple KD of endophilin A1-3 does not completely block endocytosis of the CME cargo transferrin (51). Endophilins possess a SH3 domain through which they interact with cargo receptors, and a BAR domain to induce membrane curvature. The morphology of FEME is similar to the morphology of CLIC; however, FEME needs dynamin for its execution (dispensable for CLIC-GEEC), Rac, phosphatidylinositol-3-OH kinase, Pak1 and actin polymerization. Moreover, different from CLIC, FEME is negatively regulated by Cdc42 and is upregulated in its absence (52).

FEME mediates the ligand-triggered internalization of many cargoes: different G-protein-coupled receptors such as α_{2a}- and β1-adrenergic, dopaminergic D3 and D4 receptors and muscarinic acetylcholine receptor 4; the receptor tyrosine kinases EGFR, HGFR, VEGFR, PDGFR, NGFR and IGF1R, as well as the interleukin-2 receptor.

This new pathway is prevalently working at the leading edge of migrating cells (Figure 7): in particular, endophilins are recruited at the level of lamellipodia by the formation of phosphatidynlinositol-3,4-bisphosphate ($PI(3,4)P_2$) by SHIP phosphatases. Thus, FEME may be required for large PM rearrangement required during cell migration.

The FEME pathway mediates also the entrance of cholera and shiga toxins (STx), two famous cargoes that enter the cell through a clathrin-independent pathway (53). Endophilin A2 (endo A2) recognize a highly curved membrane domain, and is involved in the pinching step of FEME structures, as a consequence of its role, endoA2 ablation causes an elongation of STx-containing structures. The complete block of STx internalization, however, was

observed only after simultaneous ablation of endo A2, actin and dynamin, which act in concert in the execution of this pathway (53).

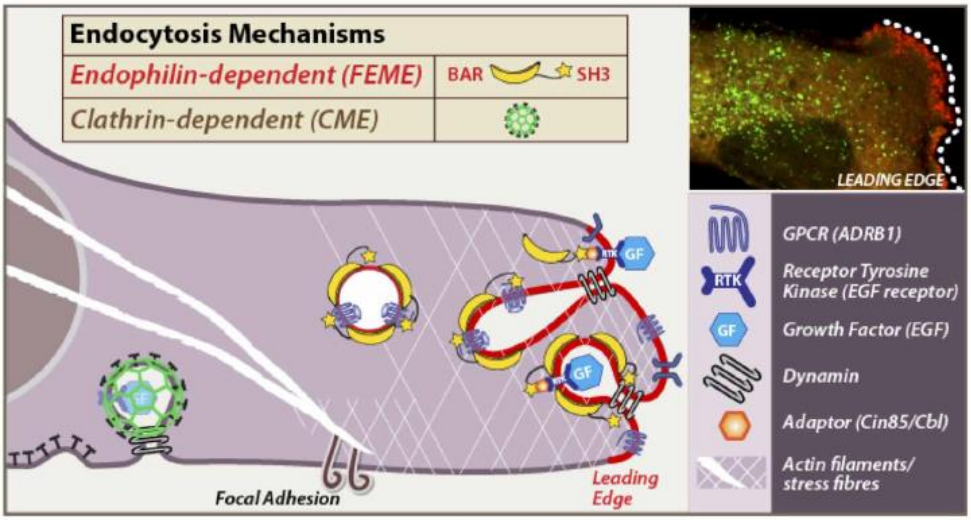

Adapted from Boucrot, *Nature*, 2015 (52)

Figure 7. Endophilin requirement at the leading cell edge.

A model of endophilin-dependent (FEME) endocytosis at the leading cell edge. Endophilin-coated vesicles/tubules associate with receptors or receptor-adaptors (like CIN85/Cbl) through their SH3 domains and promote membrane curvature through their N-BAR domains. Dynamin is recruited by endophilin and is required for the last step of detachment from the PM.

1.5 Dynamin: a master regulator of membrane trafficking

The GTPase dynamin is required for the completion of numerous endocytic pathways: CME, caveolae-mediated endocytosis, IL2-R endocytosis and FEME. Based on its function in several endocytic pathways, dynamin can be described as a master regulator of membrane trafficking. Dynamin intervenes in endocytosis at the moment of the detachment of endocytic structures from the PM when membranes are already in close apposition at the level of the so-called 'neck' of endocytic intermediates.

The first time that dynamin was associated with endocytosis was in a study of a temperature-sensitive mutant of shibire, the dynamin homologous in *Drosophila*

melanogaster (D. melanogaster). This mutant caused paralysis in the model system due to alteration in the release of synaptic vesicles (54). Further studies confirmed the fundamental role of dynamin in endocytosis, often assessed with the expression of the dominant negative K44A GTPase mutant. The expression of the dominant negative form of dynamin does not stop the formation of clathrin pits but causes the formation of elongated structures. A similar phenotype is observed upon complete ablation of dynamin, suggesting not only that dynamin is involved in the process, but that is also required for the last step of the pinching off. Indeed, in some cases, prior to dynamin action, actin and BAR proteins, like endophilins, are necessary for the stabilization of the neck of the endocytic structure (18,52,53). For instance, in cells in which the PM tension is reduced, actin is required for the stabilization of clathrin pits prior to dynamin action, otherwise, the GTPase cannot complete the pinching of the endocytic structure from the PM (55).

Mammalian cells possess three dynamin genes that encode for three proteins that share 80% homology but are differently expressed. Dynamin 1 is expressed at high levels in neurons; dynamin 2 is ubiquitously expressed; dynamin 3, like dynamin 1, is prevalently expressed in the brain, but also in testis and to a lower extent in lungs (56).

Invertebrates like *C. elegans* and *D. melanogaster* possess only a single gene for dynamin, so the existence of three genes in mammals could suggest a specific role for the different isoforms embedded in their different binding proprieties rather than related to different expression levels.

Dynamin possess different domains (Figure 8a):

- N-terminal GTPase,
- middle region: needed for the dimerization,
- pleckstrin homology (PH): binds phospholipids, especially PI(4, 5)P2
- GED: GTPase effector domain

- proline rich C-terminus domain (PRD): interacts with SH2 domain containing proteins.

To execute its function, the dynamin monomer dimerizes through the middle region with the N-terminal domain oriented in the opposite direction and combined to form tetramers (Figure 8b). The tetramers then oligomerize in a helical polymer at the neck of vesicles at the PM, and, through constriction induced by torsion, fuses the two sides of the neck, leading to vesicle separation from the PM (Figure 8c-d). To execute these functions, dynamin needs to hydrolize GTP through its GTPase domain (56).

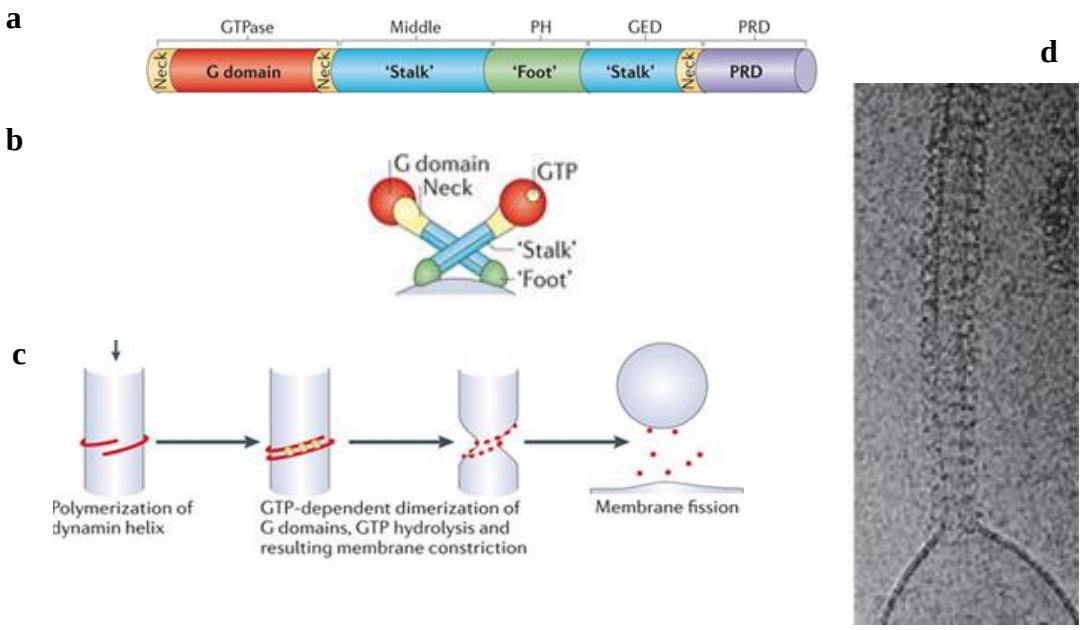

Adapted from Ferguson *Nat Rev Mol Cell Biol.* 2012 (56)

Figure 8. Dynamin structure and function.

a) Representation of the domain organization of dynamin.

b) Schematic representation of dynamin dimers.

c) Proposed GTP hydrolysis-dependent movement of dynamin neck leading to dynamin-mediated membrane fission.

d) Cryo-electron microscopy image showing a helical polymer of purified dynamin that has driven the formation of a tubule from a liposome.

1.6 After endocytosis: sorting at the endosomal level

Stereotypical view of the endosomal compartment strictly divided the endosomes into early, late and recycling endosomes. This view, however, has been revised towards a more dynamic picture, showing that this compartment is highly active and responsible for the collection of internalized cargoes and sorting to final destination (57).

The first feature that is used to categorize endosomes is the pH, which gradually decreases along with endosome maturation. This work is done by a v-type vacuolar H^+ ATPase, a transmembrane protein that pumps hydrogen ions into the lumen and decreases the pH. Considering the different pH sensitivity of ligand-receptors complexes, the decreasing pH is important for the regulation of the stability of the complexes. In particular, receptors that have to be actively recycled release the ligand already at pH 6.5, typical of early endosomes; while signaling receptors, like the EGFR, stay bound to their ligand and signal also at a lower pH, pH 4.5, typical of late endosomes.

Trough the endocytic pathway, endosomes change also their phosphatidylinositol phospholipid (PIP) composition, PIP interconversion is regulated by lipid kinases and phosphatases that act at different levels of endosomes maturation (58).

Endosomes are also characterized based on their association with different Rab GTPases, which are required for proper vesicle trafficking. Typical Rabs for the early endosomes are Rab4 and Rab5. These proteins recruit GEFs to endosome, which in turn recruit and activate Rabs in the following compartment (59,60). Following endosome maturation, Rab5 is lost and contemporary substituted by Rab7 (61). The Rab7 GTPase is active at the level of late endosomes that, while going through multivesicular bodies (MVBs), leads to cargo degradation in the lysosome. Rab11, instead, is enriched at the level of recycling endosomes and drives receptors back to the PM.

An example of the emerging plasticity of the early endosomal compartment is a recent model that revised the role of APPL-marked endosomes. More in detail, early endosomes are

marked not only by Rab5 but also by its effectors EEA1 and APPL1. APPL proteins seem to interact specifically with some types of receptors, and APPL endosomes have been considered to be intermediate structures for all endosomes before the acquisition of EEA1. Recently, new data highlights the possibility that multiple populations of endosomes coexist, one positive for APPL, one positive for EEA1 and one positive for both. Interconversion between the compartments is possible (57).

Once internalized, cargo fate is determined by sorting signals in its sequence (62) or by post-translation modifications, like ubiquitin, as in the case of EGFR ((63) and section 3.1.3). The different sorting of internalized cargoes is regulated also by the geometry of early endosomes. Indeed, the diverse shapes of the endocytic structures can facilitate the accumulation of cargoes for degradation or redistribution at the PM (64).

Sorting of endosomes is regulated by the ESCRT (endosomal sorting complex required for transport) machinery. This complex consists of four protein complexes: ESCRT-0, -I, -II and -III, according to their consecutive involvement in the sorting of cargoes into MVEs (for a recent review see (65)). The first three protein complexes contain ubiquitin-binding subunits and are responsible of the recognition of ubiquitinated cargoes. ESCRT-III, instead, forms oligomers and is involved in the interaction with deubiquitinating enzymes that are involved in the release of ubiquitin from the cargo before degradation. The ATPase VPS4 is then recruited and dissociate ESCRT-III oligomers for subsequent reuse (66,67).

2. Endocytosis and signaling

Cells have developed fine-tuned systems to regulate signaling. One of these systems is endocytosis and trafficking of PM receptors. The first line of control is represented by the regulation of the number of receptors exposed at the PM. This view is, however, simplistic, indeed, depending on the kind of receptors and on the endocytic route, signaling can continue along the endocytic pathway. Moreover, the spatial constrains of receptors into endosomes add another line of control, spatially defining the source of signaling.

2.1 Signaling from the PM

After ligand binding, PM receptors are usually removed through endocytosis in order to regulate the magnitude of the signal coming from their activation. If the ligand administration is prolonged over time, in some cases, like for example RTKs, the number of receptors at the PM is permanently reduced and can results in downmodulation of signaling but can also shift ligand concentration to higher levels to obtain the same magnitude of signal (68).

Signaling starts at the PM level and cargo clustering is often required to orchestrate a productive signaling. This is the case of RTKs and GPCRs, for which cargo clustering is absolutely required (69,70) (see (71) for a recent review). Cargo clustering can be regulated by the dynamics of pit formation. For example, the time of pit establishment can determine a different output in the case of cannabinoid receptor 1 (CB1R); thus regulating β–arrestin signaling. Depending on the type of ligand, endocytosis occurs through CCPs with different dwell times. In particular, pits that are formed in a fast process, stimulated by the agonist WIN 55,212-2, do not lead to the production of an active signal, while pits that are formed in slow process or in a prolonged period of time, stimulated by the ligand 2-AG, lead to productive clustering and, thus, to strong signaling (72) (Figure 9a).

CCP dynamics can be regulated not only by the internalized cargo but also by the lipid composition of the membranes involved. Indeed, some specific lipids are substrates for enzymes like phospholipase C (PLC), which is able to work only in the presence of the specific lipid substrate. PLC requires the presence of PI(4,5)P2 (phosphatidylinositol 4,5-bisphosphate) and PI(3,4,5)P3 (phosphatidylinositol 3,4,5-trisphosphate); and, for example, in the case of EGFR, PLC is active at the level of the PM, which is enriched in PI(4,5)P2, while it is almost completely inactive at endosomes where PI(4,5)P2 is virtually absent (73,74).

Signaling from the PM is also crucial for migrating cells. The localization of receptors in specific areas of the PM, as the leading edge, is required for a proper localization of signaling that, in turn, is crucial in the chemotactic response of the cell. Indeed, ligand sequestration at the leading edge provides spatial localization of signaling towards the migrating front, renders it less available for receptors at the lateral side; and through degradation of activated receptors cells are progressively less sensitive to the stimulus until a complete stop of migration occurs ((75), for a review see (76)).

Notch signaling is an example of the importance of endocytosis in the regulation of ligand and receptor exposure on the PM (reviewed in (68)). The signal regulation of this pathway involves the interaction between the membrane-bound ligand (e.g., Delta) on the so-called ‘signal sending cell’ and the receptor (Notch) on the ‘receiving cell’. Importantly, a recent study uncovered that Notch signaling from the PM can be regulated also by physical stimuli like temperature and mechanotension (77). Two different routes for Notch internalization are present during the development of *D. melanogaster*: at low temperature, Notch is constitutively internalized through a cholesterol-independent pathway that leads to signal activation; while at higher temperatures, a cholesterol-dependent way is prevalently activated and leads to the degradation of Notch ((77), Figure 9b).

PM tension is another feature that can regulate endocytosis and subsequent signaling; conversely, endocytosis, through the alteration of membrane composition, can modify PM

tension. This bidirectional regulation is particularly important when cells communicate with the extracellular matrix (ECM), a process that requires the active regulation of integrin signaling. In particular, the diverse rigidity of the ECM is able to regulate the recruitment of different adaptors or endocytic machineries necessary for endocytosis (78).

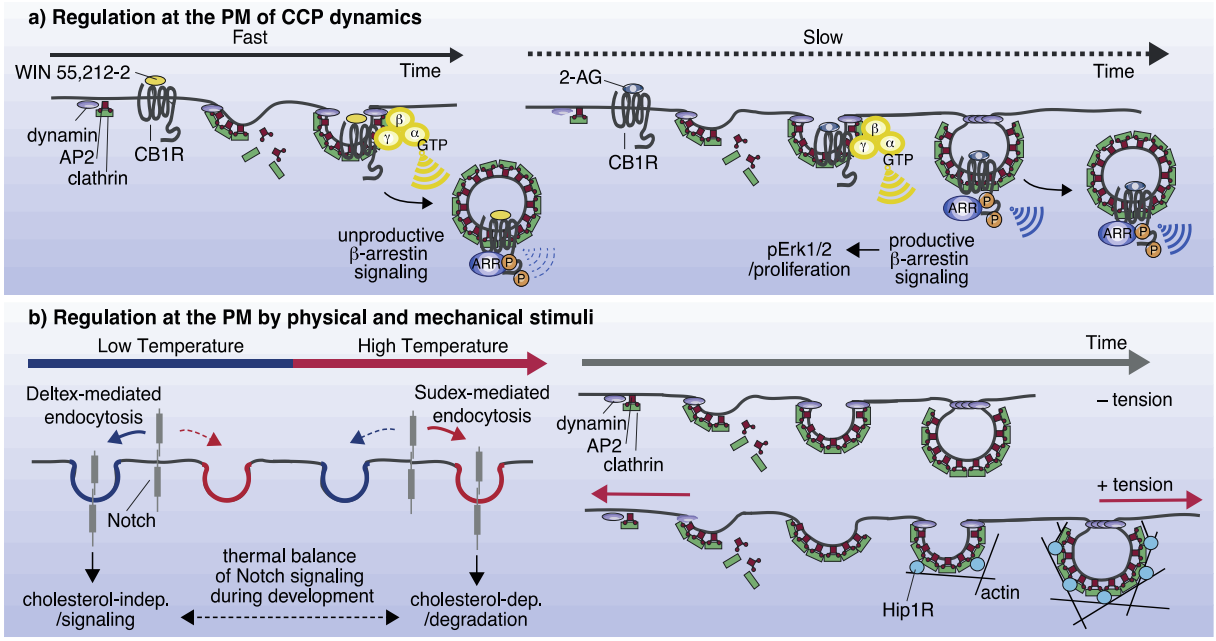

Adapted from Barbieri et al. *Current Opinion in Cell Biology* 2016 (79)

Figure 9. Endocytosis controls signaling from the PM.

a) Left, the agonist WIN 55,212-2 induces recruitment and internalization of the cannabinoid receptor (CB1R) through CCPs, which results in trimeric G-protein (α, β, γ)-mediated signaling, but fails to generate productive β-arrestin-dependent signaling. Right, the agonist 2-AG recruits CB1R into CCPs with slow dwell times allowing for both G-protein and productive β-arrestin-dependent signaling, which leads to the phosphorylation of Erk1/2 and cell proliferation.

b) Physical and mechanical stimuli, like temperature (left) or PM tension (right), control endocytosis and signaling. Left, in *D. melanogaster*, Notch is constitutively internalized, mainly via Deltex-mediated endocytosis, at low temperatures. At higher temperatures, Sudex-mediated endocytosis is enhanced and leads to Notch degradation. Right, under low PM tension (top), assembly of the clathrin coat is sufficient to deform the PM. Bottom, under high PM tension clathrin assembly is unable to counteract the tension force, and invaginations pause until actin polymerization provides the energy. In this second case, CCPs have an extended lifetime, which is necessary to allow Hip1R to be recruited and for actin polymerization to occur.

2.2 Signaling from endosomes

It is now clear that endocytosis does not block signaling after the removal of receptors from the PM; indeed, signaling can continue at the endosomal level, allowing a sustained phase of the signaling response (80). Moreover, endosomes can be seen as "signaling platforms" that organize and orchestrate specific downstream signaling pathways. Different features of endosomes make this compartment ideal for the regulation of signaling:

i) a small volume that favors the interaction between ligand and receptor,

ii) a prolonged time for activated receptor to signal,

iii) a peculiar microenvironment that can regulate receptor activity,

iv) mobility inside the cell.

Another level of regulation that can arise from endosomes is through the control of the number of endosomes, through which a cell can obtain the conversion of an analogical signal, like the concentration of a ligand, into a digital signal, like a specific cell response. This was shown for signaling receptors like EGFRs, which are not randomly distributed into endosomes but packaged in precise quantities into endosomes. The number of EGFR-containing endosomes, not the number of receptors *per* endosome, is increased with increasing EGF concentrations; this type of packaging in *quanta* allows an analog-to-digital conversion, from ligand concentration to signaling, and confers robustness to signaling which is actively regulated (81). Apparently, this control system is not restricted to EGFR signaling but is active also for hepatocyte growth factor receptor (HGFR) and nerve growth factor receptor (NGFR) (81). Importantly, the organization of receptors into endosomes defines a scaffolding role for these structures. At this level, signaling receptors can interact with adaptor proteins that are needed for the activation of downstream signaling, like growth factor receptors that activate the MAP kinase signaling.

An example of the flexibility that endosomes can give with their movement inside the cell is the regulation of cAMP signaling downstream GPCRs. After ligand-induced activation,

these receptors couple with G proteins and stimulate adenylyl cyclase that produces cAMP, which in turn regulates downstream effectors. In the case of β2-AR, after activation, receptors are internalized into endosomes and are physically moved from the PM to the nucleus, where the production of cAMP is locally required for an efficient control of transcription (82).

2.3 Endocytic routes and receptor fates

Signaling coming from receptor activation is regulated not only by the internalization of receptors into endosomes, but also by the kind of endocytic route through which they are internalized. Several receptors, like RTKs, GPCRs, TGFβR (tumor growth factor β receptor), Notch and Wnt, are internalized both through CME and NCE and the entrance into these pathways is finely regulated and results in different output (68).

The Wnt signaling pathway is fundamental for development regulation due to its regulation of the activation of β-catenin that, upon binding of transcription regulators, determines the activation of genes needed for cell proliferation. This system is finely tuned thorough the activation of two diverse endocytic routes. The transmembrane receptor Frizzled (Fz), upon binding with its ligand Wtn3a clusters with the co-receptor LRP6 (low density lipoprotein receptor-related protein 6), and through the interaction with Dishevelled (Dvl) and Rab8, promotes the internalization through the NCE caveolae pathway. This route is associated with β-catenin accumulation and, thus, with proliferation. When the Wnt3a agonist Dickkopf (DKK) is present, instead, it binds LRP6 and moves its internalization to the clathrin-mediated pathway, resulting in an increased β-catenin degradation and signal attenuation ((83) and Figure 10).

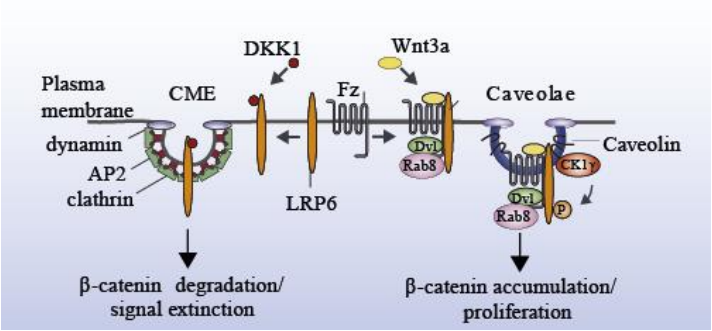

Adapted from Barbieri et al. *Current Opinion in Cell Biology* 2016 (79)

Figure 10. Different endocytic routes and different fates.

WNT3a binding to its receptor Frizzled (Fz) induces the interaction with LRP6, Dishevelled (Dvl) and Rab8, and mediates internalization through caveolae. This allows β-catenin accumulation and leads to cell proliferation. In contrast, the Wnt pathway antagonist DKK1 recruits LRP6 to clathrin-mediated endocytosis (CME), which ultimately leads to β-catenin degradation and signal extinction.

In the case of TGFβR and EGFR, the regulation is the opposite to that of LRP6. Upon ligand binding, TGFβR is activated and initiates the Smad signaling, for which the interaction with the Smad adaptor SARA (Smad anchor for receptor activation) in endosomes is important, which in turn interacts with PI3P. The characteristic of the regulation of this receptor through endocytosis is that signaling starts when TGFβR is internalized through CME, but undergoes ubiquitination and degradation when it is internalized through NCE, apparently through caveolar structures (84). A similar regulation is exerted on the endocytosis of EGFR ((63) and see section 3.2).

3. EGFR endocytosis and trafficking

EGFR, also called ErbB1, belongs to the ErbB family of RTKs, which includes ErbB2/HER2/Neu, ErbB3/HER3 and ErbB4/HER4 (85,86). These receptors are characterized by a large extracellular ligand-binding region composed of ~620 amino acids, a single membrane spanning α-helix, and a ~550 amino acids intracellular region that contains a juxtamembrane portion (composed of ~45 amino acids), followed by the tyrosine kinase domain (~270 amino acids) and the C-terminal regulatory sequence (~230 amino acids). Upon activation, the ErbB receptor undergo dimerization and autophosphorylation in trans in the C-terminal tail. This signal triggers the recruitment of downstream signaling proteins with a SH2 (Src homology 2) or a PTB domain that start the downstream signaling network (87) .

3.1 EGFR activation

3.1.1 EGFR dimerization

In the extracellular region, each single monomer of EGFR presents four subdomains, named subdomains I-IV.

- Subdomains I and III (Figure 11) are homologous and form the site where the ligand is bound.
- Subdomains II and IV (Figure 11) are also homologous, and are characterized by a high cysteine content (88).

When the ligand is not present, the EGFR extracellular region adopts a close configuration; in this condition, the subdomain II is tethered with subdomain IV (Figure 11a). Without ligand, only a minor part of the monomers is found in an “open conformation” (Figure 11b). EGFR monomers continuously alternate their status as monomers and dimers. Only upon ligand binding the open conformation is stabilized (Figure 11c) and the dimerization interfaces in subdomains II and IV are exposed, leading to proficient dimerization (88) (Figure 11d).

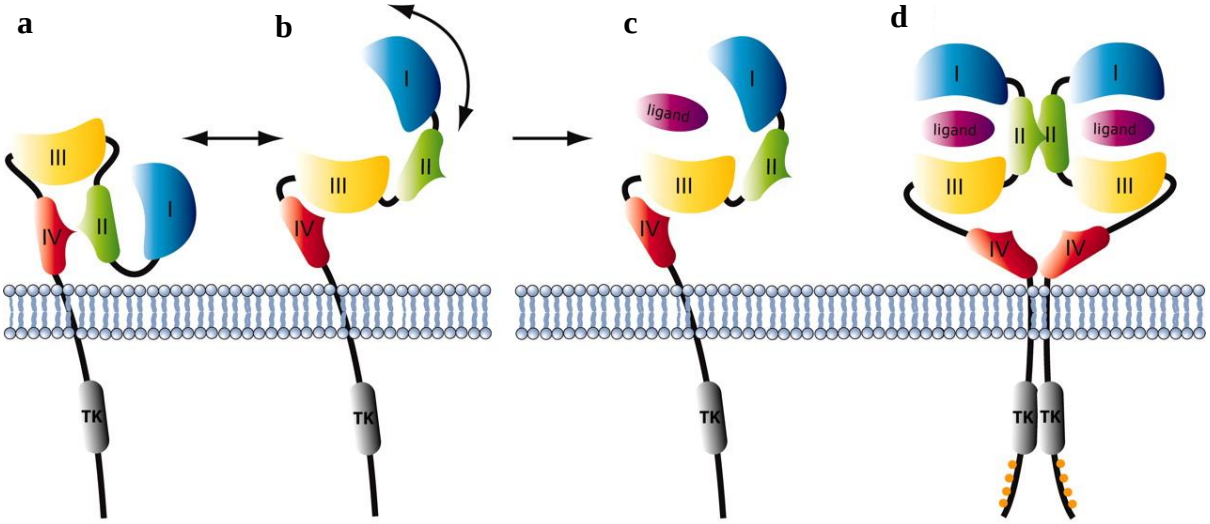

Adapted from Lammerts van Bueren JJ *PNAS*, 2008 (89)

Figure 11. Lligand-induced EGFR activation.

EGFR domains are shown (domain I, blue; domain II, green; domain III, yellow; domain IV, red; intracellular tyrosine kinase domain, gray).

a) Unbound monomer of EGFR in tethered conformation.

b) EGFR in "untethered" conformation.

c) A ligand binds an untethered ligand and interacts with domains I and III, stabilizing the extended form.

d) Dimerization of two monomers through interaction of domain II. The intracellular kinase domains cross-phosphorylate residues in the C-terminal receptor tail.

EGFR dimerization is a crucial step in receptor activation and controls the kinase activity of the receptor, which is regulated by autoinhibition. The receptor is activated by an intermolecular allosteric interaction only upon dimerization induced by the ligand. In the kinase domain of an active EGFR, the C-lobe of one monomer (the activator) takes contacts with the N-lobe of the other monomer (receiver), leading to the reversion of the auto-inihibitory interaction in the receiver monomer (90).

EGFR activation appears to be regulated also by the intracellular juxtamembrane region. Indeed, this segment is required to potentiate dimerization and to make the activation mechanism operative (91,92). To complete the activation of the receptor upon ligand binding,

also the calcium binding protein calmodulin appears to be crucial. Indeed, the EGFR juxtamembrane region possesses a positively charged calmodulin binding domain (CaM-BD) that in resting conditions is bound to the negatively charged inner leaflet of the PM (Figure 12), leading to auto-inhition in the absence of ligand. EGF stimulation leads to an increase in calcium levels and to the binding of calcium to calmodulin, forming the Ca^{2+}-calmodulin complex. One hypothesis is that the interaction with the calcium-bound calmodulin facilitates the detachment of the juxtamembrane region of EGFR from the PM, thus leading to the complete activation of the receptor (Figure 12) (93,94)

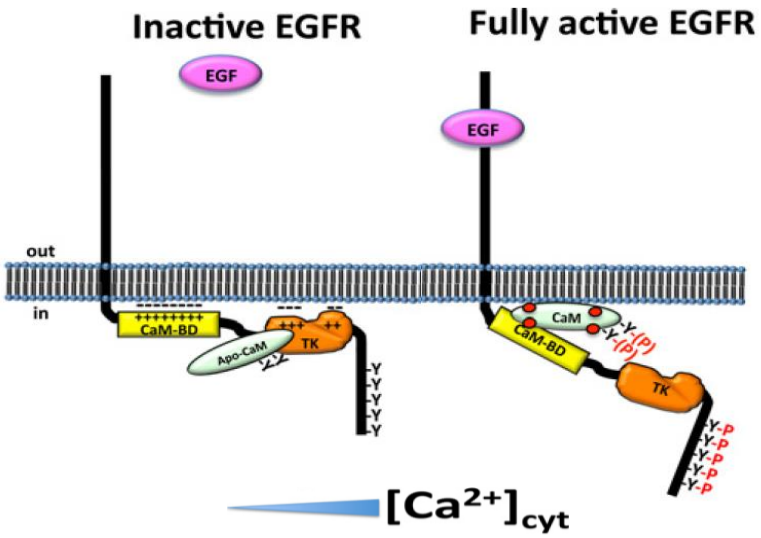

Adapted from Stateva, *Biochem Journal*, 2015 (94)

Figure 12. Calmodulin regulation of EGFR activity.

In resting conditions, both the CaM-BD and the tyrosine kinase domain (TK) of the EGFR are electrostatically bound to the inner leaflet of the PM. When calmodulin is not bound to calcium (apo-CaM), it can tether to the receptor close to its TK. After ligand binding, the cytosolic concentration of free Ca^{2+} is high enough and Ca^{2+}–CaM complexes are formed and bind to the CaM-BD of the EGFR that is completely detached from the membrane, thus activating the receptor.

3.1.2 The EGFR signaling cascade

EGFR can be activated by different ligands: EGF, TGFα (transforming growth factor α), HB-EGF (heparin-binding EGF-like growth factor), betacellulin, epiregulin, amphiregulin, and epigen. All these ligands have a so-called EGF-motif, which consists of six cysteine residues that interact through disulfide bonds (95). EGF and TGF α are specific ligands for EGFR. After activation, EGFR can start different downstream signaling pathways; the major ones are:

(1) PLC γ (phospholipase C γ), which in turn activates PKC and a calcium cascade,

(2) Ras signaling, leading to various MAPKs,

(3) PI3K, leading to AKT signaling cascade.

The final output of these signaling cascades are different and comprise: proliferation, migration, and differentiation (87). Considering the important effect of this signaling cascade on cell fate, the process is highly regulated through post-translational modifications and receptor endocytosis (for a review see (96)).

3.1.3 EGFR phosphorylation and ubiquitination

Upon ligand binding, the EGF receptor undergoes auto-phosphorylation in correspondence with tyrosine residues present at the C-terminus and phosphorylates different cytoplasmic substrates. There are several tyrosine residues on EGFR that serve as docking sites, among which:

- Tyr1068 and Tyr1086, which are crucial for the recruitment of the adaptor Grb2 (growth factor receptor-bound protein 2) that is involved in the Ras-MAPK signaling cascade (Figure 13) and in endocytosis ((97) and section 3.2.1);
- Tyr1092, which is important for the interaction with PLC γ;
- Tyr1173 and Tyr1148, which are required for the interaction with the adaptor SHC

Another crucial post-translational modification of the EGFR is ubiquitination. Ubiquitin (Ub) is a small, highly conserved, protein composed of 76 amino acids and is characterized by a di-glycine motif in which Gly76 can be conjugated by the ε-amino group to a lysine on a target protein. The modification of the target protein requires the intervention of three classes of enzymes: E1, E2 and E3 – E3 is the enzyme that covalently attaches the Ub molecule to the substrate.

Ub can be attached as: (a) monoubiquitin, when one Ub moiety is attached to one lysine residue or (b) multimonoubiquitin, when many lysine residues are modified with a single Ub moiety, or (c) polyubiquitin, when a chain of Ub is attached. All seven lysine residues in a Ub molecule can be used for chain formation *in vivo* (98), although Lys11-, Lys48- and Lys63-linked chains are the most studied and the most abundant lysines in the cell (99). In particular, Lys63-linked polyubiquitin chains play, among others, important roles in endocytic trafficking (100).

The major E3 ligase involved in ubiquitination of EGFR is Cbl (Figure 13) (101). Three Cbl genes have been identified in mammals: Cbl (also called c-Cbl), Cbl-b and Cbl-c. Cbl proteins have multiple domains:

i) the tyrosine kinase-binding domain (TKB), which can directly bind to the phosphorylated Tyr1045 of EGFR,

ii) the RING E3 ligase domain,

iii) a proline rich region, through which interact with Grb2,

iv) the UBA (ubiquitin associated) domain, responsible for Ub-binding and/or dimerization (102).

The ubiquitination sites on EGFR have been mapped and the two major modifications that occur are monoubiquitination (~49% of the modified receptor) and Lys63-linked polyubiquitination (~40% of the modified receptor) in the kinase domain of the receptor (103). EGFR ubiquitination has a fundamental role in receptor endocytosis and in the

regulation of its intracellular fate. Indeed, when EGFR is stimulated with high dose of EGF, a substantial fraction of the receptor becomes ubiquitinated and is destined to lysosomes for degradation ((22) and section 3.2.2).

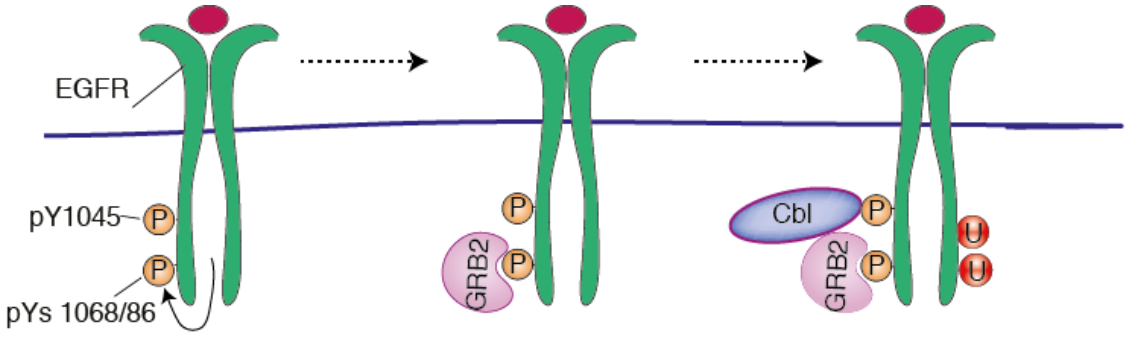

Adapted from Polo, *BMC Biology*, 2012 (104)

Figure 13. The interaction of Grb2 and Cbl with active EGFR.
Upon EGF activation, Tyr1068, Tyr1086 and Tyr1045 residues in EGFR are phosphorylated, permitting the recruitment of the adaptor Grb2. Finally, the recruitment of Cbl leads EGFR ubiquitination.

3.2 EGFR endocytosis

A critical regulator of EGFR signaling is endocytosis. Depending on ligand concentration and cell context (68), EGFR internalization can occur both via CME and NCE. At low EGF doses (≤1 ng/ml), receptors are almost exclusively internalized through CME. In contrast, at high, yet physiologically relevant, EGF doses (20 - 100 ng/ml), a substantial proportion of EGFR (around 40% in HeLa cells) is internalized, in parallel to CME, also through NCE (63). Importantly, both low and high doses of EGF are physiological; indeed, EGF concentrations vary in different bodily fluids (Table 2):

- low (1–5 ng/ml) in plasma, serum, and saliva,
- medium (5–50 ng/ml) in tears, follicular fluid, sperm, and seminal plasma,
- high (50–500 ng/ml) in bile, urine, milk, and prostate fluid.

Moreover, EGF can act as a juxtacrine stimulator as it is produced as a transmembrane precursor and is not always processed (especially in the kidney) (105). Thus, under physiological conditions, cells are exposed to a wide range of ligand concentrations but epithelial cells act as a barrier, preventing the encounter of EGF-containing fluids with EGF receptors expressed on the basolateral membrane of cells. In pathological conditions, however, like in lesions or in premalignant neoplasia, tight junctions of the epithelia become leaky and lead to elevated doses of EGF that reach and activate the EGFR. Moreover, high levels of EGFR ligands have been found in different cancer types (reviewed in (106)).

	Tissue/bodily fluids	**Concentration**
LOW	Plasma	~1 ng/ml
	Serum	~5 ng/ml
	Saliva	1-3 ng/ml
MEDIUM	Tears	10-30 ng/ml
	Follicular fluid	3-30 ng/ml
	Sperm	20-40 ng/ml
	Seminal plasma	~50 ng/ml
HIGH	Bile	~150 ng/ml
	Urine	~100 ng/ml
	Milk	~400 ng/ml
	Prostate fluid	150 ng/ml

Table 2. Different concentrations of EGF in human tissues and body fluids.

3.2.1 Clathrin-mediated endocytosis of EGFR

CME is the best-characterized endocytic route for EGFR. Indeed, EGFR possess different sequence motifs in its C-terminal tail that interact with the clathrin adaptor AP2. More in detail, the receptor directly interacts with the μ2 subunit of AP2, and mutations in this motif do not block completely EGFR entrance through CME (107). Moreover, the removal of AP2 reduces CME of EGFR, even if to a lesser extent compared to the removal of clathrin, thus suggesting the possible involvement of other adaptors ((108) and section 1.3.2).

After ligand binding, the EGFR undergoes auto-phosphorylation (Tyr1068 and Tyr1086) and Grb2 is recruited to the receptor. The phosphorylation of these residues appears necessary for CME, as when they are mutagenized, Grb2 is no longer recruited to the receptor and CME of EGFR is strongly affected (97). Grb2 can interact with Tyr1068- and Tyr1086-containing motifs of the receptor (97,109) through its SH2 domain, coupling the receptor with other proteins. One of the major Grb2-interacting proteins is Cbl: different evidences highlight a function for Cbl in EGFR internalization. Cbl has been found to translocate to CCPs upon EGF stimulation (110). Expression of Cbl mutants inhibits EGFR internalization (97) and siRNA depletion of both Cbl and Cbl-b results in partial inhibition of receptor endocytosis (103). Cbl directly ubiquitinates EGFR, but receptor ubiquitination is not always required for its endocytosis: indeed, EGFR ubiquitination is not essential for CME (22,103) but is required for NCE (22). In particular, EGFR mutants that lack Tyr1045 (the site recognized by Cbl) or the ubiquitin acceptor sites, undergo almost normal internalization via CME (22,111). Importantly, even if EGFR ubiquitination is not essential for CME, the activity of Cbl is still needed, possibly because it can ubiquitinate other components of the clathrin machinery or it can work as an adaptor in CME.

3.2.2 Non-clathrin endocytosis of EGFR

Opposite to CME, EGFR ubiquitination is absolutely required for NCE. Our laboratory demonstrated that, in HeLa cells, ubiquitination of EGFR occurs only upon stimulation with high doses of EGF and that this is coupled to the emergence of the NCE pathway (22,111). Ubiquitination is required for proper NCE; indeed, the EGFR mutant (Y1045F), which is poorly ubiquitinated, is defective for NCE but not for CME (111). Also other ubiquitin-binding proteins, Eps15, Eps15R and Epsin, appear to be recruited to the ubiquitinated EGFR and are redundantly essential but not specific, due to their involvement also in CME, in EGFR-NCE (22).

Ubiquitination is threshold controlled in different model systems and works as the molecular switch that triggers the internalization of EGFR through NCE (68). Ubiquitination is minimal at low doses and maximal at high doses of EGF, but presents a rapid increase in a narrow interval of EGF concentrations. EGFR-phosphorylation, instead, follows a typical hyperbolic dose-response curve (Figure 14). Thus, cells have the ability to convert a linear EGF signal into an on-off switch for the NCE system. By using a modeling approach, our laboratory demonstrated that a cooperative binding of Cbl and Grb2 to different phosphorylation sites on the EGFR tail is required for the proper control of this on-off system (112). Importantly, EGFR-NCE has been characterized in HeLa cells but its presence has been also verified in other cell lines, as reported in Table 3.

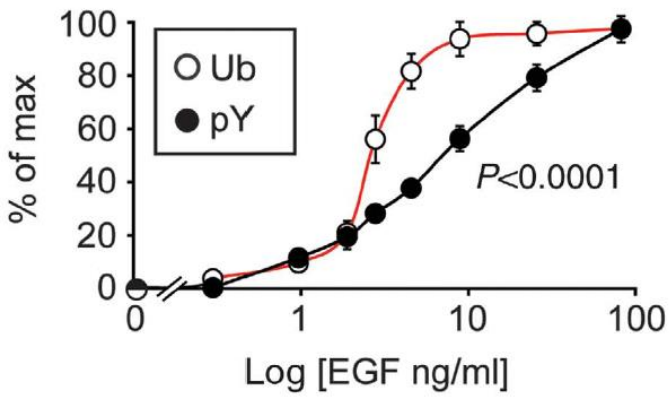

Adapted from Capuani, *EMBO Journal*, 2013 (111)

Figure 14. EGFR phosphorylation versus ubiquitination.

ELISA analysis of cell lysates after stimulation with the indicated doses of EGF and analyzed with anti-Ub or anti-pY antibodies. The results are presented as the percentage of the maximal tyrosine phosphorylation or ubiquitination (% of max). In black, the linear increase in EGFR phosphorylation. In red, the threshold behavior of EGFR ubiquitination.

Cell line (EGFRs/cell)	Low EGF Ke	High EGF Ke obs	NCE
HeLa (3.0×10^5)			
Control	0.30	0.15	Yes
Clathrin-KD	0.08	0.08	
Dynamin KD	0.07	0.03	
A431 (1.4×10^6)			
Control	0.42	0.05	Yes
Clathrin-KD	0.07	0.03	
Dynamin KD	0.08	0.01	
MDA MB-231 (0.8×10^5)			
Control	0.24	0.19	Yes
Clathrin-KD	0.04	0.08	
Dynamin KD	0.03	0.02	
BT20 (4.3×10^5)			
Control	0.10	0.06	Yes
Clathrin-KD	0.03	0.04	
Dynamin KD	0.03	0.02	
MCF10A (2.9×10^5)			
Control	0.27	0.19	No
Clathrin-KD	0.04	0.02	
Dynamin KD	0.02	0.04	
HCT116 (0.5×10^5)			
Control	0.23	0.24	No
Clathrin-KD	0.04	0.05	
Dynamin KD	0.04	0.05	
BT549 (0.5×10^5)			
Control	0.23	0.13	No
Clathrin-KD	0.04	0.02	
Dynamin KD	0.04	0.02	

Table 3. The presence of NCE in different cell lines.

The presence of EGFR-NCE was evaluated by comparing the internalization rate of EGF at low and high dose in WT *versus* clathrin-KD and dynamin-KD cells.

3.2.3 EGFR internalization: two routes, two distinct fates

In HeLa cells, CME and NCE of EGFR are linked to two different intracellular fates: EGFR molecules internalized through CME are mainly recycled back to the PM (70%), resulting in sustained signaling, while EGFRs internalized through NCE are selectively trafficked to lysosomes for degradation (90%), leading to signal attenuation (Figure 15, (63)). Thus, NCE appears to be required for suppressing EGFR signaling in response to excessive stimulus and might therefore represent a crucial safety mechanism by preventing overstimulation of the cell. Considering the frequent over activation of EGFR signaling in cancer, a thorough understanding of NCE could lead to novel insights into tumorigenesis.

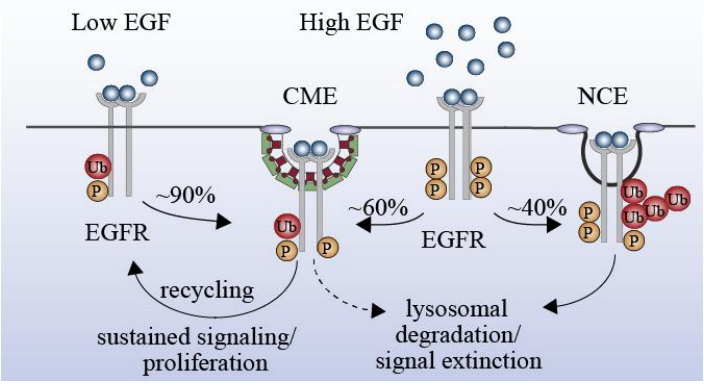

Adapted from Barbieri et al. *Current Opinion in Cell Biology* 2016 (79)

Figure 15. The effect of CME and NCE on EGFR fate.

At low doses of EGF, 90% of EGFR is internalized via CME and is targeted for recycling and sustained signaling, thus resulting in cell proliferation. At high doses of EGF, EGFR become significantly ubiquitinated concomitantly with the activation of NCE. NCE targets internalized EGFR mainly to degradation in the lysosome, leading to signal attenuation.

4. The endoplasmic reticulum: a multifunctional highway

In recent years, the endoplasmic reticulum (ER) is emerging more and more as a central system, fundamental in the regulation of different processes. One of the most intriguing characteristic of this endomembrane system is that it is spread all over the cytoplasm of a cell and is able to reach every corner of it. Being so spread, the ER can come into close proximity with many different compartments of the cell and functionally interact with these. In recent years, the study of contact sites that regulate the interaction of the ER with different organelles has evolved, opening a new field of membrane contact sites (MCS).

Contact sites are defined as any place inside the cell where organelles come into close contact with each other without membrane fusion at a distance of 20-30 nm (113). Thanks to its structure, the ER comes into contact with many organelles inside the cell; the first types of interactions studied were with mitochondria and the PM (113). In the past decade, many other contact sites between ER and other organelles have been revealed (114) and represent a new interesting field of study (Figure 16). Contact sites represent an ideal platform where organelles can exchange information and material. Indeed, MCS appear to be involved in the movement and positioning of organelles inside the cell and in the exchange of calcium and lipids ((114-116), and sections 4.2, 4.3).

The ER system is divided into “rough endoplasmic reticulum” that represent the part of ER that is enriched in ribosomes, for protein synthesis, and that is more close to the nucleus; and “smooth ER” tubules that spread into the cell, are associated with less ribosomes, and constitute a “tubular ER network” that is able to stabilize contact with other organelles. In the next sections, the role of the crosstalk between tubular ER and endosomes will be discussed.

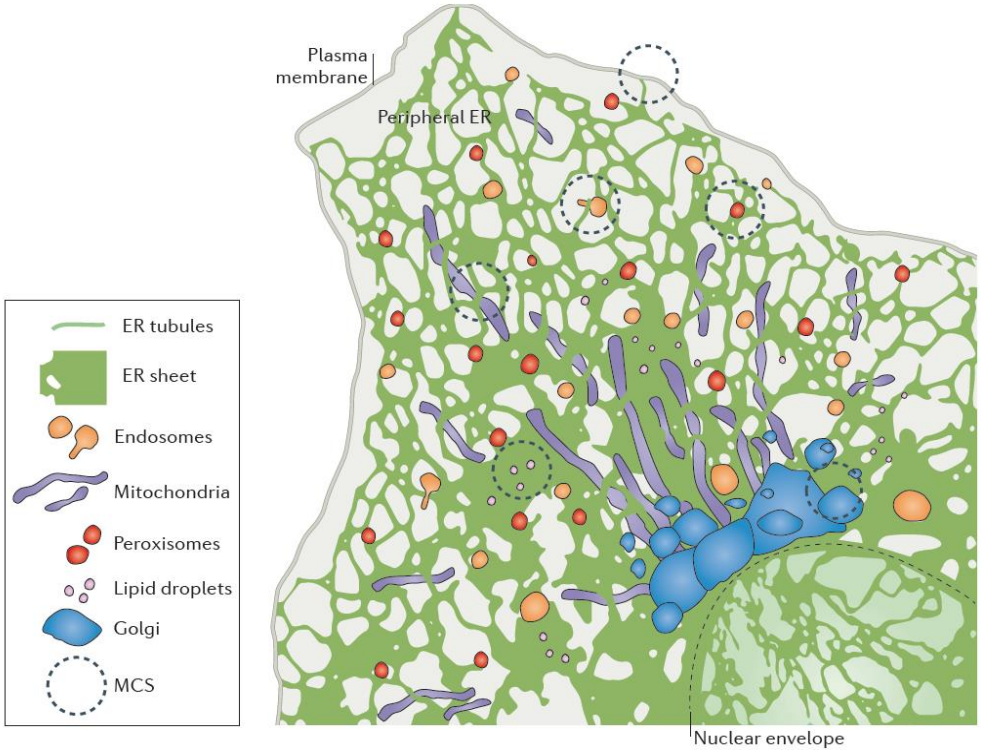

Adapted from Phillips *Nature Reviews* 2016 (114)

Figure 16. Endoplasmic reticulum and membrane-contact sites (MCSs).

The ER starts from the nuclear envelope (dashed line) and continues as peripheral ER, which diffuses into the cytosol as a network of sheets and tubules. Peripheral ER (smooth ER) forms MCSs with the PM, mitochondria, endosomes, peroxisomes, lipid droplets and the Golgi complex.

4.1 ER in the regulation of endosome dynamics

4.1.1 ER contact sites control endosome trafficking

Endosomes are engaged by the tubular ER and travel inside the cell by following the ER network, maturing along the way. This association is maintained thanks to the formation of functional MCS between endosomes and the ER, and increases with the maturation of endosomes. Indeed, it has been calculated that 55% of early endosomes are associated with the ER while this percentage increase to 99% for late endosomes (117).

The system that regulates endosome dynamic is starting to be better defined. The level of cholesterol, for example, is one feature that regulates this process. In particular, when cholesterol levels are low, late endosomes accumulate at cell periphery; while high cholesterol levels lead to the localization of endosomes close to the cell center (118). This control is exerted by the protein ORP1L (oxysterol-binding-related protein 1L), a regulator that is localized at the membrane of late endosomes and possesses an oxysterol-binding related domain (ORD) through which it interacts with sterols (118). When the ORD domain interacts with cholesterol, ORP1L changes its conformation and is able to enter in a Rab7-containing complex that directs the endosome towards the cell center. In the absence of cholesterol, ORP1L interacts, instead, with the ER-localized protein VAP (Vamp-associated protein). The interaction with VAP drives endosomes preferentially towards the cell periphery (119,120).

Another protein involved in endosome trafficking that is able to bind both Rab7 and VAP is protrudin. This protein is embedded into ER membranes and interacts with: VAP, PI3P, which is enriched at the level of late endosomes, and with the microtubule motor protein kinesin-1. At the level of MCS, protrudin, from the ER, interacts with Rab7 and PI(3,4,5)P3 in late endosomes; this interaction leads to the translocation of kinesin-1 from protrudin to the motor adaptor at the level of late endosomes. The kinesin-1 handover is a crucial step for the subsequent movement of late endosomes on the microtubule network (121). Deregulation of protrudin levels results in an alteration of endosome positioning: overexpression of protrudin and Rab7 causes an accumulation of late endosomes at the periphery, while protrudin depletion causes endosome accumulation at the perinuclear level, suggesting an impairment in their motility.

A recent discovery highlights an important function in endosome positioning also for an ubiquitin ligase located in the ER, the Ring finger protein 26 (RNF26). RNF26 has been defined as the “global architect of the entire endosomal system” (122). RNF26 is an ER resident protein that exposes its RING domain into the cytosol, and through this domain

interacts and ubiquitinate the scaffold p62/sequesosome 1 (SQSTM1). This modification leads to the interaction with endosome adaptors that possess an ubiquitin-binding motif, leading to the "binding" of endosomes to the ER. The interaction between endosome adaptors and the ER allows the formation of the so-called "cloud" of endosomes at the level of the perinuclear area. This system is reversible and is regulated by the deubiquitinating enzyme (DUB) USP15 that, by removing ubiquitin from SQSTM1, allows the detachment of the endosome from RNF26 (122).

4.1.2 ER contact sites control endosome fission and function

The ER is involved not only in the spatial localization of endosomes, but also in the localization and timing of their fission. This event occurs both at the level of early and late endosomes. A recent study assessed the binding, in correspondence with MCS, of ER to endosomes, followed by endosome fission and defined that the ER remains bound to endosomes after the process (123). The actin machinery, bound to the WASH complex, the multiprotein complex that activate actin nucleation by Arp2/3, is required to terminate the fission process. On the contrary, microtubule polymerization seems to be required for the formation of contacts with endosomes-ER, but is not required for their maintenance or activity (123).

A clear demonstration of the role of ER in endosome fission is the fact that alterations in ER shape, composition and dynamics result in a defective process in endosome fission (123). Recent evidences clarified the possible molecular mechanism involved in this process; MCS are platforms for the recruitment of all the factors necessary for the fission process and, considering the role of ER in lipid synthesis, the movement of lipids into the fission area is involved in the completion of the process (124).

A clear role of ER-endosome contact sites has been defined for EGFR-positive endosomes. EGFR interacts with the protein tyrosine phosphatase PTB1B that is localized in

the cytoplasmic part of the ER. The EGFR needs to be endocytosed and transported inside endosomes to interact with PTB1B in correspondence with endosomes-ER MCS, as demonstrated by immune-electron microscopy (Figure 17 (125,126)). PTB1B regulates EGFR through dephosphorilation and acts, not only at the level of endosomes, but is also involved in the regulation of MVB maturation, thus promoting the sequestration of EGFR into MVB vesicles and leading to degradation and signal control (125).

Of note, some evidences indicate an interaction of PTP1B with PM. This interaction highlights a function for contact sites between the ER and the PM in signaling control, at least in correspondence with cell-to-cell junction, where PTP1B can act, for example on EphA2 (127).

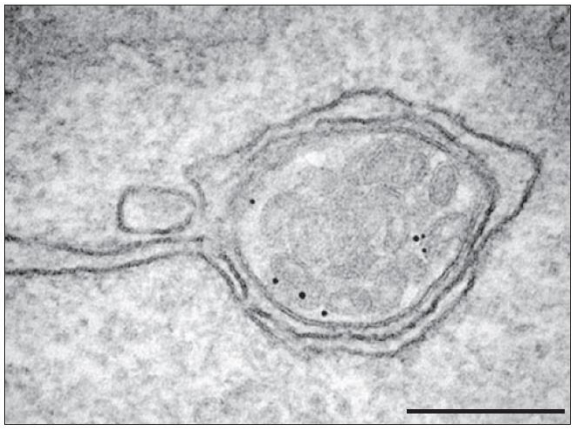

Adapted from Eden, *Nature Cell Biology*, 2010 (125)

Figure 17. PTP1B endosomes create contact sites with the endoplasmatic reticulum.
Cryo-immuno-EM of an endosome containing endocytosed EGF marked with gold EGFR and enwrapped by the ER.

4.2 ER-endosome contact sites in the regulation of lipid exchange

The ER synthetizes a vast number of phospholipids, sterols and precursor of sphingolipids that need to be moved to their active sites. However, the movement of lipids can occur also in

the other direction, from organelles to the ER, with the scope to control membrane lipid homeostasis (128). Independently of the direction, movement of lipids can be achieved by active transport through vesicles or through non-vesicular transport. An important role for MCS is emerging in this non-vesicular transport. The machinery involved in this process needs proteins that, with a hydrophobic pocket that allows the isolation of the lipid from the aqueous phase, are able to move lipids from one membrane to another. An example is the ORP5 protein, an ER transmembrane protein localized at late endosomes that is able to "accept" sterols from the protein NPC1 (Niemann-Pick C2 Protein) and to transfer them into the ER (129). Of note, ORP5 has recently been shown to be involved, together with ORP8, in the dual control of lipid composition of the PM and the ER. In particular, this protein mediates the movement of PI(4)P (phosphatidylinositol 4-phosphate) from the PM to the ER where the interaction with the phosphatase Sac1 leads to PI(4)P degradation. In the opposite direction, phosphatidylserine is moved from the ER to the PM where this lipid is enriched in specific domains (130). The ER-protein VAP, which controls the lipid composition of the PM and the ER, is crucial for the precise functioning of this system (124).

4.3 ER-endosomes contact sites and calcium

Calcium concentration [Ca^{2+}] is tightly regulated inside the cell, and its movement across membrane interfaces propagates its signal throughout the cell. The ER represents the major calcium store inside the cell, and calcium concentration in this organelle is between 60 and 500 μM (114). Calcium concentration outside the cell is around 1 nM, and endosomes, considering that they are generated from the PM, start with a similar concentration that goes from around 1nM in newly formed endosomes to 2.5 μM in late endosomes. Different mechanisms intervene to precisely control calcium concentration inside different organelles (114).

The most characterized pathway used by the ER to release calcium occurs through the opening of inositol-1, 2, 3-trisphosphate receptor (IP_3R) that is present in the ER membrane. The signaling cascade that leads to the opening of these channels starts at the PM, where external stimuli activate phospholipase C (PLC) that cleaves $PI(4,5)P_2$, releasing cytosolic IP_3 that is necessary for the opening of IP_3R on the ER membrane. The release of calcium from these receptors is massive and precisely localized but highly diffusible, and closely apposed membranes appear to be a favorite site for this type of calcium release (131,132).

The release of calcium is not only directed from the ER but is also directed back to the ER itself. Indeed, endosomes can rapidly change their pH after their formation and release calcium as a "stimulus" to trigger more calcium release from the ER, suggesting a bidirectional regulation between these two organelles (114).

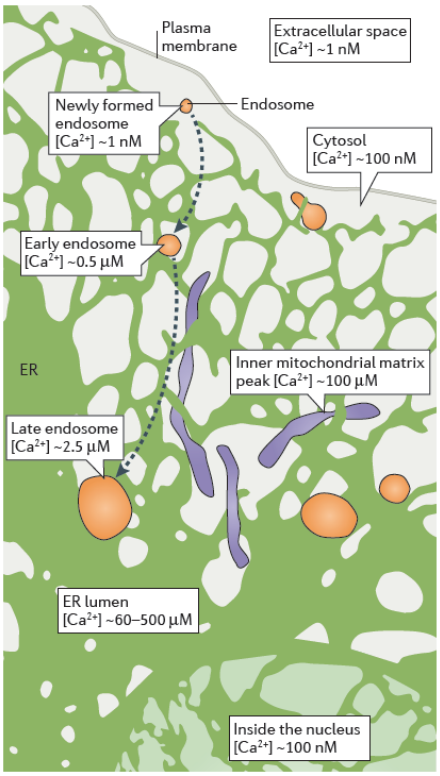

Adapted from Phillips, *Nature Reviews*, 2016 (114)

Figure 18. Calcium (Ca^{2+}) exchange at endoplasmic reticulum membrane contact sites. Ca^{2+} concentration [Ca^{2+}] in different organelles is presented.

AIM OF THE PROJECT

EGFR internalization via NCE is essential for receptor degradation in the presence of high EGF concentrations, safeguarding cells against excessive EGFR signaling. Since NCE appears to be a crucial negative regulator of EGFR signaling in response to excessive stimulus, we hypothesized that loss of this route could lead to aberrant EGFR signaling in cancer and that NCE could therefore be a novel tumor suppressor pathway.

The aim of this thesis was to define the molecular mechanisms underlying EGFR-NCE by combining a candidate gene approach with an unbiased proteomic approach. Through high-resolution studies, we established that the EGFR-NCE pathway is distinct from other previously described clathrin-independent endocytic routes. We performed a proteomic analysis of NCE vesicles to identify NCE-specific regulators, and identified nine proteins with no previously defined role in endocytosis, four of which are ER proteins. Further investigation of one of these ER proteins, Reticulon 3 (RTN3), which is involved in the ER tubulation pathway, revealed that this protein is located in close proximity to active EGFR that internalizes via NCE, suggesting the existence of contact sites between the ER and the PM at sites of NCE. Thus, we set out to characterize the precise molecular mechanisms governing EGFR-NCE, taking advantage of RTN3 as a molecular tool, to elucidate the role of RTN3 in the crosstalk between the ER and the PM.

Considering the regulatory role of EGFR-NCE, the definition of its molecular mechanism should provide insights into unexplored mechanisms of EGFR overactivation in cancer and could lead to the identification of novel cancer-relevant endocytic proteins that might represent useful tumor biomarkers or targets for therapeutic intervention.

RESULTS

1. Functional characterization of EGFR-NCE

In order to characterize the EGFR-NCE pathway, we initially exploited a candidate gene approach, selecting players that have been described to have a fundamental role in clathrin-independent endocytic routes.

We analyzed the effect of Rac1 and Rac2, two GTPases involved in macropinocytosis; Cdc42 and GRAF1, two players mainly involved in the CLIC-GEEK pathway; RhoA, involved in IL-2Rβ endocytosis, among others; Arf6, involved in the internalization of different non-clathrin endocytic cargoes like MHCI and MHCII (see "Introduction" for a more detailed description of these endocytic routes). To define the possible role of these players in EGFR-NCE, we followed EGFR internalization with iodinated ^{125}I-EGF in HeLa cells upon knockdown (KD) of the candidate genes alone or in combination with clathrin KD.

We assessed first EGF internalization upon clathrin and dynamin KD. Stimulation of HeLa cells with low dose of EGF (1 ng/ml) showed that ~75% of the ligand is internalized through CME, as represented by the inhibition of internalization upon clathrin KD or dynamin KD; the residual endocytosis could be due to an incomplete KD or due to the existence of a third pathway of internalization that is insensitive to clathrin/dynamin depletion, possibly representing the constitutive pathway of EGFR endocytosis (111). At high dose of EGF (30 ng/ml), clathrin KD reduced the internalization only ~50%, while dynamin KD reduced the internalization ~80%; indicating that in these conditions clathrin KD is not sufficient for blocking EGF internalization due to an active NCE. Then, we assessed the role of the factors described above, both at high and low dose of EGF, in order to clarify whether they may have a specific role in EGFR-NCE. At high dose of EGF, Cdc42 KD and Rac 1/2 KD reduced EGF internalization ~20-50%. When the KD was combined with clathrin KD, we observed a

further reduction of ~80% of EGF internalization (Figure 19a, left). These results indicate that Cdc42 and Rac 1/2 may be involved in EGFR-NCE. However, their role is not exclusive to this pathway as their KD blocks EGFR internalization also at low dose of EGF when NCE is not activated (Figure 19a, right). Note that Cdc42 KD and Rac 1/2 KD reduced EGFR internalization at low dose of EGF also when the KD was combined with clathrin KD, suggesting a more general role for these players in EGFR endocytosis, possibly also in the constitutive endocytosis of EGFR (Figure 19a, right). We did not score any significant effect on EGFR endocytosis upon KD of GRAF1 (Figure 19b), Arf6, RhoA and caveolin-1 (Figure 19c) upon stimulation with high or low dose of EGF. The results obtained with caveolin-1 KD support our previous data that caveolin-1 KD does not affect EGFR degradation and signaling (63).

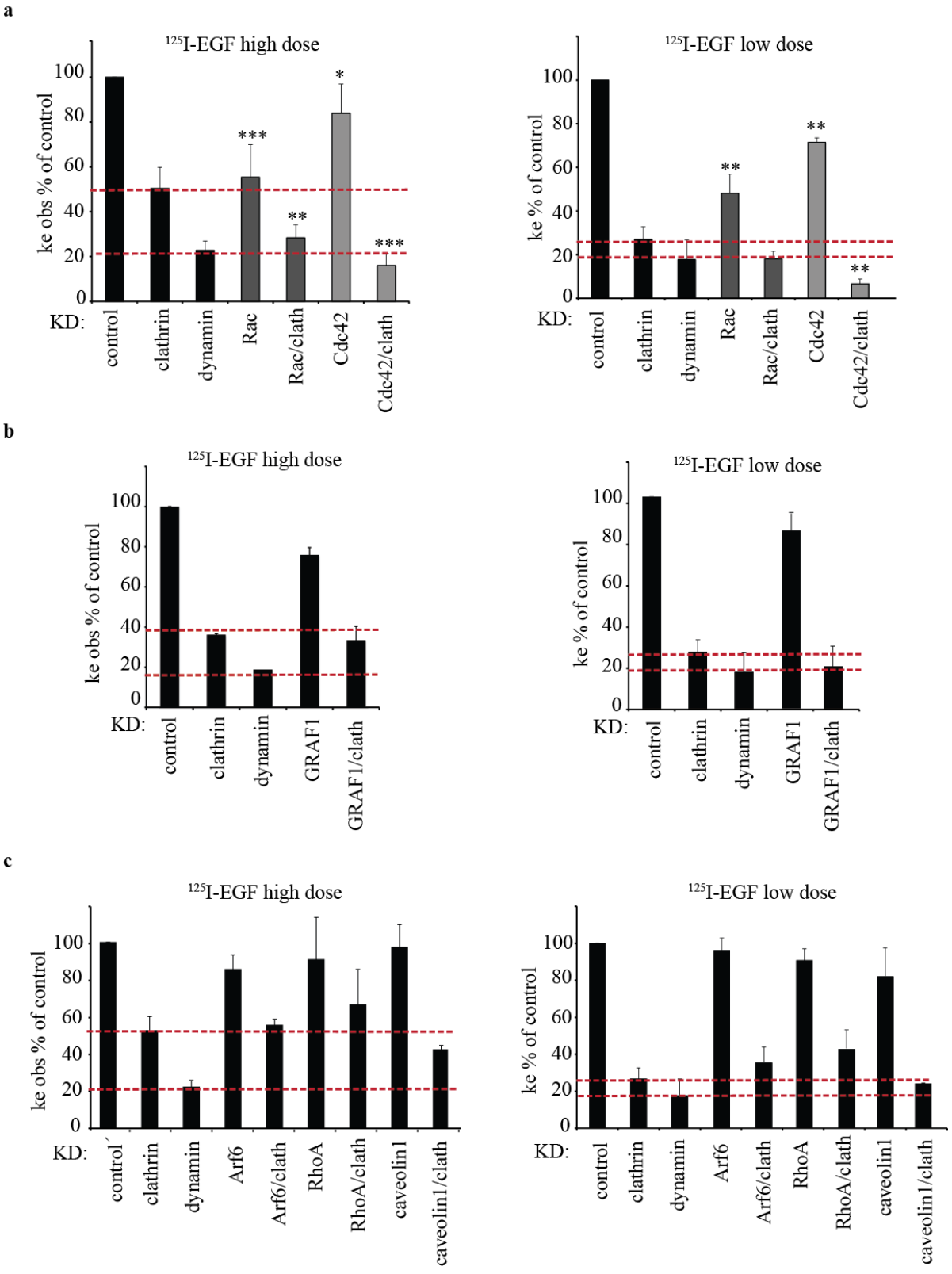

Figure 19. ^{125}I-EGF internalization assays upon candidate gene ablation.

a), **b)** and **c)** HeLa cells were transiently KD for the indicated proteins. Internalization constants (Ke) are plotted in the chart as % internalization compared to the control. High dose internalization rates (Ke obs) are plotted in the chart as % of the control. Red lines indicate the effect of clathrin KD and dynamin KD on ^{125}I-EGF internalization.

1.1 EGFR-NCE is independent of endophilins

The FEME pathway, a recently described novel clathrin-independent pathway, requires endophilin A proteins. This endocytic route is involved in the internalization of many PM receptors, including the EGFR, specifically in migrating cells (see also section 1.4.6, Introduction). Thus, we tested the possible involvement of endophilin A (EndoA) in EGFR-NCE.

We initially tested the expression levels of the three endophilin A genes (A1, A2 and A3) in our HeLa cells by RT-QPCR analysis. We found that only endophilin A1 and endophilin A2 were expressed in our cells. Importantly, the KD of endophilin A1 and endophilin A2 did not have any significant impact on EGFR endocytosis, neither at low nor at high dose of EGF (Figure 20a,b). The combination of endophilin A1 and endophilin A2 KD with clathrin KD did not have any additive effect, suggesting that EGFR-NCE is functionally distinct from the FEME pathway (Figure 20a,b), at least in the model under scrutiny.

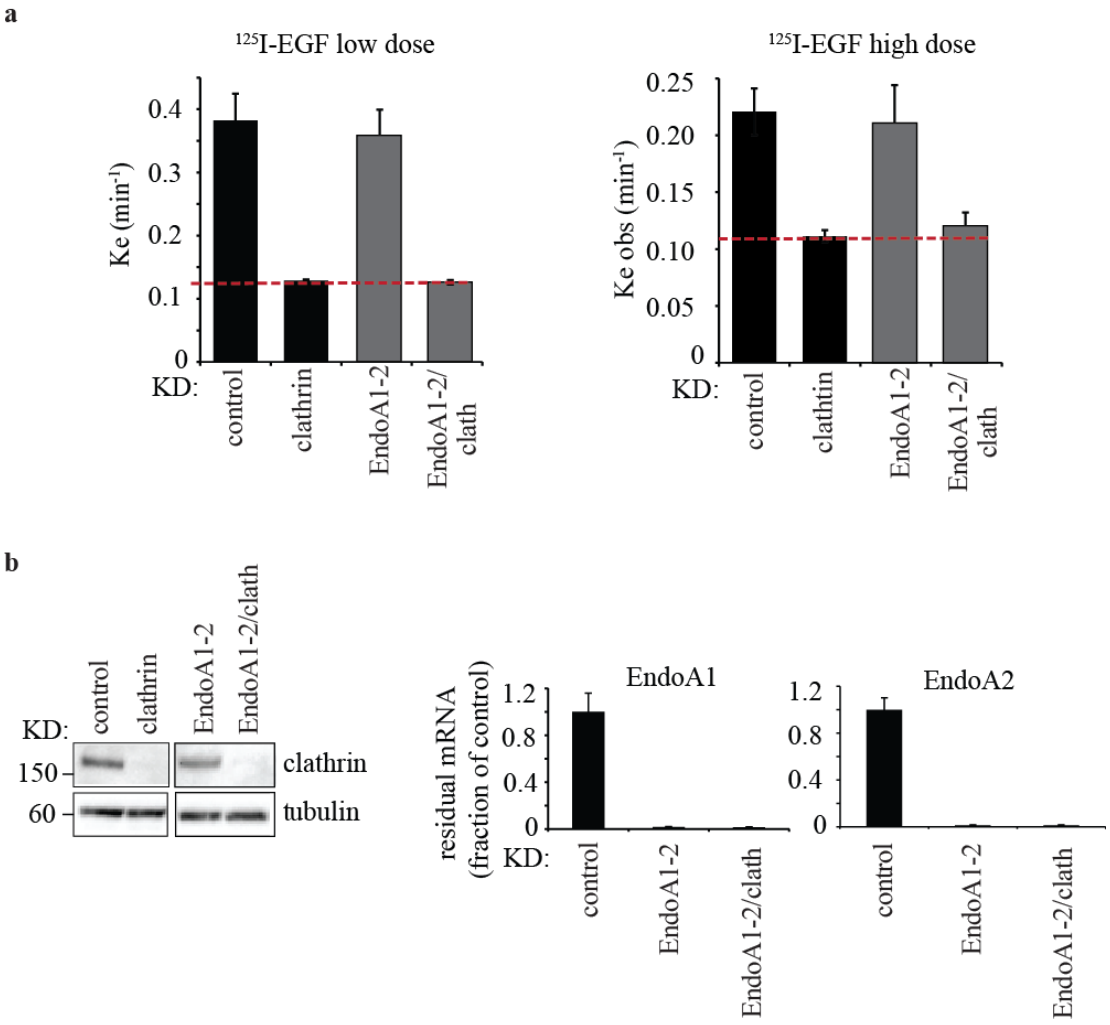

Figure 20. EGFR-NCE and endophilins.

a) Low (1 ng/ml, left) and high (30 ng/ml, right) internalization assay in control and clathrin KD cells for endophilin A1/2 (grey bars). Controls are in black. Red lines indicate the effect of clathrin KD on ^{125}I-EGF internalization.

b) Left: efficiency of clathrin KD in the indicated samples was determined by IB. Tubulin was used as loading control. Right: efficiency of endophilins KD in the indicated samples was determined by RT-QPCR and is represented as residual mRNA as a fraction of the control.

2. Molecular dissection of EGFR-NCE

2.1 Unbiased proteomic approach to identify specific EGFR-NCE components

Given the results above, we hypothesized that there might be unidentified, specific regulators of the EGFR-NCE pathway. To address this point, an unbiased approach was previously developed in our laboratory, based on the purification of NCE-EGFR vesicles in clathrin KD cells and on a quantitative mass spectrometry analysis using SILAC (Stable Isotope Labeling with Amino Acids in Cell Culture (133). From this analysis, we derived a list of 101 NCE candidates that were enriched in NCE-vesicles.

2.2 Validation of the involvement of SILAC candidates in NCE

To test the involvement of these candidates on EGFR-NCE, we performed KD of each single gene alone or in combination with clathrin and assessed its impact on EGFR internalization both at high (both CME and NCE are active) and at low dose of EGF (only CME is active) by ^{125}I-EGF internalization assays. We also evaluated the possible effect of the candidate genes on EGFR surface number, as alterations in receptor number might affect the internalization rate of EGFR. To exclude the involvement of candidate genes in CME, we assessed if their ablation could have an impact also on Tf internalization, which occurs only through CME. The rationale for this screening is presented in Figure 21.

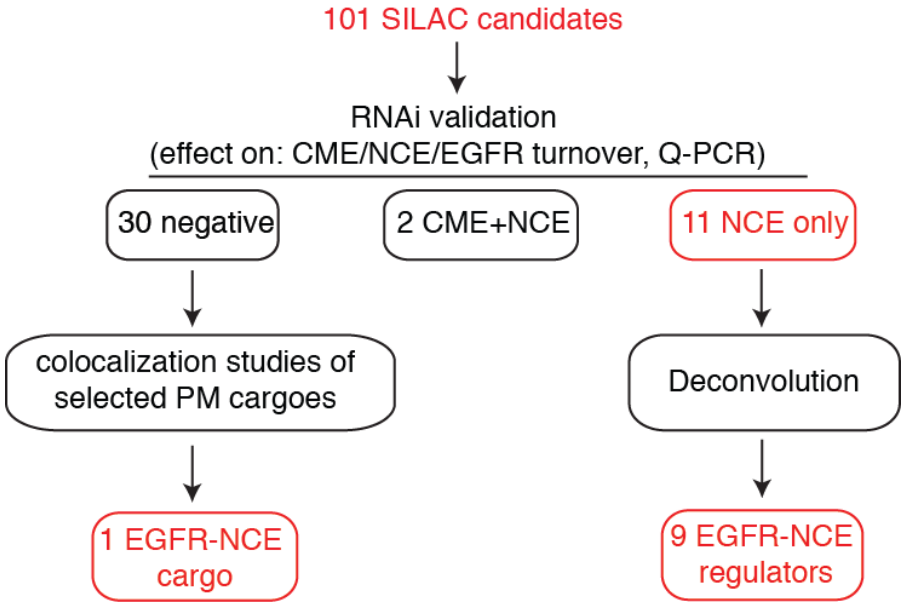

Figure 21. Flowchart of the unbiased screening and the validation procedure of NCE candidate genes.

The 101 NCE candidates were selected from the SILAC list. The expression of these candidates was ablated, with a pool of four oligos, alone or in combination with clathrin KD, and the effect of the KD was assessed in ^{125}I-EGF internalization assays at low and high dose of ligand. Also EGFR turnover was assessed. Deconvolution analysis resulted in the identification of 9 genes as regulators of NCE. The genes that scored "negative" in the initial round of validation were further analyzed and characterized by colocalization studies with internalized EGF, leading to the identification of a specific NCE cargo (see section 2.3).

Nine bona-fide EGFR-NCE regulators were identified. These players have different functions, are involved in signal transduction, RNA-binding or are ER and mitochondrial proteins; none of them has previously been involved in endocytosis. Importantly, these proteins are found associated with NCE vesicles and their ablation specifically blocks EGFR-NCE but has no effect on CME. These EGFR-NCE regulators and their involvement in EGFR internalization are listed in Table 4.

		EGFR Ke reduction (%) in high EGF	
Gene	**Localization/ function**	**Gene KD**	**Gene KD + clath. KD**
RTN3	ER membrane	42	68
REEP5	ER membrane	33	68
P4HB	ER enzyme	28	69
PLOD1	ER enzyme	50	71
ECHS1	Mito. enzyme	16	72
LRPPRC	Mito/RNA bind.	24	71
KHDRBS1	RNA bind/sign.	16	65
ZFR	RNA bind/Zn fin.	22	70
TPR	nuclear export	15	68
dynamin	CME + NCE	80	80
clathrin	CME	50	-

Table 4. NCE functional regulators.

The nine regulators of EGFR-NCE with their gene names and putative localization/function are presented in the table. For EGFR internalization, results are expressed as a reduction of the Ke of internalization compared to control (high dose of ligand). The effect of genes ablation alone or in combination with clathrin KD is reported. Mito: mitochondrial, bind: binding, sign: signaling, fin: finger.

2.3 Subcellular localization of the non-regulatory protein CD147

In the initial list of 101 proteins, there were a number of PM-resident proteins, whose ablation did not alter EGFR-NCE, that might represent cargoes of this internalization pathway. Among these, we analyzed in detail the matrix metalloproteinase inducer CD147/BSG. Considering the regulatory role of EGFR-NCE, we focused on CD147 known to be a tumor-associated antigen highly expressed on the surface of diverse tumors, analyzing in detail its subcellular localization and co-trafficking with the EGFR.

To this aim, HeLa cells were stimulated with high dose of Alexa555-labelled EGF for 2 and 8 minutes, fixed and stained for immunofluorescence (IF) analysis with anti-CD147 antibody. We found that in non-stimulated cells, CD147 was mainly localized at the PM. Stimulation with EGF for 2 minutes, instead, resulted in the internalization and colocalization of EGF and CD147. The colocalization of EGF and CD147 was even more clear in cells stimulated for 8 minutes with EGF. These results indicate a possible co-trafficking of CD147 with activated EGFR (Figure 22, upper panel). Note that a strong CD147 signal at the PM was present also upon EGF stimulation. CD147 internalization and colocalization with internalized EGF was scored also in clathrin KD cells (Figure 22, lower panel), suggesting that the co-trafficking may occur through NCE and that it may represent a good tool in the validation of this pathway.

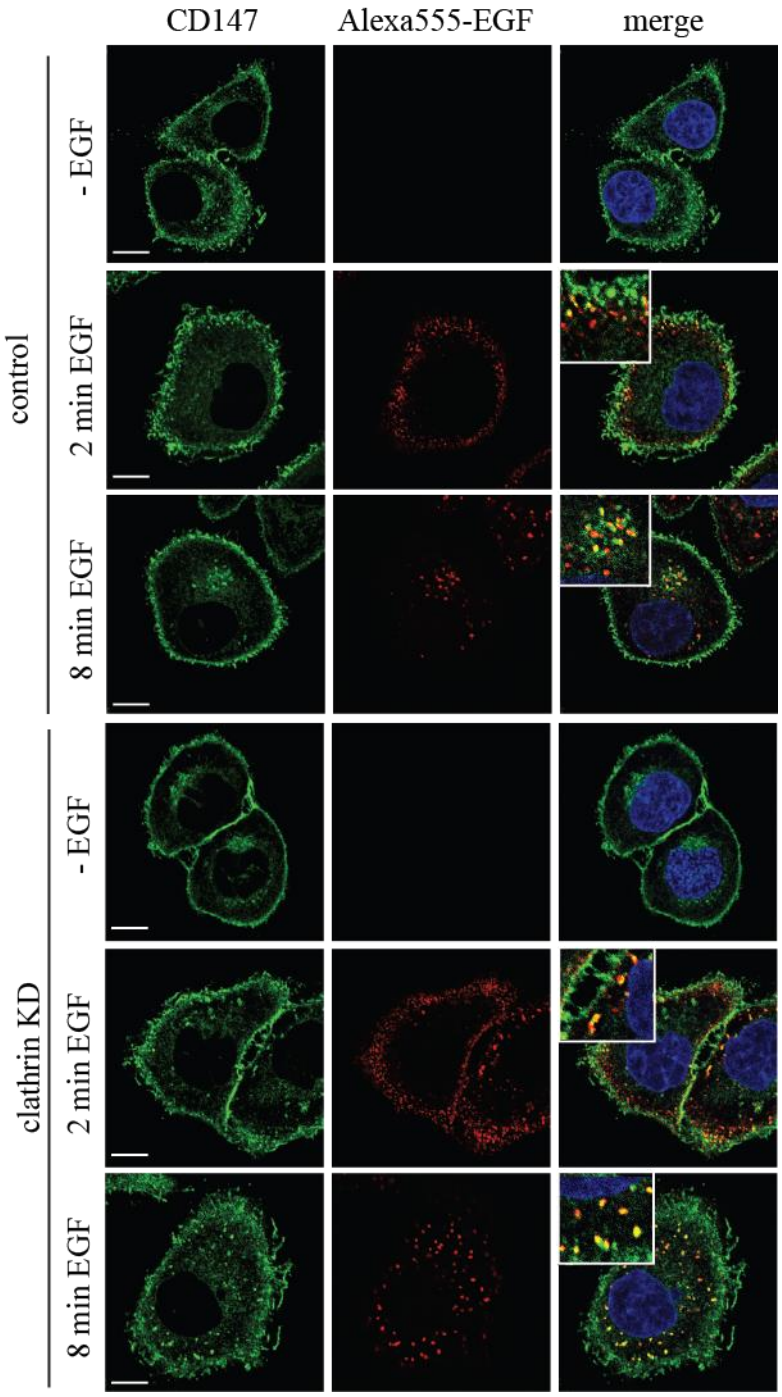

Figure 22. CD147 internalization together with EGF.

The localization of CD147 (green) in control or clathrin KD cells, in unstimulated or stimulated cells with Alexa555-EGF (red) for 2 or 8 minutes. DAPI (blue). Inserts highlight colocalization (yellow) between EGF and CD147. Scale bar, 10 μm.

2.4 Cross validation of NCE regulators and the CD147 cargo protein

In order to further validate CD147 as a NCE cargo and, at the same time, to reinforce the role of the identified NCE regulators, we decided to test the impact of their ablation on CD147 internalization. Given that the majority of CD147 remains at the PM and that only a small percentage of the protein is internalized upon EGF stimulation (see Figure 22), we set up a protocol to distinguish between PM CD147 and the internalized counterpart (45). In detail, to specifically follow the internalized CD147, we labeled cells *in vivo* with an antibody that recognizes the extracellular domain of the protein without interfering with its endocytosis (45), followed by stimulation with Alexa-conjugated EGF and fixation. To saturate the signal coming from CD147 at the PM, we proceeded with a first staining of the antibody at the PM without any permeabilization (Figure 23, magenta), after which we proceeded with a classical IF protocol, permeabilizing the cells and using a different secondary antibody for staining of CD147 (Figure 23, green). This second staining colors the internalized counterpart and the non-saturated CD147 at the PM.

With this procedure, we confirmed the co-internalization of CD147 with EGF (Figure 23), and found that the KD of all 9 identified regulators affected CD147 endocytosis, while EGF was still internalized, presumably through CME. Figure 23 shows representative data obtained from this analysis. Table 5 summarizes the quantitation of the inhibition of CD147 internalization induced by the KD of each candidate. This analysis allowed us to cross validate the cargo and the regulators, and to demonstrate that CD147 represents a specific marker for NCE as ablation of the identified NCE regulators is able to impair its internalization upon EGF stimulation.

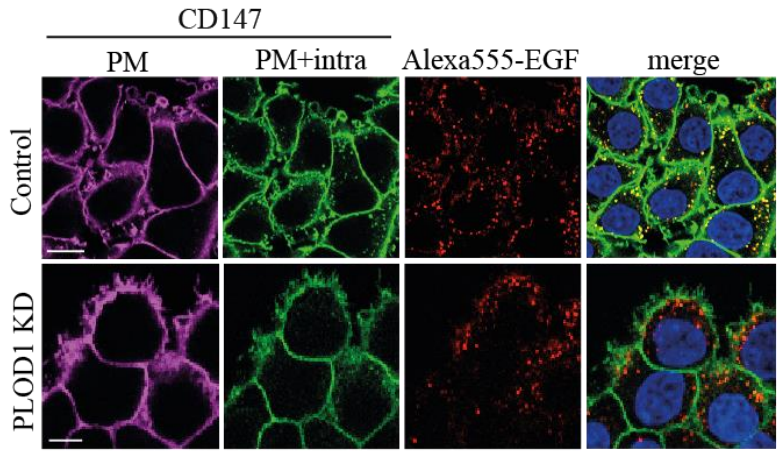

Figure 23. **CD147 internalization.**

CD147 internalization was followed in control cells or in PLOD1 KD cells with a specific antibody. Cells were stimulated with high dose of Alexa555-EGF for 8 minutes (red). PM CD147 staining was performed before cell permeabilization (magenta, PM CD147). After cell permeabilization, staining of residual PM and intracellular CD147 (green, PM+intra CD147) was performed. Blue, DAPI. Scale bar, 10 μm.

		CD147 inhib. (% of cells)
Gene	**Localization/ function**	**Gene KD**
RTN3	ER membrane	80
REEP5	ER membrane	50
P4HB	ER enzyme	45
PLOD1	ER enzyme	72
ECHS1	Mito. enzyme	50
LRPPRC	Mito/RNA bind.	45
KHDRBS1	RNA bind/sign.	52
ZFR	RNA bind/Zn fin.	67
TPR	nuclear export	67
dynamin	CME + NCE	80
clathrin	CME	10

Table 5. The effect of NCE regulators on CD147 internalization.

The percentage of cells in which CD147 internalization was blocked upon the KD of indicated genes is reported. At least 100 cells were counted in each condition. Dynamin (CME and NCE) and clathrin (CME only) are reported as controls.

3. RTN3 has a pivotal role in NCE

Four out of nine NCE-functional regulators are ER proteins (see Table 4 and 5). We focused our efforts on analyzing reticulon 3 (RTN3), which showed one of the strongest phenotypes on EGFR and CD147 endocytosis (Table 4 and Table 5). RTN3 is an ER tubulation factor and belongs to the reticulon protein family (134). Interestingly, another reticulon family member, REEP5, that is involved in ER tubulation as well, is also present in our list of NCE regulators.

3.1 RTN3 has specific effects on NCE

3.1.1 RTN3 KD but not RTN4 KD blocks EGF and CD147 entrance trough NCE

We performed ^{125}I-EGF internalization assays to test the effect of RTN3 KD on EGFR-NCE. RTN3 KD reduced EGF internalization by ~50% at high dose of EGf (Figure 24a), which is compatible with the amount of EGFRs entering via NCE (22). The double KD of RTN3 and clathrin reduced EGF internalization almost to the same levels observed under conditions of dynamin KD (Figure 24a), demonstrating the requirement of RTN3 for EGFR-NCE. On the contrary, RTN3 KD showed only a minor impact on EGFR internalization at low EGF dose (Figure 24b) and no effect on Tf internalization, which is known to occur only via CME (Figure 24c).

We then assessed the effect of REEP5 KD on EGFR internalization and found that it reduces EGFR-NCE (Figure 24a). However, REEP5 KD is less efficient and less reproducible than RTN3 KD, thus we decided to start analyze the effect of RTN3 ablation on EGFR-NCE to obtain more reliable results. RTN3 and REEP5 form a complex with another reticulon, RTN4. The RTN3/REEP5/RTN4 complex has been implicated in cortical ER tubulation (135,136). Although RTN4 was not enriched in our MS screening, we decided to verify the effect of its KD on EGFR and CD147 NCE as a test of specificity. We found that RTN4 KD

did not affect EGFR internalization, neither at low nor at high dose of EGF (Figure 24a,b), arguing for a specific function of RTN3, and REEP5, in NCE.

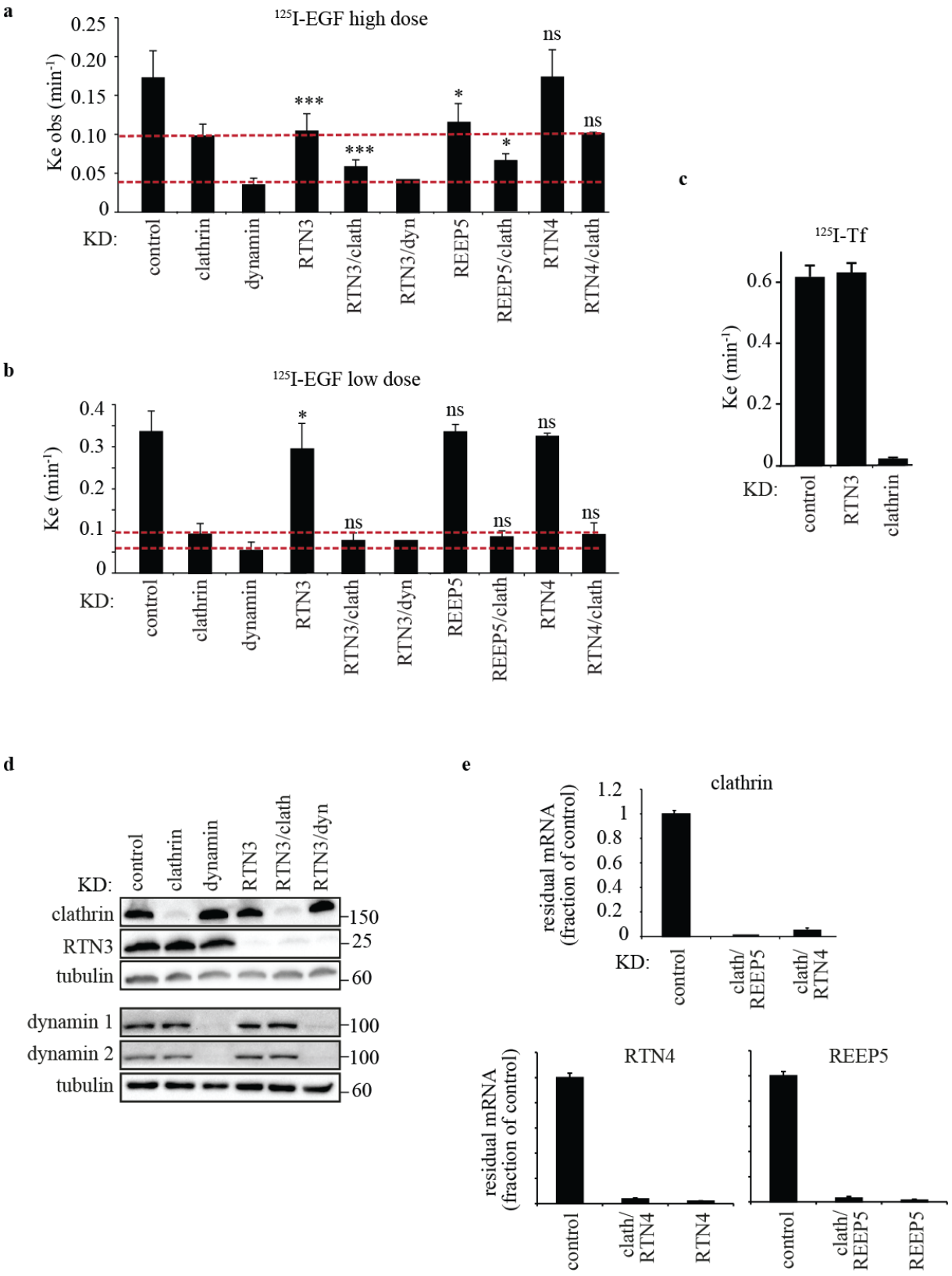

Figure 24. The effect of RTN3, REEP5 and RTN4 on EGFR-NCE.

a) and **b)** EGF internalization rate constants (Ke) at high (a) and low (b) dose of EGF in the indicated conditions.

c) Ke of ^{125}I-Tf internalization in the indicated conditions.

d) Efficiency of RTN3 KD alone or in combination with the indicated genes was assessed by IB. The samples were loaded on two parallel gels (top and bottom). Dynamin 1 was blotted on the same membrane of dynamin 2 after stripping and re-blotting.

e) Efficiency of RTN4 KD, REEP5 KD and clathrin KD was assessed by RT-qPCR. Residual mRNA expression in the KD samples was normalized using a housekeeping gene (GusB) and expressed as a fraction of the control.

The strong and specific effect of RTN3 *vs.* RTN4 on NCE was confirmed by exploiting CD147 internalization. CD147 internalization was assessed *in vivo* as described in section 2.4 by stimulating the cells with Alexa555-EGF for 8 minutes. CD147 and EGF internalization proceeded in clathrin KD cells (see also Figure 22) but CD147 was blocked upon RTN3 KD, showing that RTN3 is indeed required for NCE (Figure 25a,b). The double KD of clathrin and RTN3 resulted in the inhibition of both CD147 and EGF endocytosis (Figure 25a), suggesting a comprehensive impairment of both CME and NCE.

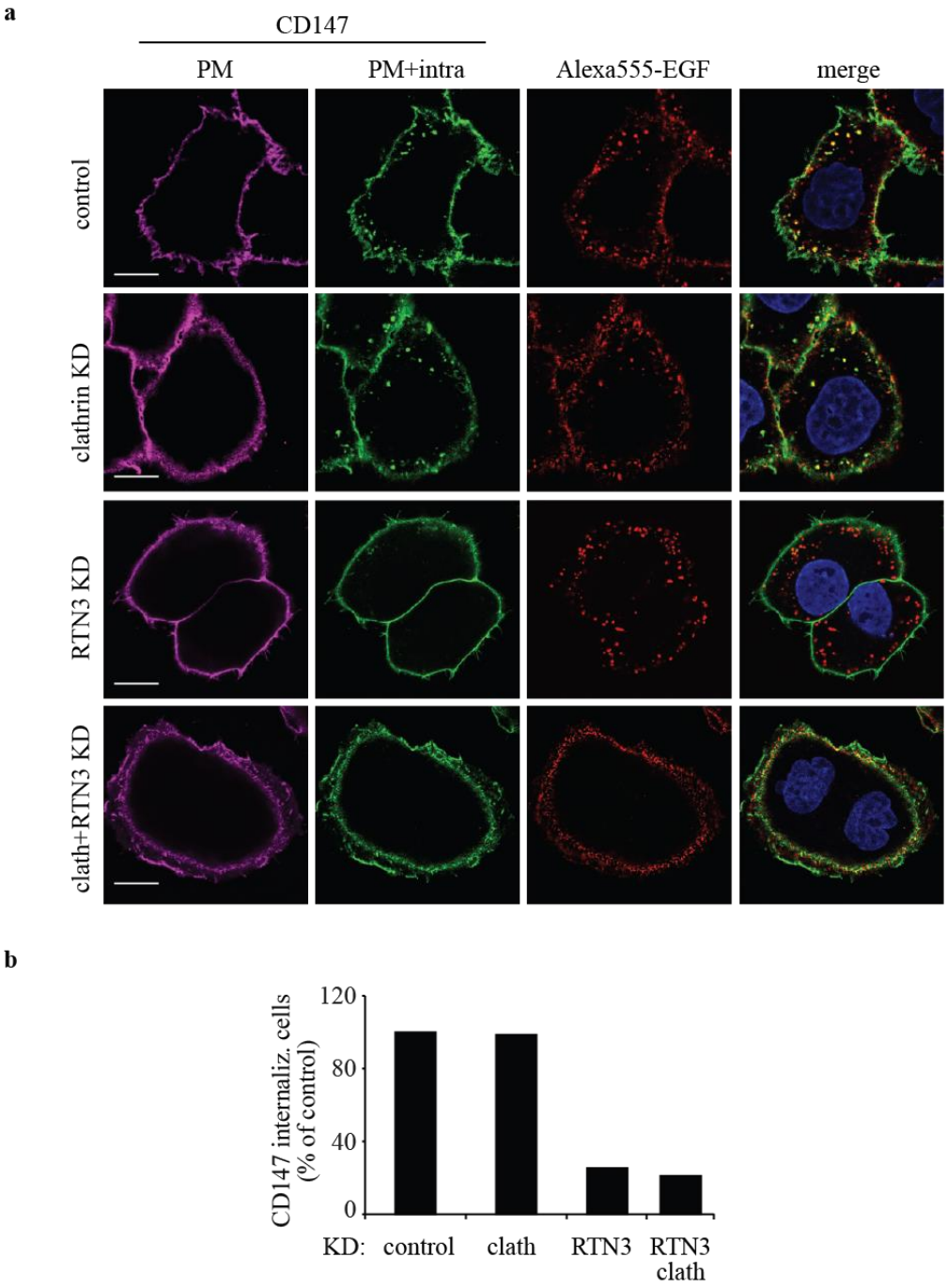

Figure 25. RTN3 KD affects NCE.

a) CD147 internalization was followed with a specific antibody in cells stimulated with high dose of Alexa555-EGF for 8 minutes (red) in the indicated conditions. PM CD147 staining was performed before cell permeabilization (magenta, PM CD147). After cell permeabilization, staining of residual PM and intracellular CD147 (intra) was performed (green, PM+intra CD147). Scale bar, 10 μm. Blue, DAPI.

b) Quantification of CD147 internalization in the indicated conditions, expressed as percentage of cells in which CD147 is internalized compared to the control.

We then tested also the effect of RTN4 ablation on CD147-NCE. RTN4 KD did not show any impairment of CD147 internalization (Figure 26a,b), confirming that it does not play a functional role in NCE. These results reinforce the relevance and specificity of RTN3 function in EGFR/CD147-NCE.

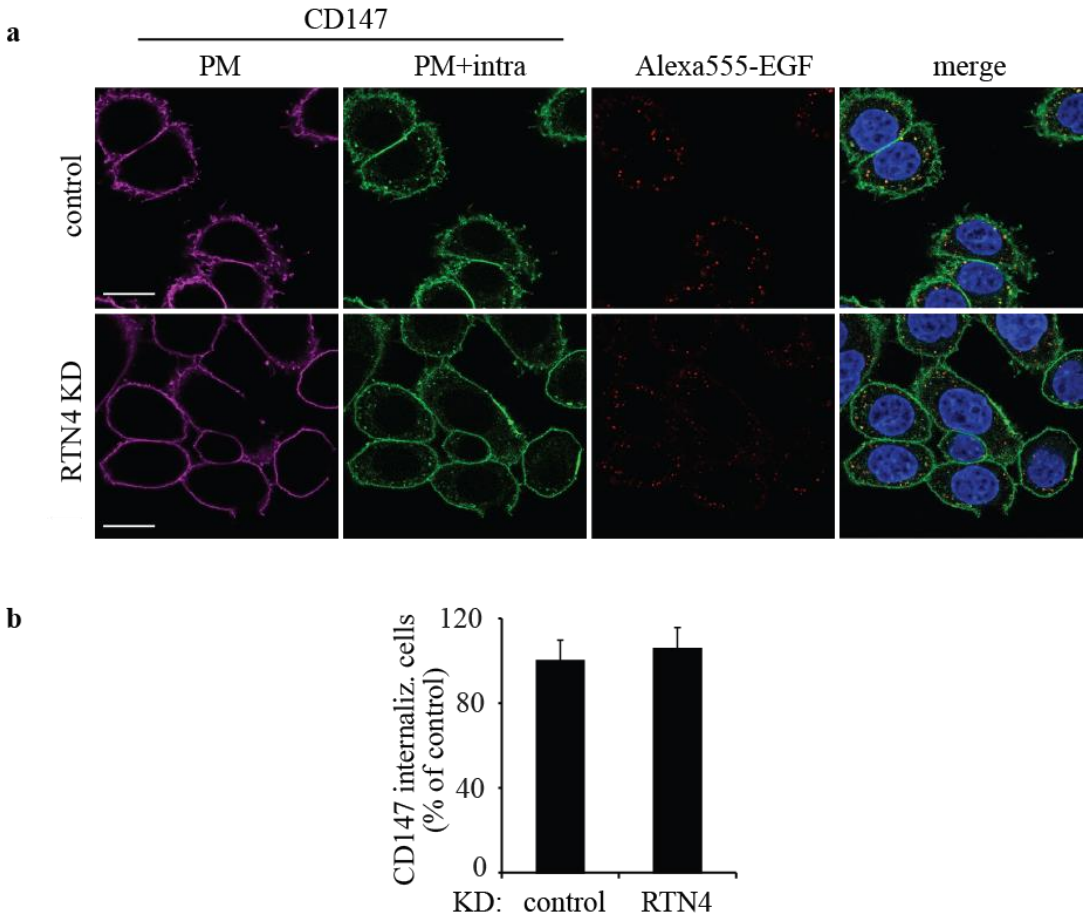

Figure 26. RTN4 does not affect CD147 NCE.

a) CD147 internalization was followed with a specific antibody in cells stimulated with high dose of Alexa555-EGF for 8 minutes (red) in control and RTN4 KD cells. PM CD147 staining was performed before cell permeabilization (magenta, PM CD147). After cell permeabilization, staining of residual PM and intracellular CD147 (intra) was performed (green, PM+intra CD147). Scale bar, 10 μm. Blue, DAPI.

b) Quantification of CD147 internalization in the indicated conditions, expressed as percentage of cells in which CD147 is internalized compared to the control.

3.1.2 Reintroduction of RTN3 restores EGFR and CD147 NCE

In order to test if the effect of RTN3 ablation on NCE was specific and not due to an unspecific effect of the RNAi, we performed reconstitution experiments. There are seven isoforms described for RTN3 (Figure 27a). We initially evaluated if the RTN3 isoforms are expressed in our cell system (HeLa cells) by RT-QPCR analysis. We designed specific primers in order to discriminate between the different RTN3 isoforms and found that the most expressed isoform was isoform A (Figure 27b). Therefore, we decided to introduce a siRNA resistant form of RTN3A in our HeLa cells: we generated a cDNA of RTN3A that was resistant to the RNAi oligo used for RTN3 KD by introducing 8 silent mutations in the region targeted by the siRNA oligo by site-directed mutagenesis. The cells were then infected with pBABE-RTN3A siRNA-resistant and a clone expressing the transgene at endogenous levels was selected (Figure 28a). We then assessed that the exogenous expression of RTN3 was not affected by RTN3 siRNA oligo (Figure 28a). We evaluated the reconstitution of NCE upon RTN3 KD by RTN3A expression, both in ^{125}I-EGF (Figure 28b) and CD147 internalization assays (Figure 28c). Results from both assays showed that the phenotype of EGFR and CD147 internalization was restored almost to wild-type (WT) levels by the reintroduction of RTN3A, indicating an almost complete rescue of the NCE pathway (Figure 28b,c). However, we cannot exclude that other isoforms may contribute to the NCE, possibly through oligomerization.

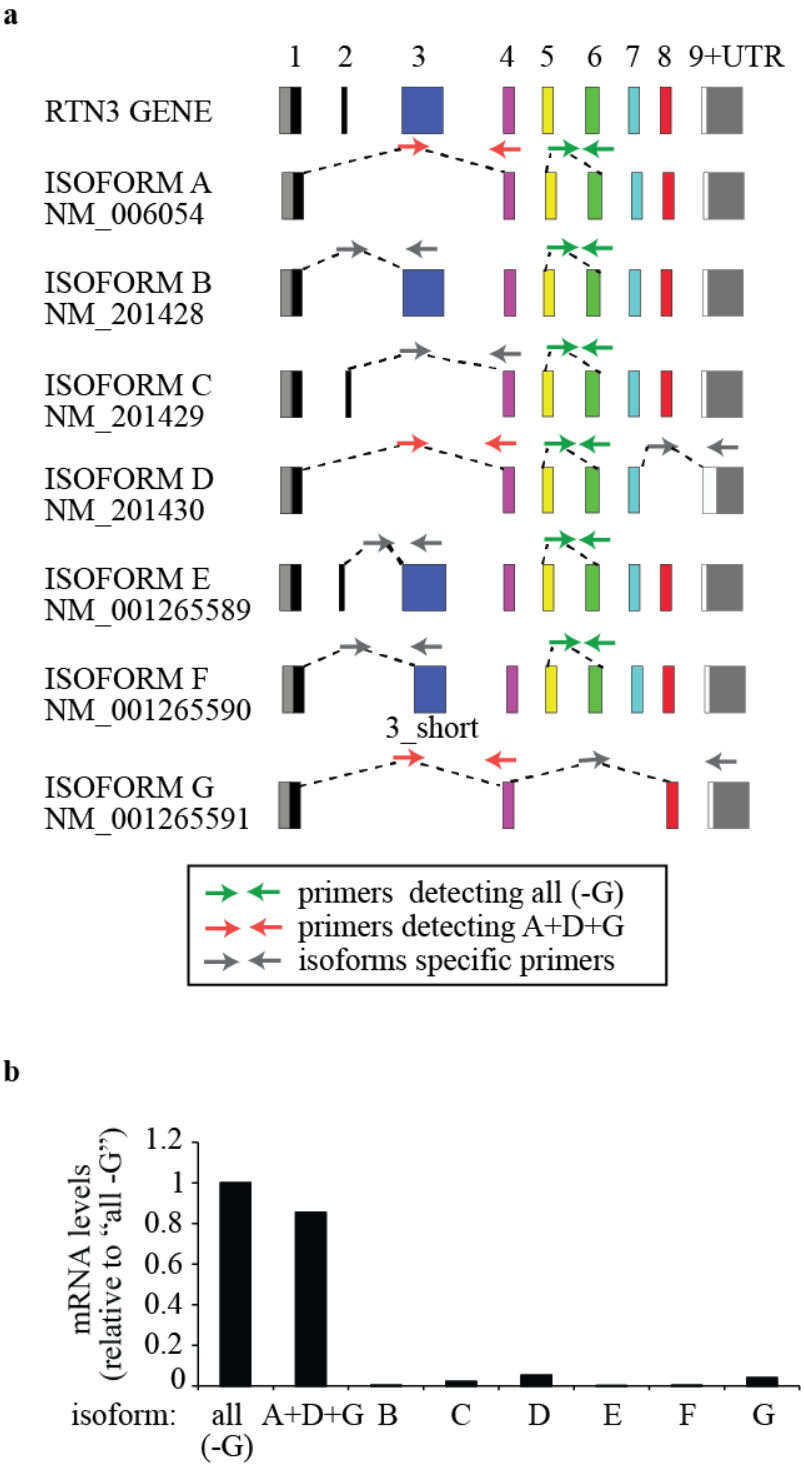

Figure 27. RTN3A isoforms.

a) A schematic representation of the RTN3 gene and its 7 isoforms. Left, isoform name and accession number. The different exons are labeled with different colors and the corresponding number is indicated on the top. Oligos used in the qPCR analysis are indicated with arrows in different colors: green arrows indicate primers recognizing all isoforms except for isoform G; gray arrows indicate isoform-specific primers; red arrows indicate primers recognizing isoforms A, D and G.

b) Relative mRNA expression levels of the indicated isoforms were assessed by qPCR analysis. The normalization was performed using a housekeeping gene (GAPDH), expressed as relative to levels detected with primers recognizing all isoforms (except for isoform G).

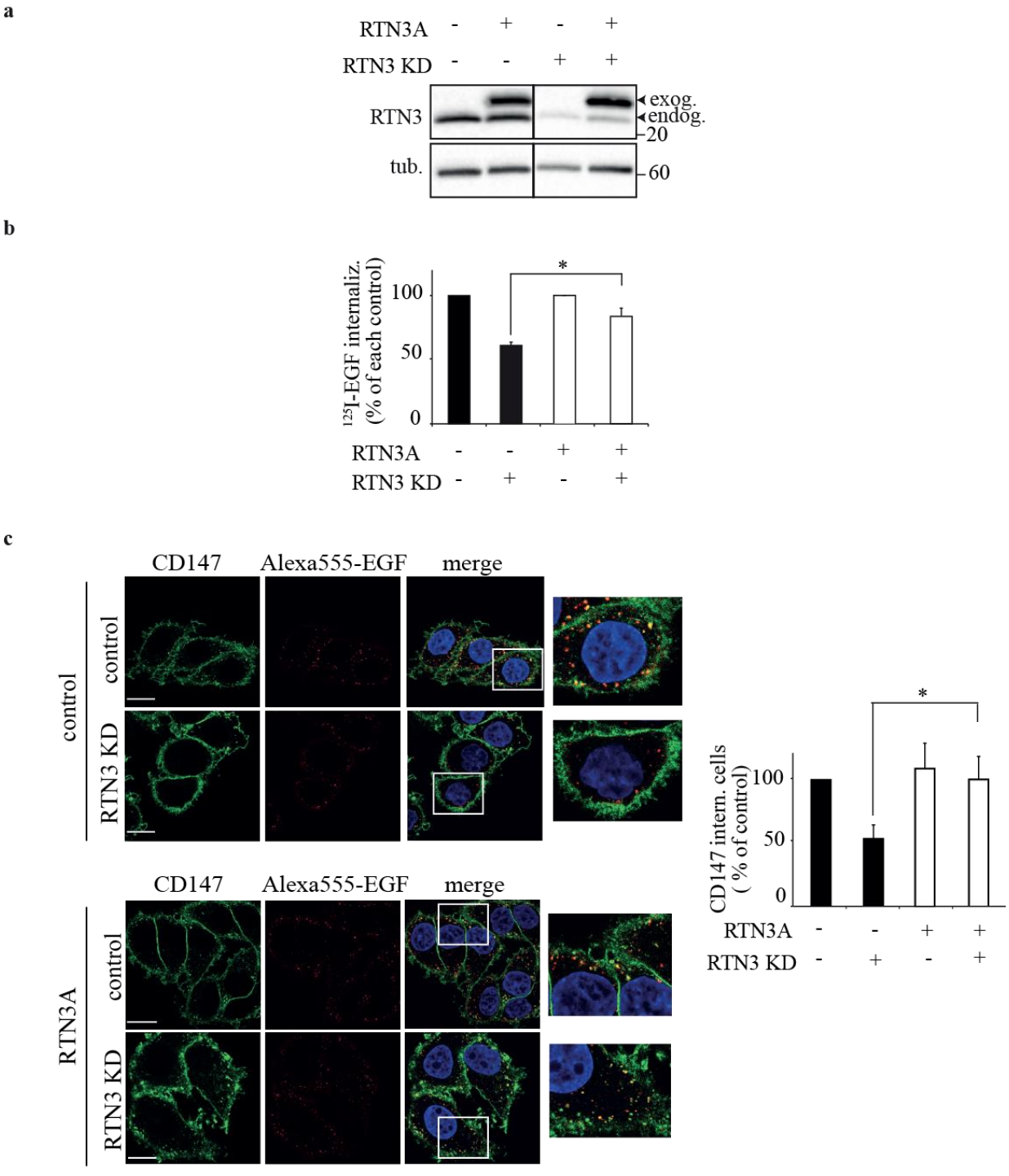

Figure 28. NCE restoration by exogenous RTN3A.

a) RNAi resistant Isoform A of RTN3 was expressed in HeLa cells at endogenous levels. RTN3 endogenous and exogenous levels (indicated by arrows) were analyzed by IB in the

indicated conditions. Tubulin was used as loading control. This panel was assembled from samples run on the same gel.

b) Internalization constants were measured by ^{125}I-EGF internalization at high dose of ligand upon RTN3 KD or in control samples. Data are presented as the mean of duplicates of three independent experiments ± SD and are normalized to each control clone. *, P-value <0.05.

c) CD147 internalization was followed *in vivo* as described in Figure 25 in the indicated conditions. Quantification of the percentage of CD147 internalizing cells in the different samples relative to control cells is indicated. Scale bar, 10 μm. Data are are presented as the mean of two independent experiments ± SD.

3.2 RTN3 ablation affects EGFR degradation and increases its recycling

We wanted to test the impact of RTN3 ablation also on the fate of internalized EGFR and analyzed the impact of RTN3 ablation on EGFR degradation. Considering that NCE destines the vast majority of internalized EGFR to degradation, impairment of the pathway should delay receptor degradation. We thus analyzed EGFR degradation in cells stimulated with high EGF doses (100 ng/ml) for increasing time points in order to follow EGFR degradation. Total EGFR levels were then detected by immunoblot (IB) analysis. In control cells, the receptor was almost completely degraded at 180 minutes post stimulation, while its degradation was delayed upon RTN3 KD (Figure 29a), thus confirming the role of RTN3 as a regulator of EGFR-NCE. These results were then confirmed in a more quantitative assay by following ^{125}I-EGF degradation in cells stimulated with high dose of EGF. By measuring, at increasing time points, the ratio of degraded ^{125}I-EGF compared with the total receptor, we observed a significant reduction in EGF degradation upon RTN3 KD (Figure 29b).

Based on these results, we hypothesize that the ablation of RTN3 may skew EGFR fate from a degradative to a recycling route. We thus followed EGFR recycling using ^{125}I-EGF and found that stimulation of RTN3 KD cells with high dose of EGF resulted in an increased recycling of EGFR (Figure 29c), suggesting that, in these conditions, only the CME pathway, which is mainly devoted to receptor recycling, is active.

a

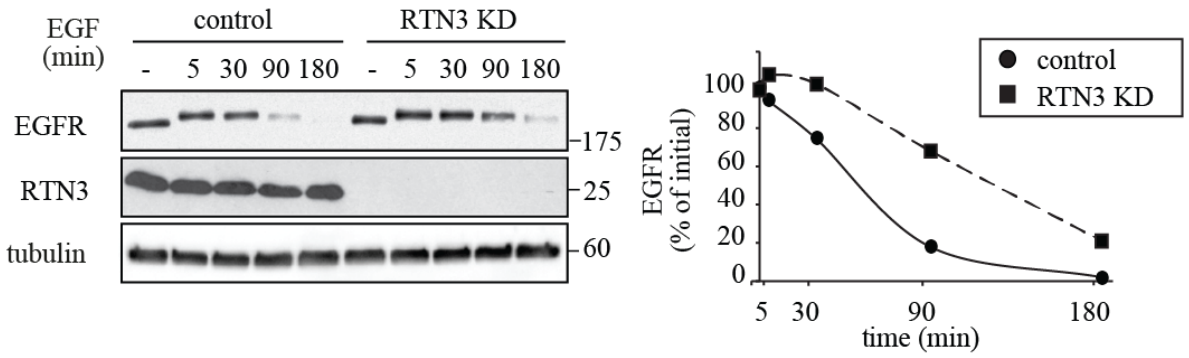

b

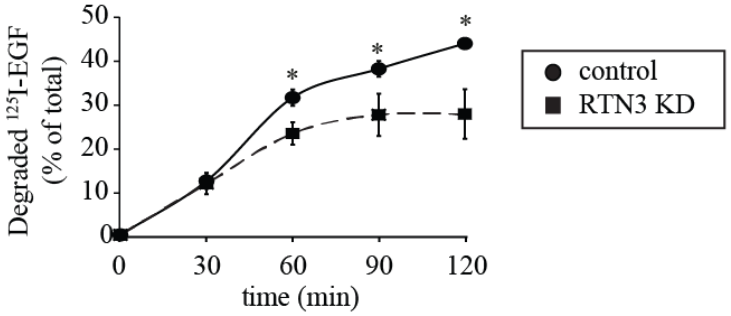

c

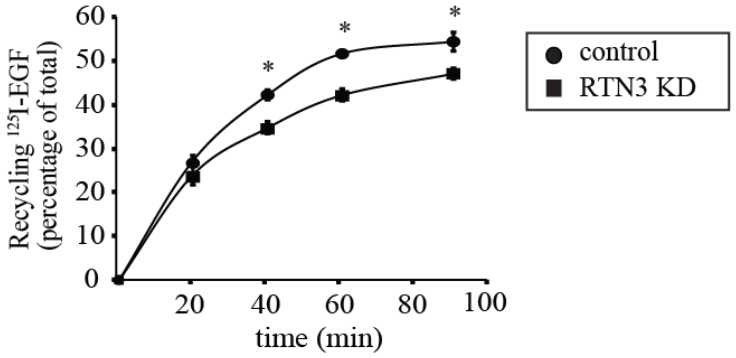

Figure 29. The effect of RTN3 ablation on EGFR degradation and recycling.

a) Left, EGFR degradation (EGF, 100 ng/ml) was analyzed in control and RTN3 KD cells. Right, densitometric quantification, expressed as the percentage of EGFR levels relative to the initial amount.

b) Quantitative ^{125}I-EGF degradation assay. Data are expressed as percentage of degraded EGF. *, $p < 0.05$ (*vs.* control).

c) Quantitative ^{125}I-EGF recycling assay. Data are expressed as percentage of recycled EGF. *, $p < 0.05$ (*vs.* control).

4. Contact sites between the ER and the PM are involved in EGFR-NCE

4.1 Identification of NCE intermediates

In order to obtain information about the morphology of EGFR-NCE structures, we used high-resolution electron microscopy (EM) technique in collaboration with Andrea Raimondi at the San Raffaele Institute, Milan.

We employed pre-embedding immunolabeling for labeling of EGFRs *in vivo* with an antibody that does not interfere with receptor endocytosis (22) and marked it for EM with gold protein A. We then followed receptor internalization after stimulation with high dose of EGF for 5 minutes and we marked the structures that were still connected with the PM with Ruthenium Red (RuR). In control cells, gold-labeled EGFR was detectable both in clathrin-coated pits (CCPs) and in tubular invaginations (TI, Figure 30a left). TIs persisted in clathrin KD cells (Figure 30a center), suggesting that they may represent the structures that mediate EGFR-NCE.

We also assessed whether the formation of EGFR internalizing structures is affected by RTN3 KD, and found that upon RTN3 KD TI structures where significantly reduced in number, suggesting that these are indeed NCE intermediates and that their formation/stabilization is RTN3-dependent (Figure 30b); while RTN3 KD had no effect on CCPs (Figure 30c).

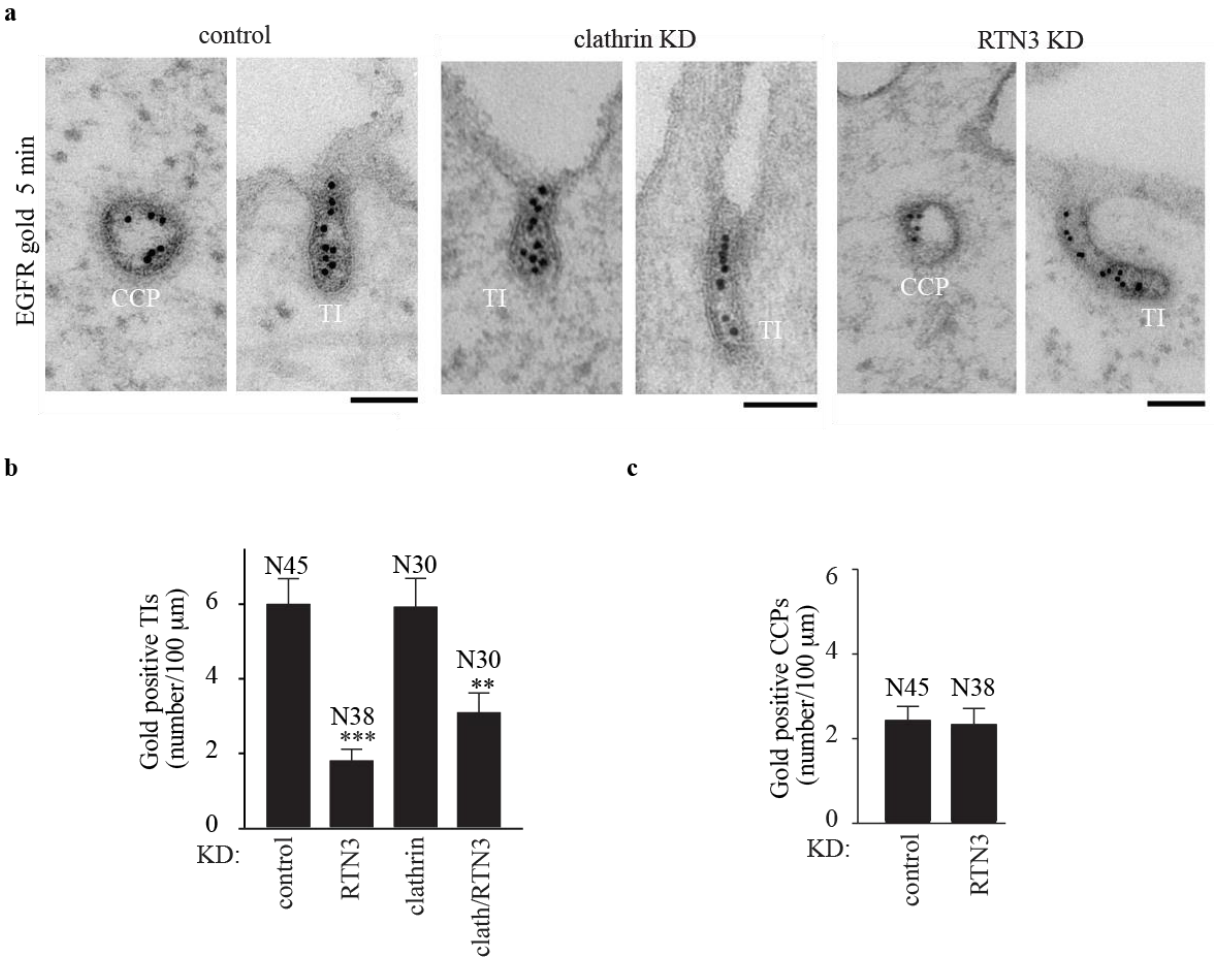

Figure 30. Characterization of EGFR-NCE by EM.

a) Representative images of EGFR endocytic structures upon stimulation with high dose EGF in the indicated conditions. Scale bar 100 nm.

b) and **c)** Quantification of gold-EGFR positive Tis and CCPs at 5 minutes of stimulation with high dose of EGF. Only RuR-stained structures were counted. N, number of cell profiles analyzed. Data are expressed as number of gold-positive structures normalized to PM profiles of 100 µm length. **, <0.01; ***, <0.001 (*vs*. control).

4.2 RTN3 is an ER-localized protein

To study the endogenous localization of RTN3, we produced a rabbit polyclonal antibody against amino acids (aa) 1-47, which are located in the N-terminal loop of RTN3 facing the cytosol (this region is common to all 7 RTN3 isoforms) and tested the specificity of its signal in IF analysis. We found that RTN3 showed the typical pattern of an ER protein and that the signal was significantly reduced upon RTN3 KD (Figure 31a).

To confirm the ER localization of RTN3, we tested the colocalization of endogenous RTN3 and the ER-resident protein Sec61β, expressed as a GFP-tagged chimera (Figure 31b top). We also co-transfected a tagged version of RTN3 together with the ER-localized protein ESYT1 (GFP-tagged) (137). We found that both RTN3 and ESYT1, showed a similar ER-pattern as both proteins were enriched in cortical ER (Figure 31b bottom). We also tested the localization of RTN3 upon EGF stimulation but did not score any clear changes in RTN3 localization by standard IF analysis except for a juxtaposition of cortical RTN3 signal and EGF (Figure 31b merge, enlargement).

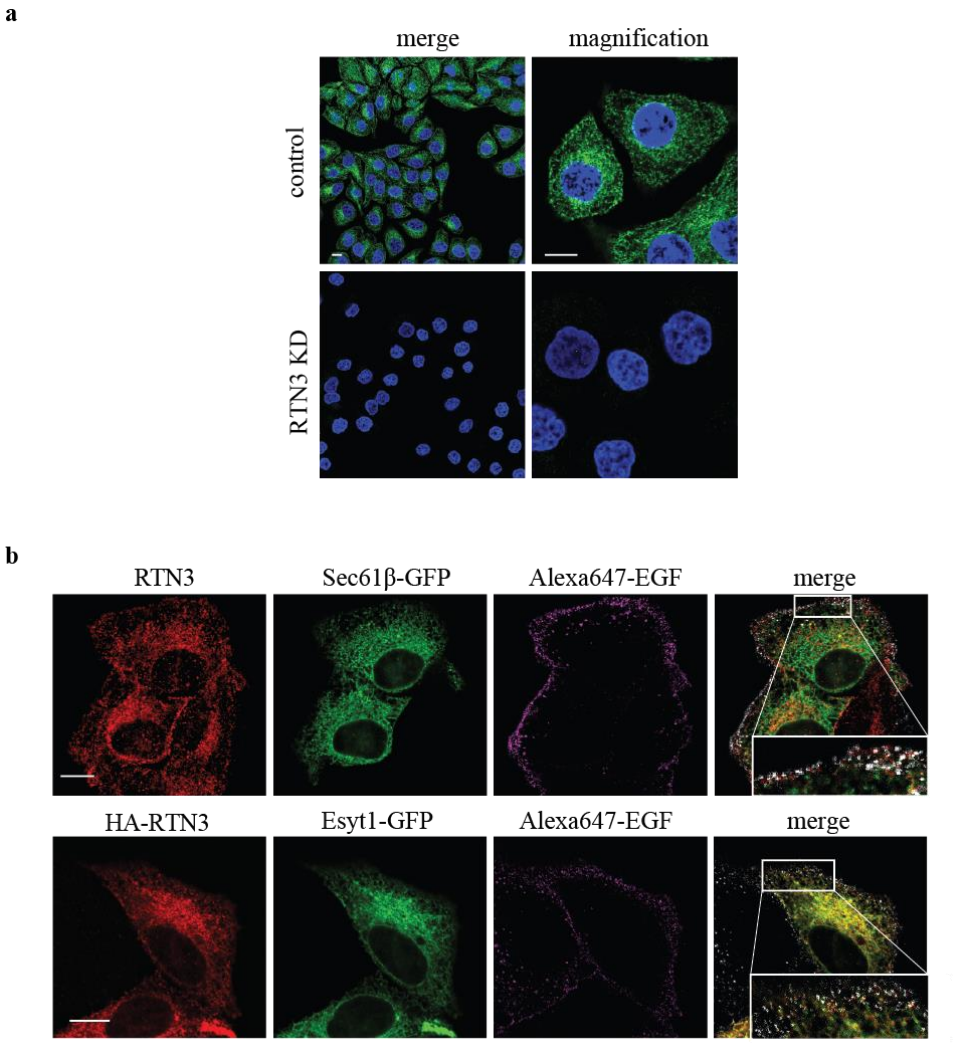

Figure 31. ER localization of RTN3.

a) Characterization of the specificity of an anti-RTN3 antibody by IF analysis in HeLa control and RTN3 KD cells. Scale bar, 10 μm. Blue, DAPI.

b) Upper panel, colocalization, of endogenous RTN3 (red) and the ER-resident protein Sec61β-GFP (green) in HeLa cells stimulated with high dose Alexa647-EGF (magenta) for 2 minutes. EGF Alexa647-EGF is shown as pseudocolored in grey (merge). Scale bar, 10 μm.
b) Lower panel, colocalization of HA-RTN3 (red) and the ER-resident protein Esyt1-GFP (green) in HeLa cells stimulated with high dose Alexa647-EGF (magenta) for 2 minutes. EGF Alexa647-EGF is shown as pseudocolored in grey (merge). Scale bar, 10 μm.

4.3 RTN3 and EGFR do not co-immunoprecipitate

In order to investigate whether RTN3 is recruited in complex with the EGFR upon activation, we undertook co-immunoprecipitation (co-IP) studies. Clathrin KD cells were stimulated or not with high dose of EGF and subjected to IP analysis. In parallel, we also performed IP for RTN3, both in clathrin KD cells and in clathrin KD cells ablated also for RTN3 as a control for specificity. No co-IP was scored between EGFR and RTN3 in any of the conditions tested (Figure 32a,b). This data indicates that EGFR and RTN3 do not stably interact upon EGF. Considering that the interaction between RTN3 and EGFR could be indirect and/or transient, we decided to perform an image-based analysis, see section 4.4.

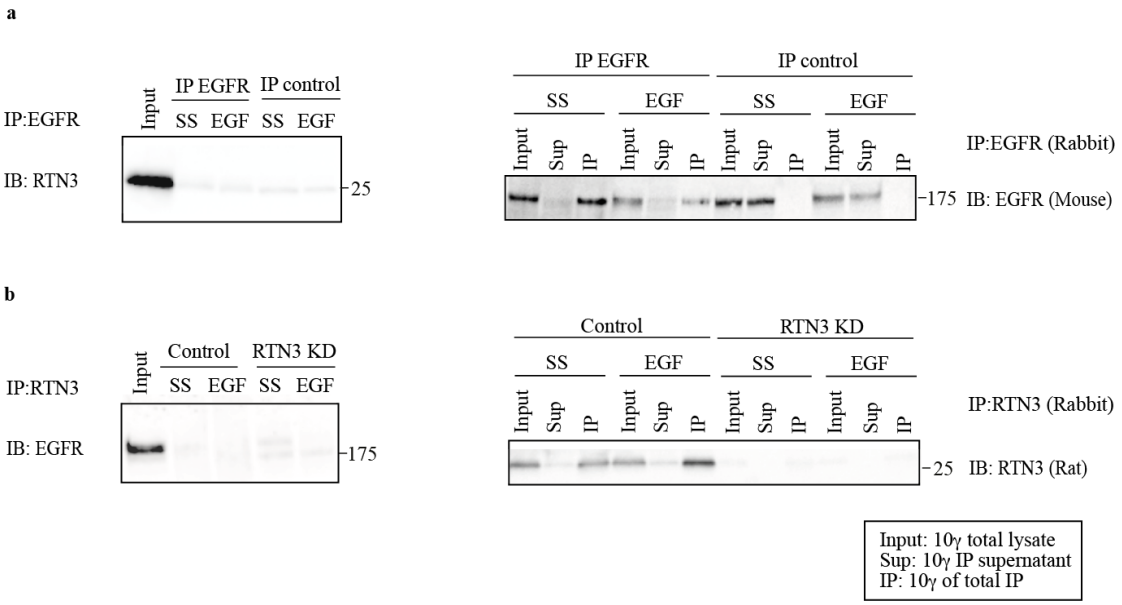

Figure 32. Immunoprecipitation of RTN3 and EGFR.

a) Left, clathrin KD cells were stimulated for 2 minutes with high dose of EGF or left unstimulated in the indicated conditions and subjected to IP with a specific EGFR antibody (mouse). Right, controls of the IP efficiency were loaded and revealed with an EGFR antibody (rabbit).

b) Left, clathrin KD cells were stimulated for 2 minutes with high dose of EGF or left unstimulated in the indicated conditions and subjected to IP with a RTN3 antibody (rabbit). Right, controls of the IP efficiency were loaded and revealed with a RTN3 antibody (rat).

4.4 RTN3 is localized in close proximity to active EGFR

4.4.1 Super resolution analysis to study signal clustering upon EGF stimulation

To define the relationship between RTN3 and activated EGFR, we decided to employ super-resolution microscopy and Förster resonance energy transfer (FRET) analysis due to the diffuse distribution of both RTN3 and EGFR. With the super-resolution microscopy technique it is possible to eliminate background signal coming from the presence of multiple fluorophores and to specifically localize the source of the signal. In particular, we took advantage of direct stochastic optical reconstruction microscopy (dStorm) (138) in

collaboration with Davide Mazza at the San Raffaele Institute, Milan. Cells were first incubated with an anti-EGFR antibody that does not alter its activation and endocytosis, and then stimulated with low or high dose of EGF for 2 minutes in order to follow the initial steps of endocytosis. Finally, cells were fixed and processed for IF by labeling EGFR with a secondary antibody (Cage550) that is specific for dStorm, and RTN3 with an Alexa-labeled (Alexa647) antibody that possesses the characteristics needed for this kind of microscopy (see Materials and Methods). The images of the channels of the two secondary antibodies were acquired and the list of detected molecules in the two channels was used to compute the cross-correlation of the two images as described in (139) as follows: the cross-correlation curve was fitted by an exponential decay to quantify the degree of colocalization between EGFR-Cage500 and RTN3-Alexa647 and the size of the co-clusters, respectively, provided by the cross-correlation amplitude C_0 and the correlation length R_c.

Upon EGF stimulation, we observed an increase in the proximity between the two signals (Figure 33a) quantified as co-clustering (C_0) and cluster size (R_c). Only localization events occurring at the periphery of the cell were considered. This EGF-induced increase was significantly greater in cells stimulated with high dose of EGF compared to cells stimulated with low dose of EGF (Figure 33b). The two parameters were not measurable for serum-starved cells. The increase in proximity induced by high EGF dose suggests that EGFR and RTN3 come into close proximity upon ligand stimulation.

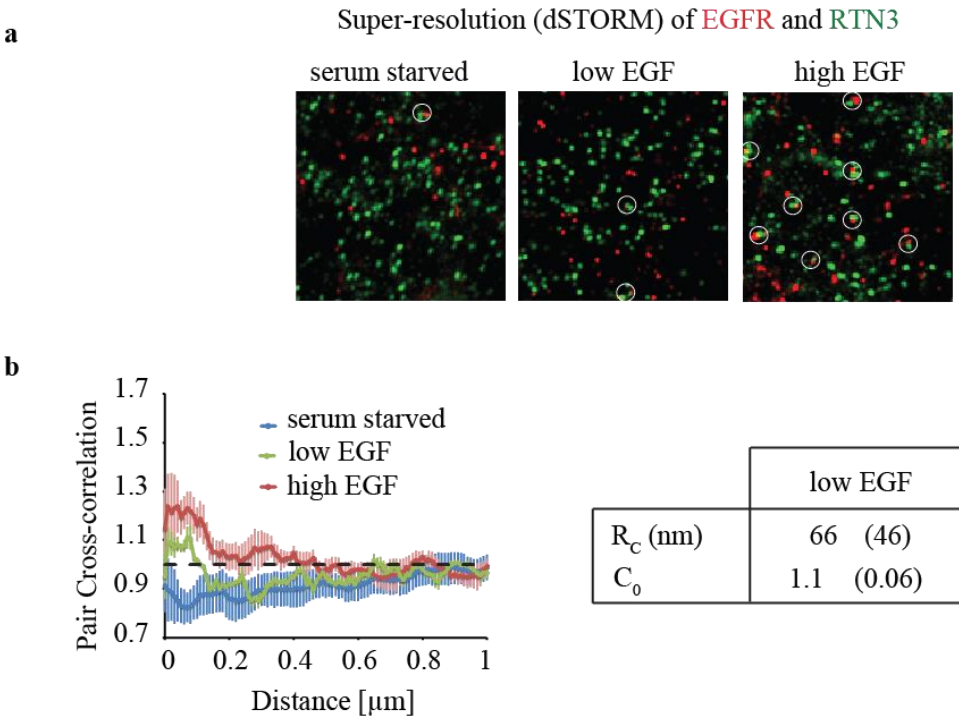

	low EGF	high EGF
R_C (nm)	66 (46)	205 (41)
C_0	1.1 (0.06)	1.25 (0.04)

Figure 33. EGF induced proximity between RTN3 and EGFR.

a) dSTORM of RTN3 (green) and EGFR (red). Representative images of HeLa cells in the indicated conditions (low EGF, 1 ng/ml; high 100 ng/ml). Scale bar, 0.7 µm.

b) Left, cross-correlation between the two channels as a function of distance (139). No significant cross-correlation of the signal was observed in serum-starved conditions, indicating negligible co-clustering of the two proteins and implying that the size of the co-clusters could not be estimated in these conditions. For EGF-induced samples, the cross-correlation curves were fit to an exponential decay, providing (right): i) the amplitude of the correlation (C_0) proportional to the fraction of co-clustered RTN3 and EGFR signals, and ii) the spatial extent of the cross-correlation curve (R_C), which is an estimate of the size of the co-clusters. Stimulation of cells with high dose of EGF resulted in increased R_C and C_0 *vs.* low dose of EGF. 95% confidence intervals (CI) are presented in parenthesis.

4.4.2 Live FRET to study of EGFR-RTN3 proximity kinetic

To kinetically follow the interaction between RTN3 and EGFR, prior and after EGF administration, we used live-FRET analysis, which allows the detection of transient/low affinity and indirect interactions with a resolution of 10-30 nm. To this aim, we transiently co-transfected cells with EGFR-YFP/RTN3-CFP and measured the basal FRET level and followed its kinetics for 5 minutes of EGF stimulation. A significant increase in maximal FRET was registered upon cell stimulation with high dose of EGF, compared to basal conditions, (Figure 34b, red dots), suggesting that RTN3 and EGFR come into close proximity upon EGF stimulation.

As controls, we also verified FRET of EGFR with different ER markers: STIM1 and RTN4 as markers enriched in peripheral ER (where also RTN3 is enriched), Sec61□ and the ER-localized construct CER17 (140) that labels all ER (Figure 34a). Interestingly, proteins enriched in cortical ER, like RTN3, gave a positive FRET signal within 5 minutes of EGF stimulation (Figure 34b, black dots), while proteins not enriched in the peripheral ER did not give a positive FRET signal ("all ER" markers, Figure 34b, grey dots). Representative images of the localization of the ER proteins and EGFR-YFP upon Alexa555-EGF stimulation of cells are shown in Figure 34a.

In order to follow only FRET signal coming from activated EGFR, we restricted our analysis to the PM region by applying a mask based on Alexa555-EGF signal and followed the FRET signal for 3 minutes of EGF stimulation. We also discarded the signal coming from endosomes, excluding structures bigger then 0.2 μm^2 (see Materials and Methods). We found that, among peripheral ER proteins, RTN3 was the one that gave the highest FRET signal in this specific setting (Figure 34c). All together, these results suggest that upon EGF stimulation, all cortical ER comes into close proximity with EGF-activated EGFR and that the first recruited protein is RTN3 (Figure 34b,c).

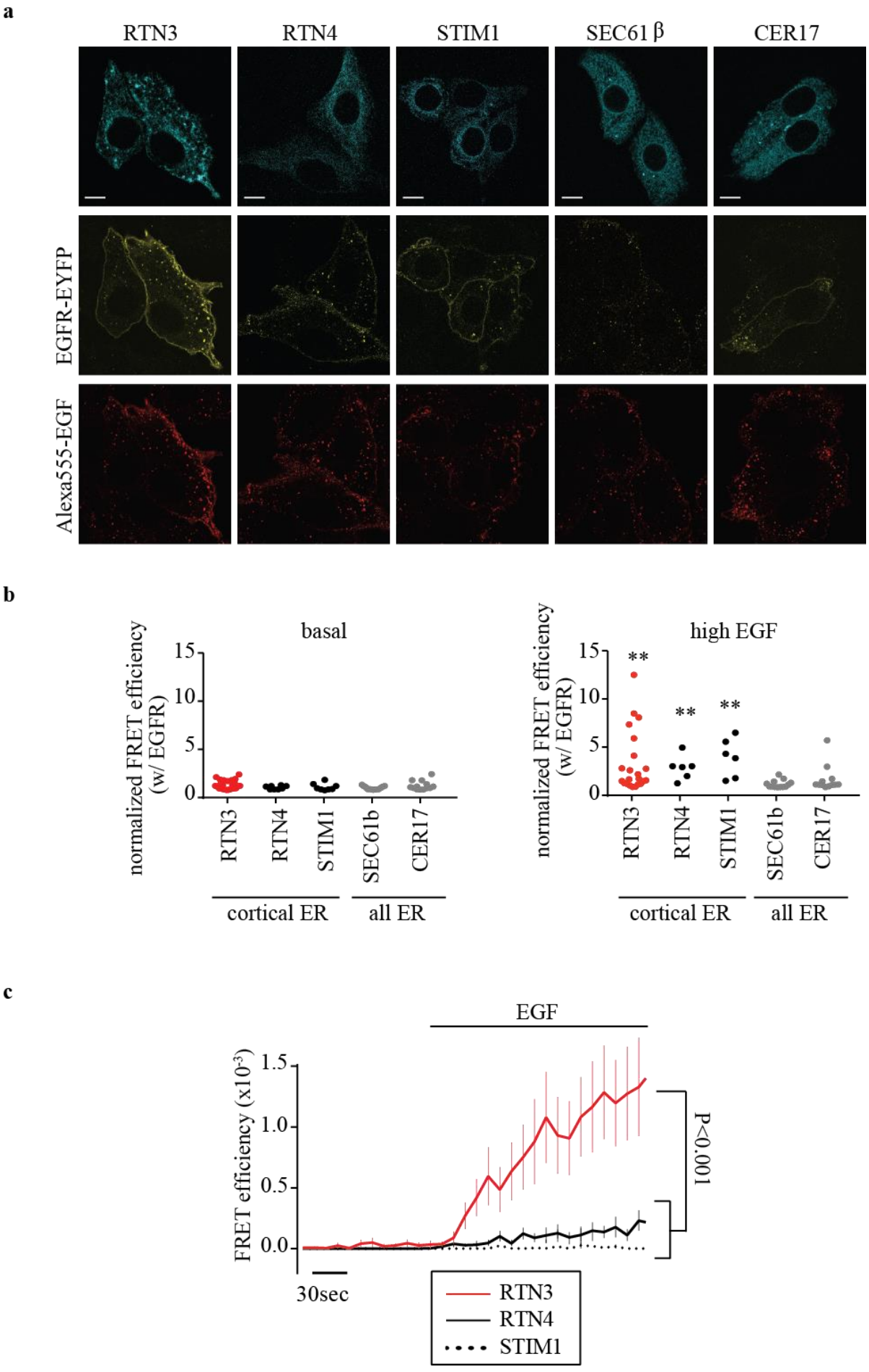
a
RTN3
RTN4
STIM1
SEC61 β
CER17
EGFR-EYFP
Alexa555-EGF
b
basal
high EGF
normalized FRET efficiency (w/ EGFR)
15
10
5
0
**
RTN3
RTN4
STIM1
SEC61b
CER17
cortical ER
all ER
c
EGF
FRET efficiency (x10-3)
1.5
1.0
0.5
0.0
30sec
P<0.001
RTN3
RTN4
STIM1

Figure 34. RTN3 proximity with EGFR is specific.

a) Localization of the indicated CFP-tagged constructs or cerulean, and EGFR-YFP upon stimulation with Alexa555-EGF for 5 minutes. Scale bar, 10 μm.

b) Sensitized Emission FRET analysis (SE-FRET). Normalized SE-FRET efficiencies of EGFR-EYFP in pair with the indicated ECFP-tagged constructs or cerulean-17, before (basal, left) and after stimulation with high dose of Alexa555-EGF for 5 minutes (high EGF, right). Red, RTN3; black, proteins enriched in cortical ER ("cortical ER"); grey, ER proteins not enriched in cortical ER ("all ER"). CER17, cerulean-1. **, P-value <0.01 (EGF-stimulated *vs.* basal condition).

c) Measurement of close proximity at the PM. SE-FRET as in b) was restricted to regions where EGFR is activated at the PM by applying a mask based on Alexa555-EGF signal and following FRET for 3 minutes of EGF stimulation.

4.5 ER contact sites with EGFR positive TIs are formed upon EGF stimulation and are RTN3-dependent.

Our results obtained with super resolution and FRET were compatible with the proximity between activated EGFR at the PM and RTN3 in the ER through the formation of EGF-induced ER-PM contact sites. To further explore this possibility, we took advantage of EM resolution. To better visualize the ER, HeLa cells were transiently transfected with HRP-KDEL, a construct that is localized in the ER and that is visible as a black electrondense precipitate, leading to a clear visualization of the ER ((141,142) and Figure 35a). Cells were then labeled with anti-EGFR, as described in chapter 4.1, and stimulated with high dose of EGF. To test the presence of contact sites between activated EGFR and the ER, each EGFR-positive structure (CCP or TI) was subjected to serial section analysis because gold-labeled EGFR and ER profiles were often not visible in the same section (Figure 35b for a scheme). We defined contact sites as those instances in which ER proximity (≤ 20 nm) to EGFR-gold-positive PM invagination was present in at least one out of three sections (Figure 35c). We found that ~20% of EGFR-containing TIs were in contact with peripheral ER and observed

that no contact sites were present between ER and EGFR-containing CCPs (Figure 35d), suggesting that this might be a specific feature for EGFR-NCE.

We then tested whether RTN3 is required for the formation of contact sites between the ER and EGFR-positive TIs. Serial section analysis showed that TIs that are retained in RTN3 KD cells had lost contact with the ER (only one out of 37 structures retained contact with the ER , Figure 35d). As control, we tested the effect of RTN4 KD on ER-TIs proximity but did not score any alterations in ER proximity with NCE structures (Figure 35e). These results show that RTN3 is required for the formation of specific contacts between the ER and sites of EGFR-NCE. RTN3-dependent contact sites are in turn required for TI formation/stabilization, as RTN3 KD inhibits their biogenesis.

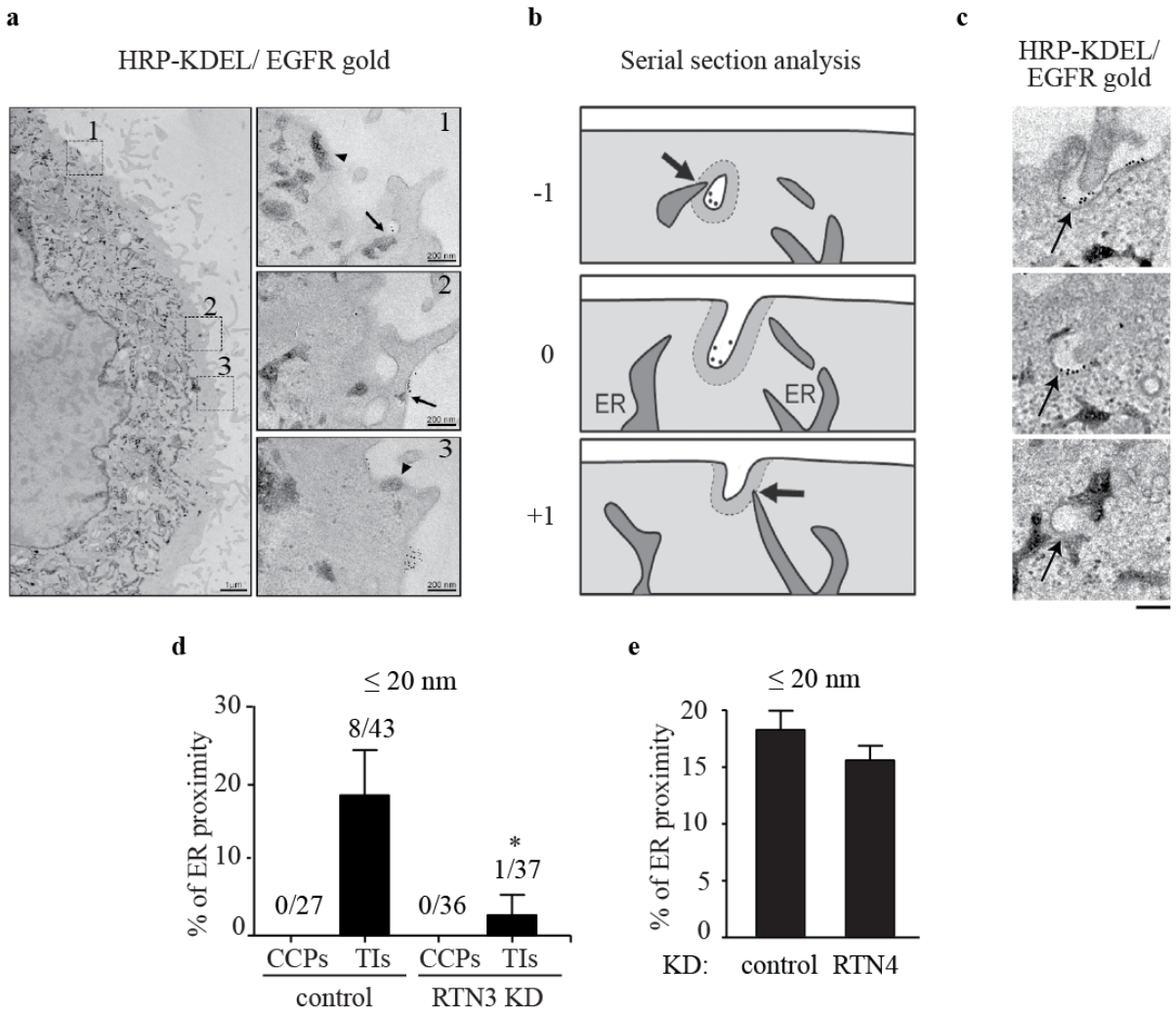

Figure 35. ER-PM contact sites.

a) HeLa cells were transfected with HRP-KDEL, visible as an electrondense precipitate, and stimulated with high dose of EGF (EGFR labeled with gold). Insets magnified on the right show the ER in contact with the PM (gold-labeled PM domains). Scale bar, left 1 µm, right 200 nm.

b) Cartoon depicting the rationale of serial sectioning. Arrows indicate ER-PM contacts.

c) An example of serial sections showing contact sites (≤ 20 nm) between ER and gold-EGFR-positive structures. Arrows indicate the same structures across the sections. Scale bar, 100 nm.

d) Mean frequency of ER proximity with gold EGFR-labeled CCPs or TIs expressed as percentage ± SEM. Absolute numbers above the bars indicate how many of the counted structures are in contact with the ER (distance ≤ 20 nm). Note that EGFR-positive CCPs were not found at ER contact sites. *, $p < 0.05$ (*vs*. control TIs).

5. NCE PM-ER contacts are sites of local calcium release

5.1 High dose of EGF induces a calcium wave at the inner leaflet of the PM

ER contact sites are known to have a fundamental role in localized Ca^{2+} release (114) and high doses of EGF (10-100 ng/ml) are reported to induce a rapid increase in cytosolic Ca^{2+} concentration (143,144). We, therefore, decided to assess whether this is the case for ER-PM contact sites involved in EGFR-NCE.

In order to test if EGF is able to induce a Ca^{2+} wave in correspondence with the PM, we exploited the calcium-activated photoprotein aequorin, isolated from the hydrozoan *Aequorea victoria*. In the presence of calcium, the protein undergoes a conformational change and, through oxidation, converts its prosthetic group, coelenterazine, into coelenteramide and CO_2; blue light (wavelength of 465 nm) is emitted during this reaction and, once registered, can be converted into a calcium response. We compared the cytoplasmic version (cyto-aequorin) with a version targeted to the inner leaflet of the PM by using aequorin fused with SNAP25, a neuronal protein that is recruited to the PM after the post-translational addition of a lipid anchor (PM-aequorin (145)).

Cells were transiently transfected with aequorin and after probe reconstitution (see Materials and Methods), the calcium response was registered prior and after EGF addition. Aequorin detected a rapid peak of Ca^{2+} induced by high dose of EGF (100 ng/ml). This peak was higher when detected with PM-aequorin compared to the cytoplasmic form, (Figure 36a, left), as also evidenced by measurement of the area under the curve (AUC, Figure 36a, right). This data suggests that the increase of $[Ca^{2+}]$ induced by EGF occurrs in proximity to the PM. The calcium wave was not detected at low EGF concentration (1 ng/ml, Figure 36b), indicating a correlation between EGFR-NCE activation and EGF-induced calcium release at the PM.

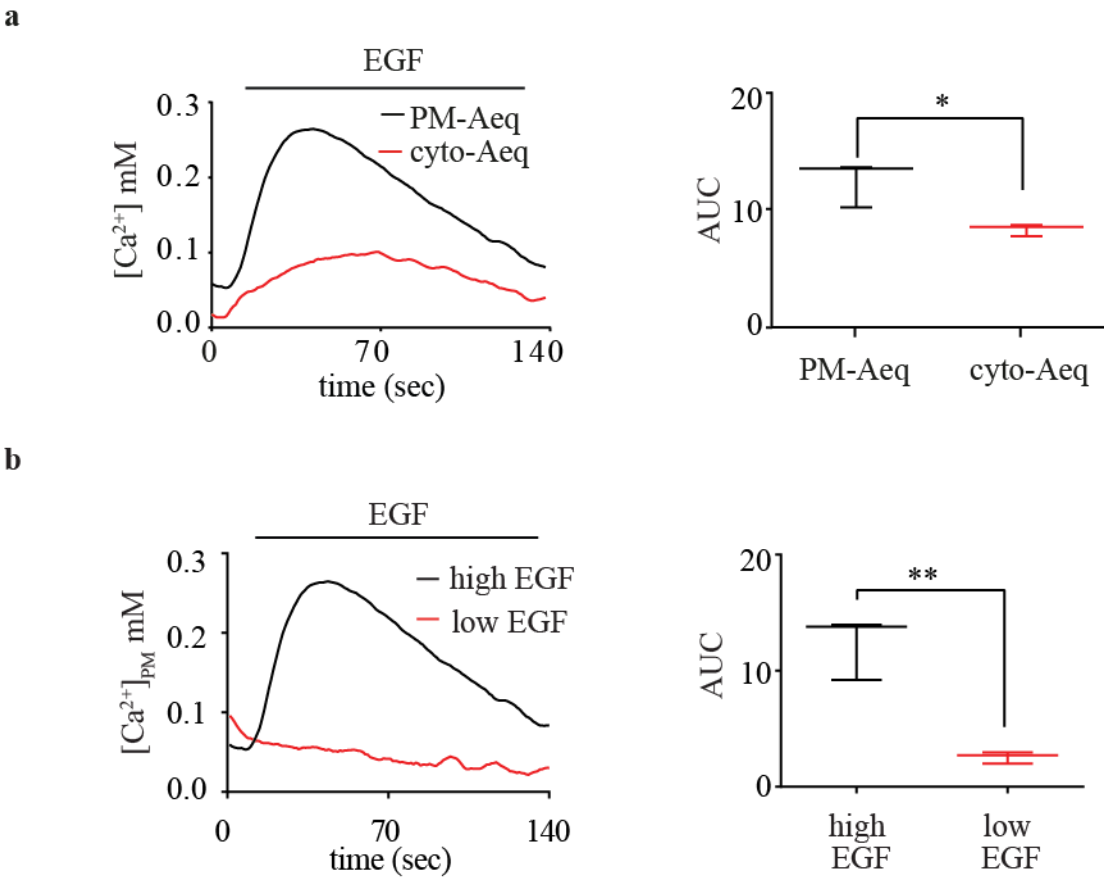

Figure 36. Ca^{2+} wave induced by EGF.

a) Left, measurements of $[Ca^{2+}]$ upon stimulation with high dose of EGF, using aequorin (cyto-Aeq, red curve) and a recombinant aequorin targeted at the PM inner leaflet (PM-Aeq, black curve). The corresponding area under the curve (AUC) in the two conditions is reported in the box plot on the right. *, P-value <0.05.

b) Measurements of $[Ca^{2+}]_{PM}$, using PM-Aeq upon stimulation with high (100 ng/ml, black curve) or low (1 ng/ml, red curve) dose of EGF in control cells. The control curve is the same as in panel a). The corresponding AUC in the two conditions is reported in the box plot on the right. **, P-value < 0.01.

5.2 EGF-induced calcium flux does not depend on extracellular calcium

The source of calcium flux in the cell could derive from intracellular stores or from extracellular space. To test whether the Ca^{2+} flux induced by EGF was coming from the extracellular space, we sequestered extracellular Ca^{2+} with the Ca^{2+}-chelator EGTA. Removal of extracellular calcium did not result in alteration of the EGF-induced peak intensity (Figure 37, lower panel, right), but only minor effects on the decay phase of the curve were observed (Figure 37, upper panel and lower panel, left; see Discussion for possible explanations). This result shows that the EGF-induced Ca^{2+} wave comes from intracellular compartments, possibly from the ER, which is the major storage compartment for intracellular Ca^{2+} (114). This result suggests that EGF induces a Ca^{2+} release from the ER, possibly in correspondence with RTN3-dependent ER-PM contact sites.

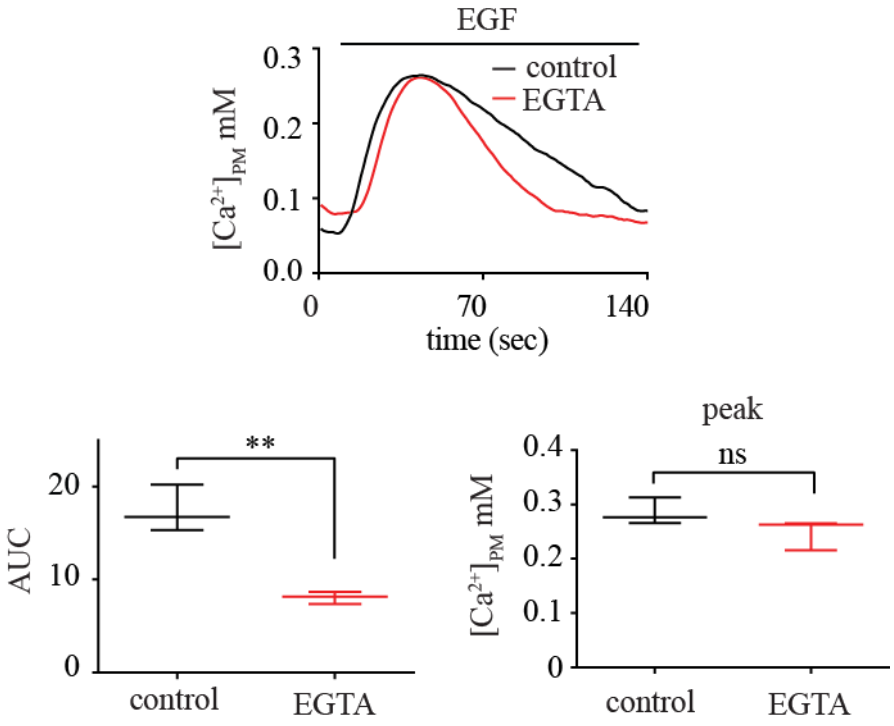

Figure 37. EGF-induced Ca^{2+} wave in the absence of extracellular calcium.

Upper panel, measurements of $[Ca^{2+}]_{PM}$, using PM-aeq upon stimulation with high dose of EGF (100 ng/ml) in the presence or absence of extracellular calcium. Control cells where stimulated in saline buffer with calcium (black curve) or in saline buffer without calcium in the presence of the extracellular calcium chelator EGTA (red curve). The control curve is the

same as in the Figure 36a. The corresponding AUC in the two conditions is reported in the box plot on the right in the lower panel. **, P-value < 0.01. On the left, calcium peak values in the two conditions are reported.

5.3 RTN3 KD affects EGF-induced calcium release

Considering that RTN3 is required for the formation of contact sites between the ER and the PM (section 4.5), we wanted to test whether RTN3 ablation could have an effect also on the EGF-induced calcium wave observed with aequorin. We observed a strong reduction in Ca^{2+} response upon stimulation with EGF in RTN3 KD cells (Figure 38a). We also tested the effect of RTN4 KD as a control and found that it had no effect on the EGF-induced calcium wave (Figure 38b). These findings corroborate the possibility that Ca^{2+} is released upon EGF at ER-PM contact sites and that these specifically depend on RTN3 function.

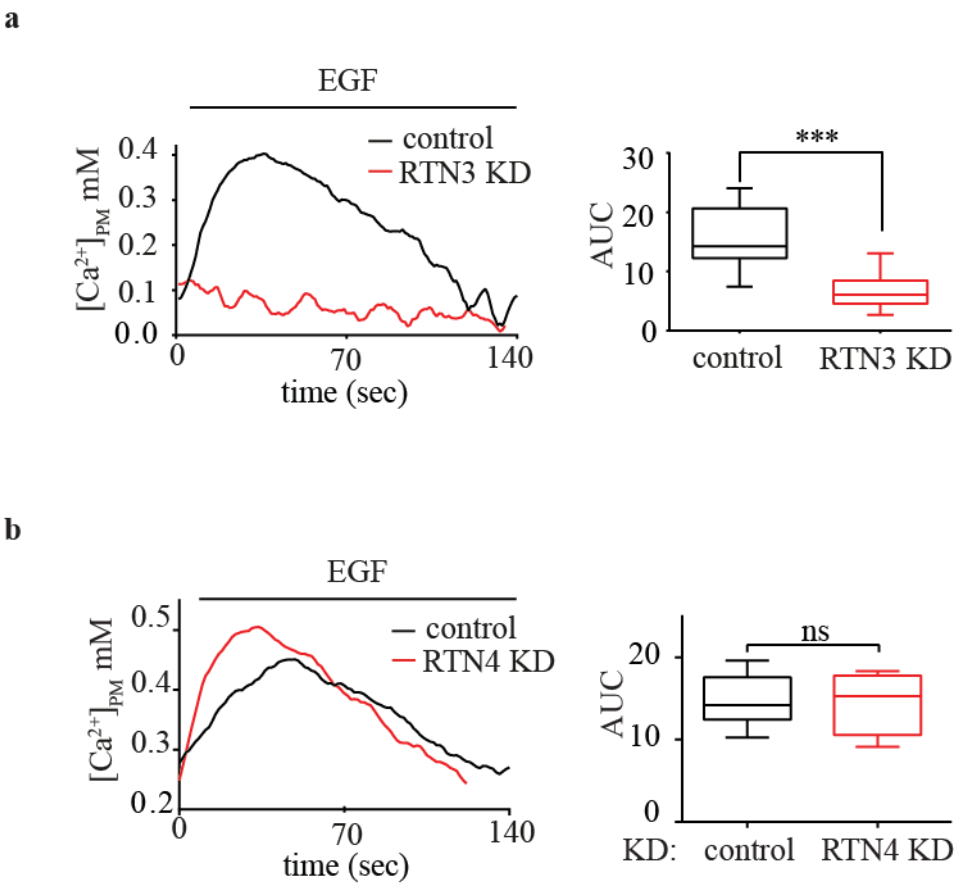

Figure 38. The effect of RTN3 KD and RTN4 KD on the EGF-induced Ca^{2+} wave.
a) Measurements of $[Ca^{2+}]_{PM}$, using PM-aeq upon stimulation with high dose of EGF in control (black curve) and RTN3 KD cells (red curve). The corresponding AUC in the two conditions is reported in the box plot on the right. ***, P-value <0.001.
b) Measurements of $[Ca^{2+}]_{PM}$, using PM-aeq upon stimulation with high dose of EGF in control (black curve) and RTN4 KD cells (red curve). The corresponding AUC in the two conditions is reported in the box plot on the right.

5.4 Calcium is necessary for internalization of EGFR via NCE

Once the dependence on RTN3 was defined also for the EGF-induced calcium wave, we wanted to test if the calcium movement induced upon stimulation with EGF was only a consequence or whether it is necessary for EGFR-NCE. We performed a calcium depletion procedure by combining EGTA and ionomycin treatment of the cells (146). The cells were kept in the presence of the calcium chelator EGTA and ionomycin to facilitate calcium exit from the ER to the extracellular space. After calcium depletion, intracellular calcium stores are emptied. We tested the effect of calcium depletion on endocytosis by stimulating the cells with Alexa555-EGF and assessing EGF and CD147 internalization. We observed that the internalization of CD147 was blocked, while the internalization of EGF was unaffected in cells treated with ionomycin. By combining ionomycin treatment with clathrin KD, both CD147 and EGF were blocked at the PM, suggesting that in these conditions both CME and NCE were blocked (Figure 39a) and that calcium depletion was sufficient to block the internalization of EGFR and CD147 through NCE.

To verify the impairment of NCE upon intracellular calcium depletion, we performed ^{125}I-EGF internalization assays. We found that ionomycin treatment does not alter EGF internalization at low dose of the ligand (Figure 39b, upper graph), while, at high dose of the ligand, the effect was comparable to that of RTN3 KD (Figure 39b lower graph), suggesting that calcium depletion, indeed, affects EGFR-NCE but not CME. The combination of

ionomycin treatment with clathrin KD at high dose of EGF reduced the internalization to levels comparable with those observed in cells depleted of both RTN3 and clathrin, confirming that intracellular Ca^{2+} is required for the internalization of EGFR via NCE (Figure 39b).

a

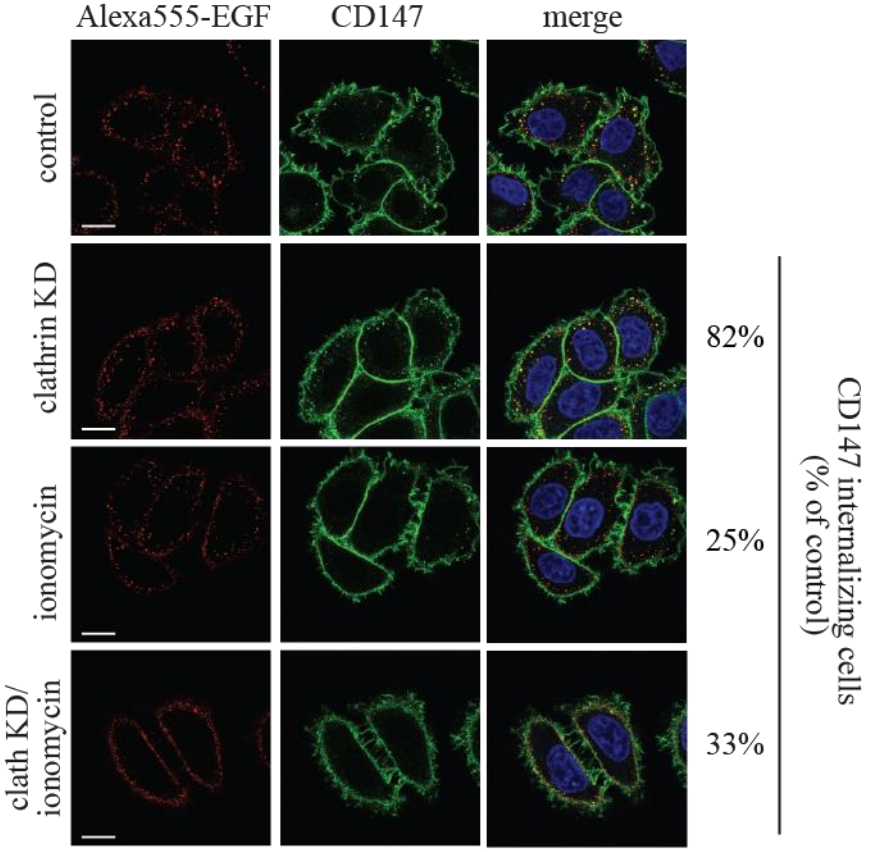
Alexa555-EGF
CD147
merge
control
clathrin KD
ionomycin
clath KD/
ionomycin
82%
25%
33%
CD147 internalizing cells
(% of control)

b

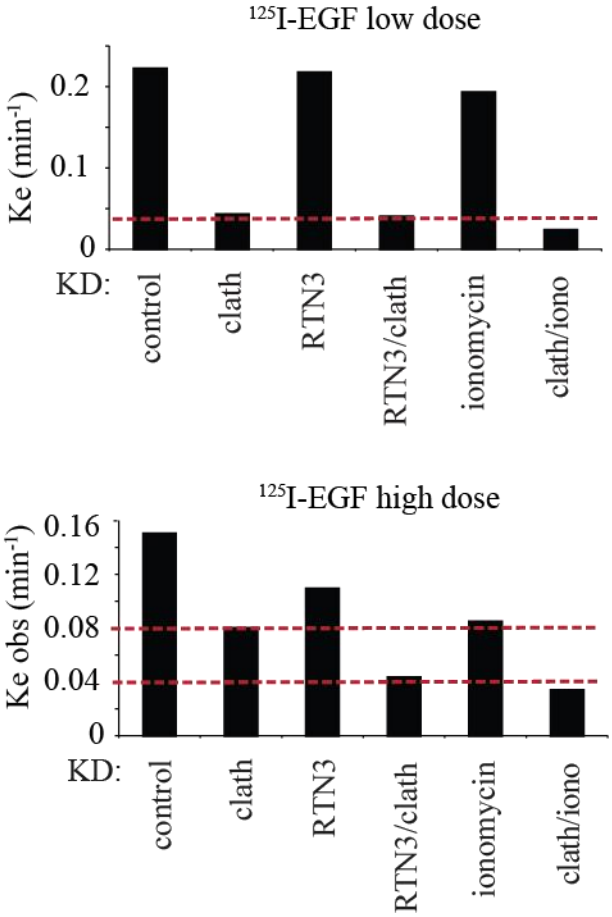
125I-EGF low dose
Ke (min-1)
0.2
0.1
0
KD:
control
clath
RTN3
RTN3/clath
ionomycin
clath/iono
125I-EGF high dose
Ke obs (min-1)
0.16
0.12
0.08
0.04
0
KD:
control
clath
RTN3
RTN3/clath
ionomycin
clath/iono

Figure 39. The effect of calcium on EGFR-NCE.

a) CD147 (green) internalization was followed using a specific antibody *in vivo* as described in Figure 25, in control and clathrin KD cells, treated or not with EGTA and ionomycin and stimulated with high dose of Alexa555-EGF for 8 minutes (red). Scale bar, 10 μm.

b) Internalization constants (Ke) were measured by ^{125}I-EGF internalization at low (upper graph) and high (lower graph) doses of EGF in the indicated conditions. Mean of duplicates of a single experiment are shown.

5.5 EGF-induced calcium release occurs through the activation of the IP3 receptor on the ER

5.5.1 Detection of EGF-induced calcium response at single cell level

Considering the relative low sensitivity of aequorin, in parallel to the aequorin experiments, we validated some of the observed phenotypes with the ratiometric dye Fura-2 AM, a highly sensitive system that allows the evaluation of calcium response at single cell level. Note that, differently from aequorin, Fura-2, AM is more sensitive but measures the calcium movement in the cytosol and cannot be targeted to specific areas. Also in this case, we observed a calcium peak upon stimulation of cells with high dose of EGF, which was strongly affected by RTN3 KD but not by RTN4 KD (Figure 40a). Differently from PM-aequorin, we observed a calcium response also in cells stimulated with low dose of EGF, even if greatly reduced compared to the stimulation with high dose of EGF (Figure 40b, see Discussion for possible explanation).

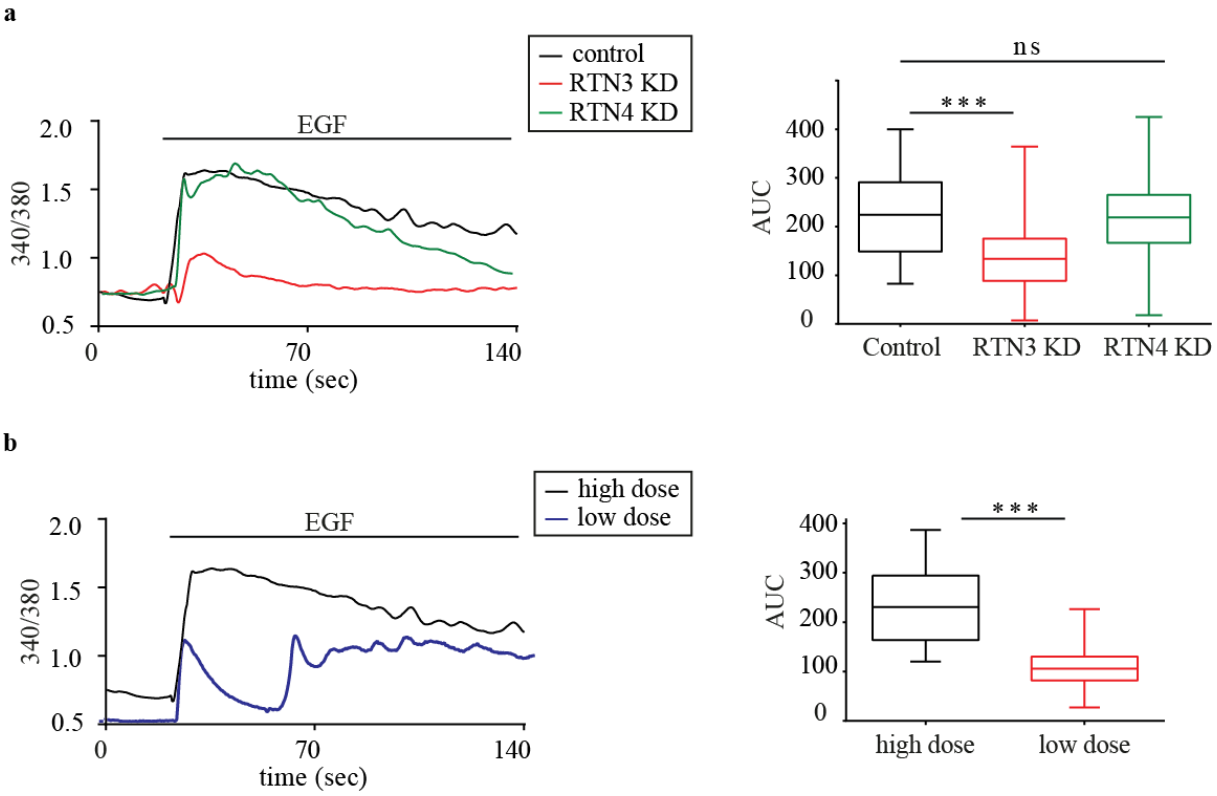

Figure 40. Measurements of EGF induced calcium wave.

a) Representative (single cell) cytosolic Ca^{2+} response induced by stimulation with high dose of EGF, in control (black curve), RTN3 KD (red curve) and RTN4 KD (green curve) cells loaded with Fura-2, AM. The kinetics of Ca^{2+} response is presented as the ratio of the fluorescence at 340/380 nm emission. The corresponding AUC in the different conditions is reported in the box plot on the right. ***, P-value <0.001.

b) Representative (single cell) cytosolic Ca^{2+} response induced by stimulation with high dose of EGF, (black curve) or low dose of EGF (blue curve) of cells loaded with Fura-2, AM. The kinetics of Ca^{2+} response is presented as the ratio of the fluorescence at 340/380 nm emission. The control curve is the same as in panel a). The corresponding AUC in the different conditions is reported in the box plot on the right. ***, P-value <0.001.

5.5.2 IP3R inhibition affects EGF-induced calcium wave and NCE progression

The activation of the ER receptor inositol-3-phosphate (IP3R) is the main pathway that promotes Ca^{2+} release from the ER in HeLa cells (147). In order to test if this pathway is implicated in the calcium wave observed upon EGF stimulation, we tested the effect of

xestospongin C, a selective IP3R inhibitor, on the EGF-induced calcium wave by using Fura-2 AM. We observed that xestospongin C treatment strongly affected EGF-induced Ca^{2+} flux to an extent comparable to RTN3 KD (Figure 41), suggesting that the EGF-induced calcium release occurs through the opening of IP3Rs on the ER membrane.

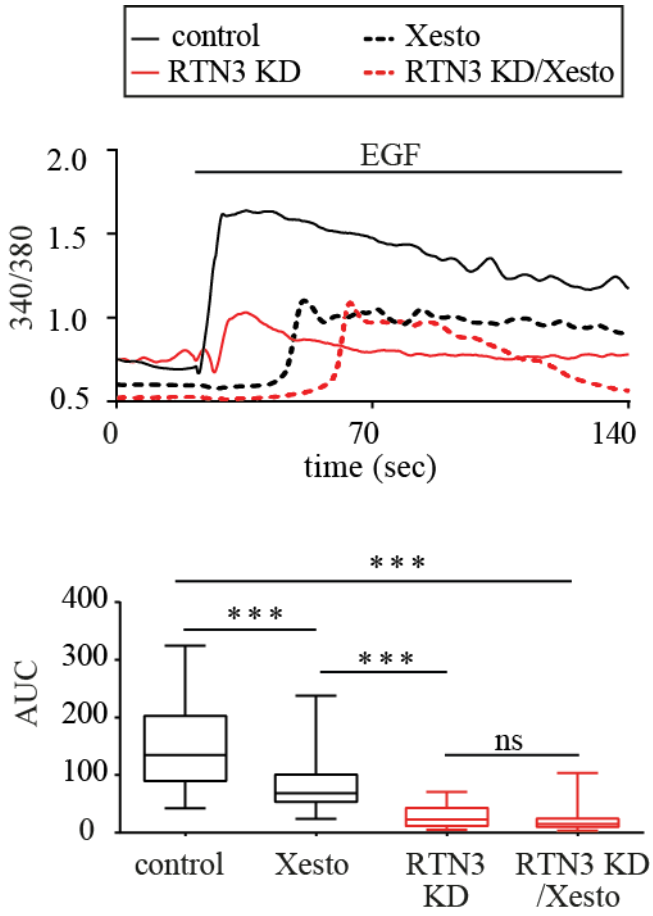

Figure 41. The effect of xestospongin on the EGF-induced calcium wave.

Top, representative (single cell) cytosolic Ca^{2+} response induced by stimulation with high dose of EGF, in control (black curve), xestospongin C-treated (Xesto, dotted black curve), RTN3 KD (red curve) and xestospongin C-treated RTN3 KD (dotted red curve) cells loaded with Fura-2, AM. The kinetics of Ca^{2+} response is presented as the ratio of the fluorescence at 340/380 nm emission. The corresponding AUC in the different conditions is reported in the box plot at the bottom. ***, P-value <0.001.

Considering that EGFR-NCE requires both ER-PM contact sites and calcium release from the ER to the PM, we wanted to define if the calcium release is required for contact site formation or if it is an event that occurs after their establishment. To study the timing of these events, we tested if the blockage of IP3R-dependent calcium release induced by EGF could alter the formation of ER-PM contact sites in EGFR-NCE. Since the proximity between RTN3 and EGFR can be assessed by FRET analysis (see Figure 34), we tested if xestospongin C treatment could lead to an alteration of this proximity induced by EGF using this method. We did not observe any alterations in the proximity between EGFR and RTN3 upon xestospongin treatment (Figure 42). These data suggest that Ca^{2+} release by IP3R is downstream of ER-PM contact site formation.

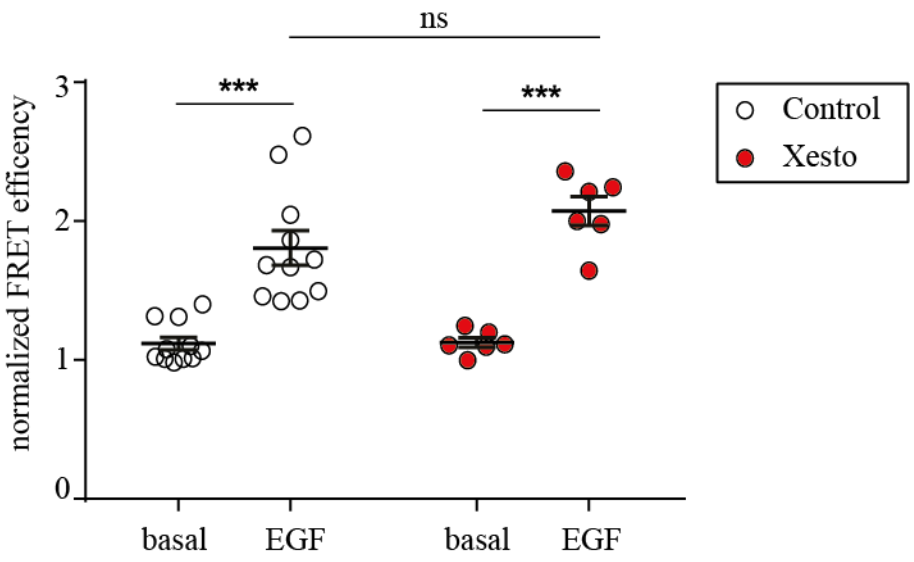

Figure 42. Xestospongin treatment does not alter EGFR-RTN3 proximity.
Sensitized Emission FRET analysis (SE-FRET). The figure shows the normalized SE-FRET efficiencies of EGFR-EYFP in pair with the RTN3-ECFP, before (basal) and after stimulation with high dose of Alexa555-EGF for 5 minutes (EGF) in cells treated (red dots) or not (white dots) with xestospongin C. ***, P-value <0.001 (EGF-stimulated *vs.* basal condition).

Finally, we tested whether the calcium needed for NCE progression was the one released from IP3R by assessing EGFR and CD147 internalization after xestospongin C treatment. We found that xestospongin C is able to impair CD147 internalization, indicating that it inhibits NCE. When we combined xestospongin C treatment with clathrin KD to block both NCE and CME, we observed an inhibition of both EGF and CD147 internalization (Figure 43). Overall, these results are compatible with the possibility that high doses of EGF induce a calcium wave through the opening of IP3R at ER-PM contact sites, which is in turn required for NCE to proceed.

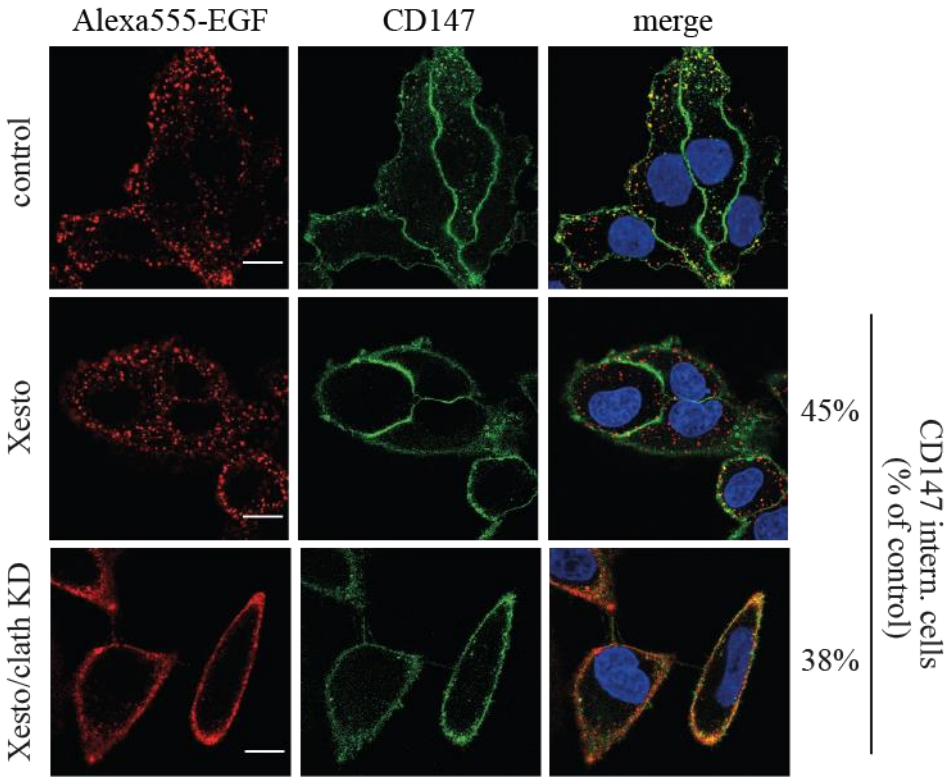

Figure 43. The effect of xestospongin C on NCE internalization.
CD147 (green) internalization was followed using a specific antibody *in vivo*, as described in Figure 5, in control cells, treated or not with xestospongin C (Xesto), and in xestospongin C-treated clathrin KD cell, stimulated with high dose of Alexa555-EGF for 8 minutes (red). Scale bar, 10 μm. Blue, DAPI. Right, percentage of cells in which CD147 is internalized in the different samples is indicated.

6. A new probe to study calcium release at the PM

We wanted to increase the "resolution" in the study of the EGF-induced calcium wave and to use a probe targetable at the inner leaflet of the PM, as aequorin, but that gives information at single cell level, as Fura-2, AM. To do so, we tested the chimeric protein GCaMP6f, that for its relative low affinity for calcium is also ideal for the evaluation of calcium potentials closely spaced in time (148). We used both the cytosolic version of this probe and a version fused with SNAP25 (see section 5.1 for aequorin). First, we evaluated the PM staining of the SNAP25 version and we confirmed that the presence of the protein at the PM did not alter EGF internalization upon stimulation of cells with Alexa555-EGF (Figure 44a). We found that the internalization of EGF was not altered by GCaMP6f transfection. Then, we compared the cytosolic and the PM version of the probe. We did not observe any significant calcium response upon EGF stimulation with the cyto-GCaMP6f. The PM-GCaMP6f probe, instead, showed an oscillatory calcium response with pronounced and repetitive calcium peaks (Figure 44b, black curve). This data highlights an interesting calcium response *in quanta* that we were not able to observe with PM-aequorin.

This preliminary data supports our previously observed phenotype; the reduced calcium response upon RTN3 KD and xestospongin C treatment (Figure 44b, red and green curves); thus confirming that the calcium release induced by EGF is occurring through IP3R specifically in correspondence with the PM.

a

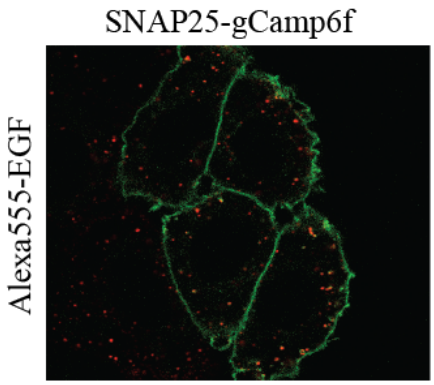
SNAP25-gCamp6f
Alexa555-EGF

b

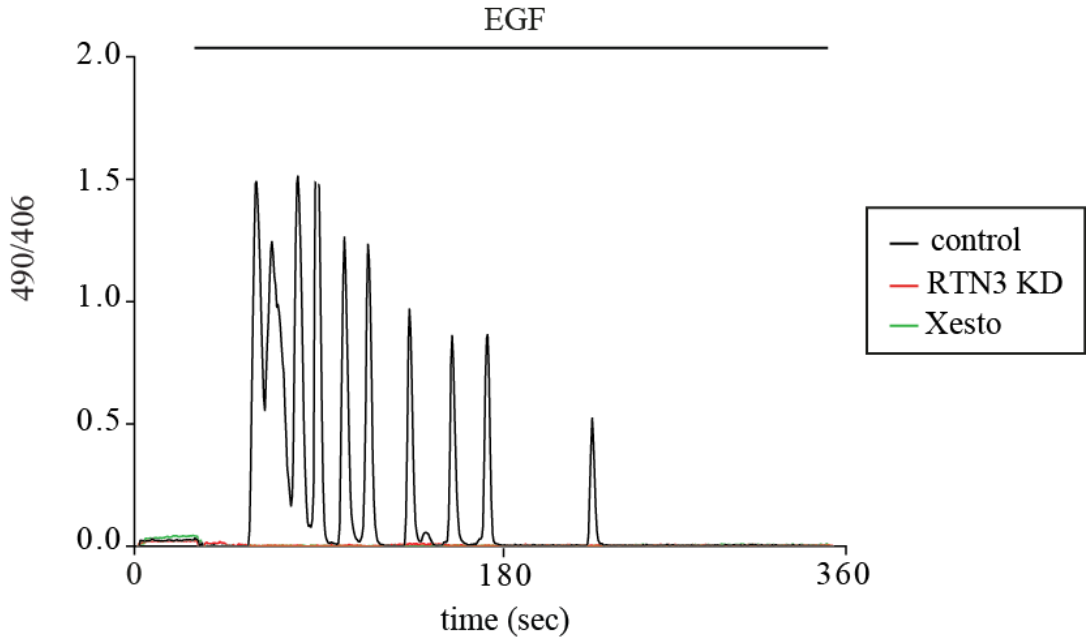
EGF
2.0
1.5
1.0
0.5
0.0
490/406
0
180
360
time (sec)
control
RTN3 KD
Xesto

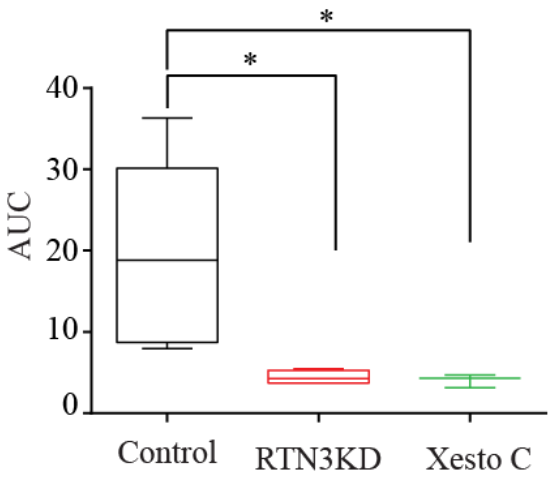
*
*
40
30
20
10
0
AUC
Control
RTN3KD
Xesto C

Figure 44. EGF-induced calcium wave detected by PM-GCaMP6f.

a) HeLa cells were transfected with the PM-GCaMP6f construct (SNAP25 fusion) and stimulated with Alexa555-EGF.

b) Top, representative (single cell) Ca^{2+} response at the PM induced by stimulation with high dose of EGF in control (black curve), RTN3 KD (red curve) and xestospongin C-treated (Xesto, green curve) cells transfected with PM-GCaMP6f. The kinetics of Ca^{2+} response is presented as the ratio of fluorescence at 490/406 nm emission. The corresponding AUC in the different conditions is reported in the box plot at the bottom. *, P-value <0.05.

DISCUSSION

1. The uniqueness of EGFR-NCE

We have characterized a new clathrin-independent endocytic pathway, responsible for the internalization of the EGFR and triggered by stimulation with high dose of EGF. The uniqueness of this pathway relies on the fact that it is functionally distinct from all other NCE pathways described so far in the literature (8,27,42,45,48,50,52,53,149-151). Indeed, our extensive analysis, performing KD of players known to be involved in other clathrin-independent endocytic routes and evaluating their effect on EGFR-NCE, did not identify any player that is specific only for NCE: we either scored no effect or a more general effect on endocytosis. This is the case for the actin-regulators Cdc42 and Rac, which appear to alter not only NCE, but also CME and the constitutive pathway, suggesting that their effect can be due to a general alteration of the actin machinery affecting the structure of the cell.

With the scope to identify key molecular players specifically involved in EGFR-NCE, we developed a protocol to isolate and molecularly characterize EGFR-NCE vesicles. This analysis was followed by an extensive validation procedure and led us to the identification of a number of regulators that have not been implicated in endocytic routes but are specifically involved in EGFR-NCE. We dissected the pathway by following EGFR internalization and found an additional PM cargo, CD147, with no active role in EGFR-NCE, but that, upon EGF stimulation, exploits the same route as EGFR for its internalization.

The great novelty of the EGFR-NCE pathway relies on the finding that it requires the establishment of contact sites between the ER and the PM for its execution, a feature that until now has not been addressed for any endocytic pathway. However, the width of the impact of EGFR-NCE in different cellular contexts, and if this pathway always relies on the same mechanism of internalization, is an issue that remains to be addressed.

We have previously shown that a clathrin-independent, dynamin-dependent pathway for the EGFR, which is activated at high EGF concentrations, is not restricted to our model system, HeLa cells, but can be observed in different cell lines, although its existence is clearly cell context dependent (111). When this analysis was performed, we did not have molecular tools, like RTN3 as a functional regulator or CD147 as a marker of NCE, to investigate the system. Therefore, we are currently screening different cell lines again, using these more specific tools to define the presence of EGFR-NCE in other model systems. This analysis will clarify if EGFR-NCE relies on the same molecular mechanism and players in different cellular contexts. Moreover, we plan to widen the analysis to test if other receptors, particularly other RTKs, exploit the same endocytic route.

2. ER resident proteins regulate EGFR-NCE

Among the identified EGFR-NCE players, four are proteins resident in the ER (RTN3, REEP5, PLOD1, P4HB); RTN3 and REEP5 showed one of the strongest and more specific effects on EGFR-NCE upon ablation. RTN3 is an ER membrane-associated protein of the reticulon family and REEP5 is closely related. Four RTN genes have been identified in mammals: RTN1, RTN2, RTN3 and RTN4. The RTN proteins have been found to be primarily associated with the ER, where they act as shaping factors, and in some cases a small fraction has been found present also at the level of the PM (136,152).

Reticulon proteins contain a Reticulon Homology Domain (RHD) at the C-terminus, formed by two hydrophobic patches flanking a hydrophilic loop. There are different hypotheses regarding the topology of the RHD region, this segment can span the membrane or double back on itself to form a hairpin (Figure 45).

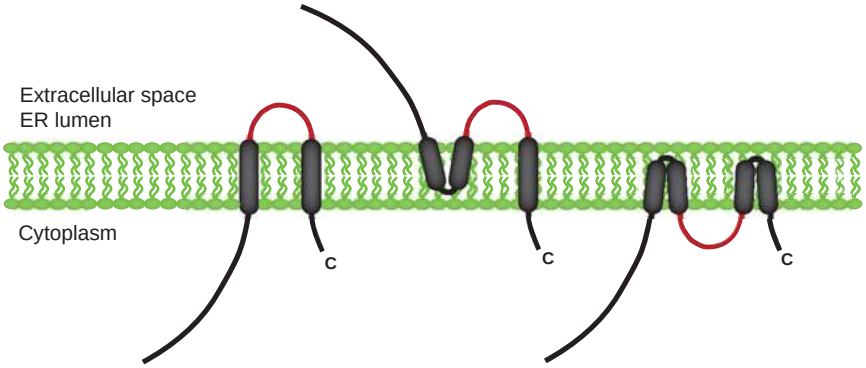

Adapted from Yang and Strittmatter, *Genome Biology*, 2007 (134)

Figure 45. Possible topologies of reticulon proteins.
Several topologies have been hypothesized for reticulon proteins but only the three topologies depicted in the figure have been verified.

Considering several evidences supporting diverse possible RTN structures, the best explanation is that, in mammals, reticulon proteins can adopt different conformations, conferring to this protein the ability to carry out multiple roles inside the cell (134). This diversity is present also at the gene level, for example, RTN3 has seven different isoforms (see Results Figure 27) and whether these can have a different localization, function or tissue expression is still unknown. Differently from RTN3, REEP5 has only one single isoform but possess the RHD region and possibly adopts the same structure as RTN3. Importantly, it has been demonstrated that RTN3 and REEP proteins oligomerize at the level of the ER, and that this interaction is required for tubulation of cortical ER (136).

Considering the hairpin-like topology, reticulon structure could resemble the structure of caveolins and flotillins at the PM (Figure 46). Like caveolins and flotillins at the level of the PM, RTN3 and REEP5 can induce membrane curvature and generate tubules at the level of peripheral ER membranes (136). In particular, our data suggest that RTN3 might exert its function in EGFR-NCE from an ER location, without any translocation at the level of the PM, supported by the fact that we could not detect any RTN3 at the PM. However, we cannot exclude that a minor fraction of RTN3 might have escaped our detection.

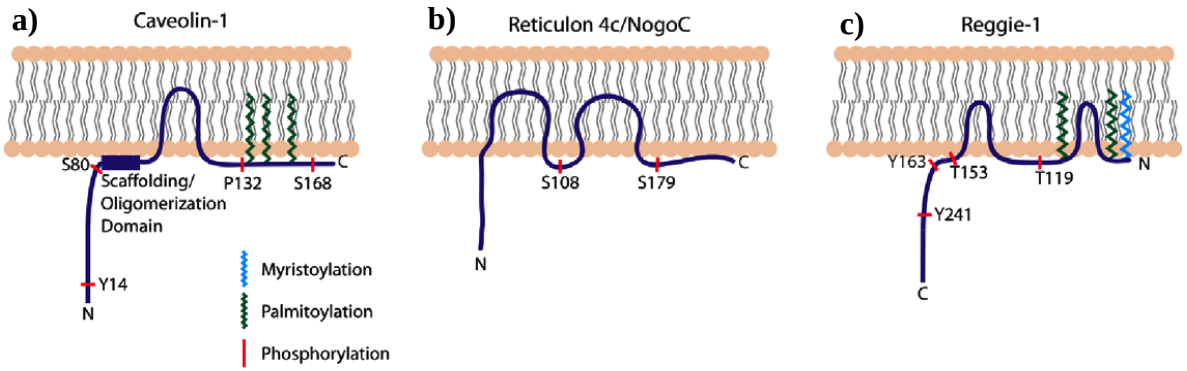

Adapted from Bauer and Pelkmans, *FEBS Letters*, 2006(153)

Figure 46. Putative membrane topologies of membrane-coat proteins and reticulons. Membrane topologies of caveolin-1 **a)**, RTN4c/NogoC **b)** and Reggie-1/Flotillin-2 **c)** are depicted. All three proteins possess a hydrophobic sequence that does not cross the membrane. Putative phosphorylation sites are also represented.

It would be interesting to evaluate the specific function of the other two ER-associated proteins PLOD1 and P4HB. PLOD1 (Procollagen-Lysine, 2-Oxoglutarate 5-Dioxygenase 1) is an ER membrane-bound lysyl hydroxylase and catalyzes the hydroxylation of lysyl residues in collagen-like peptides, a modification that is critical for the stability of mature collagen. P4HB (the beta subunit of prolyl 4-hydroxylase) is a disulfide isomerase that, among other functions, is involved in the hydroxylation of prolyl residues in preprocollagen, in the regulation of disulfide bonds, and in the control of misfolded proteins. Since these two proteins are enzymes, it would be interesting to study if their function is specifically required for EGFR-NCE.

3. ER-PM contact sites are required for EGFR-NCE

We used RTN3 as a molecular tool to characterize EGFR-NCE since it has all the characteristics of a specific regulator of this pathway. In particular, we observed that the RTN3 KD blocks EGFR internalization through NCE and leads to a complete inhibition of EGF internalization when combined with clathrin KD at high EGF dose. Moreover, the KD of RTN3 delayed EGFR degradation, leading to an increase in its recycling - as expected under conditions of EGFR-NCE inhibition, which preferentially devotes receptors to degradation into lysosomes (63). Furthermore, RTN3 ablation blocked the internalization of the cargo protein CD147 through NCE.

One issue that arises from our purification procedure is why we recovered ER-resident proteins associated with NCE vesicles. This is reminiscent of the so-called "mitochondria-associated ER membranes" (MAMs). Indeed, MAMs were initially considered "contaminants" of the mitochondrial fractions (154,155), but successive studies defined MAMs as ER structures in close contact with mitochondria (156). Similarly, our morphological studies by EM suggest an extensive association of the ER with sites of EGFR-NCE that may be responsible for the recovery of the ER fraction in our vesicle purification. These contacts seem to be a peculiarity of NCE; indeed, we could not identify any contact sites between the ER and EGFR-containing CCPs.

There are multiple evidences of contact sites between the ER and endocytic organelles, as well as with the PM in the literature. A direct role for contact sites in the internalization step has, however, never been described (117,121,157,158). Given that the ER is one of the main calcium and lipid reservoirs in the cell, it is not surprising that ER contact sites with the PM are requested for phosphoinositides and calcium signaling, and for lipid transport (90,141,159,160). Considering the great mobility of the ER to precisely locate enzymes and proteins with a specific function, contact sites can have a role also at endocytic sorting stations where they can establish a functional crosstalk between different

compartments without fusion of the two (119,121,161,162). An example of this crosstalk between ER and endosomes is the regulation of EGFR fate by the action *in trans* of the ER-phosphatase PTP1B on the internalized receptor localized at the endosomal level (125). Importantly, ER-contact sites also have a more active role as they are, together with dynamin and actin, involved in the regulation of fission events of endosomes or mitochondria (117,123). Interestingly, EGFR-NCE requires dynamin and we have evidence that show that also actin is required in this process (preliminary data, not shown). Thus, we could speculate that the cell may use the same molecular machinery for different functions, which, like in this case, may be related. The involvement of ER in membrane fission might be not only at the level of mitochondria and endosomes, as already reported, but also at the level of the PM in correspondence with EGFR-NCE sites.

4. What is the role of RTN3 in EGFR-NCE contact site formation and stabilization?

RTN3 is necessary for the formation of ER contact sites with EGFR-positive PM structures and for the maturation of TIs, which represent the NCE intermediates. Moreover, we showed that ER-localized RTN3 is recruited in close proximity to active EGFR, specifically upon EGF stimulation (Figure 34). Considering the great mobility and flexibility of the ER, we can hypothesize that the tubulating function of RTN3 is necessary for the function of ER in EGFR-NCE. The strongest evidence in support of this hypothesis is the fact that RTN3 is required for the formation of ER-PM contact sites induced by EGF. In favor of this idea, another ER tubulation factor, REEP5, has a similar function. The two proteins, RTN3 and REEP5, are reported to be able to form a complex (136). Moreover, we can envision specificity in the system, since another member of the reticulon family, RTN4, also involved

in the tubulation of the ER, apparently does not have an active role in NCE. One hypothesis could be that specific regions (or domains) of the ER can be under the control of dedicated factors to execute precise functions. Thus, RTN3 and REEP5 might represent prototypes of such "dedicated" tubulation factors. At present, however, we cannot exclude that the function of RTN3 might depend on activities other than ER tubulation.

Another hypothesis is that RTN3 acts as a tethering factor between the ER and the PM after EGFR activation by the ligand. In support of this hypothesis, we observed close proximity between RTN3 and activated EGFR, and specific FRET signal between the RTN3-EGFR pair specifically upon EGF treatment. Other cortical ER proteins showed FRET with EGFR after EGF stimulation; however, analyzing the FRET signal in correspondence with the PM and during the first minutes of stimulation, thus excluding EGF-positive endosomes, we found that RTN3 was the only protein under scrutiny that gave a strong FRET signal. We failed, however, to detect co-immunoprecipitation between the EGFR and RTN3. We can speculate that a putative RTN3-EGFR association is labile or stoichiometrically below detection limits; another possibility is that a protein bound to RTN3 acts as a tethering factor or that RTN3 interacts with a PM protein that is close to the EGFR.

5. The role of ER-PM contacts in NCE: TI maturation and local Ca^{2+} release

ER-PM contacts appear to be required for EGFR-NCE at the level of TI formation and maturation. One possibility is that the ER may work as an anchor for TI stabilization, which otherwise are instable and do not mature. Although we cannot exclude a structural role for ER-contact sites in EGFR-NCE, our data shows that they could have a functional role, working as platforms for EGF-induced local Ca^{2+} release from the ER at a location close to

the PM, which is, in turn, required for the completion of the internalization process. These findings integrate well with previous knowledge that ER-PM contacts are sites of localized calcium signaling (114) and with the fact that stimulation with high dose of EGF induces an intracellular calcium wave (143,144). However, this is the first evidence that EGF-induced calcium release occurs at ER-PM contact sites and that it is directly involved in EGFR internalization. We showed that the massive calcium wave is triggered only upon stimulation with high dose of EGF. This is critical since EGFR-NCE is also activated only at high EGF concentrations. We have previously shown that EGFR ubiquitination, which is required for EGFR-NCE, has a similar behavior (68). The two systems may be related in their regulation and we can speculate that the existence of multiple controls on EGFR-NCE activation is needed to ensure the activation of the pathway only at high doses of the ligand.

We have also dissected the signaling cascade, showing that stimulation with high dose of EGF is required to activate the IP3R on the ER, leading to Ca^{2+} release from this organelle to the PM. Our data indicate that this calcium release is needed to complete the internalization process: blocking the IP3R calcium release with the drug xestospongin, as well as ER-calcium deprivation, impairs EGFR-NCE. Importantly, the calcium release is downstream the RTN3-depedent formation of contact sites since blocking calcium release from the ER did not affect the proximity between active EGFR and RTN3. Thus, our data suggest a positive feedback loop that links EGFR-NCE and Ca^{2+} signaling: high dose of EGF triggers ER-PM contact site formation and NCE activation, which induces local Ca^{2+} release at contact sites and, in turn, the Ca^{2+} flux is required to finalize EGFR-NCE.

Upon EGF-induced release of calcium, the ER needs to reload it, and we can hypothesize that this operation may include the induction of store-operated-calcium-entry (SOCE). In the ER, the transmembrane protein STIM1 acts as a calcium sensor; when calcium is released from the ER is also detached from STIM1, inducing conformational changes that lead to the relocalization of STIM1 to ER sites near the PM where it can

associate with Orai1 to induce SOCE. These events lead to the entrance of calcium into the cytoplasm, sustaining the calcium elevation. Calcium is then re-acquired into the ER thanks to the action of sarco/ER Ca^{2+}-ATPase (SERCA) (163). We can, thus, hypothesize that this system of calcium re-acquirement by the ER is present also after the calcium release induced by EGF. Indeed, when we analyzed the EGF-induced calcium wave in the presence of EGTA, an extracellular calcium chelator, we did not observe any effect on the EGF-induced calcium peak; however, we scored an effect on the second phase of the curve (Figure 37, Results), which decayed more abruptly, likely due to the lack of activation of SOCE as a consequence of the extracellular calcium depletion. The activation of SOCE, however, should represent a secondary effect due to the emptying of ER-calcium, and should not have a direct role in EGFR-NCE. Indeed, our preliminary data shows that STIM1 KD does not affect EGFR-NCE. Further investigations will be needed to reinforce this possibility. Interestingly, another reticulon, RTN4, has been linked to ER tubulation-dependent calcium regulation. In particular, upon RTN4 KD, the ER changes its morphology profoundly, moving from tubules to ER sheets, and the blocked ER tubulation appears to be sufficient to impair the coupling between STIM1-Orai1, representing the first demonstration of a role of RTNs in calcium signaling (164).

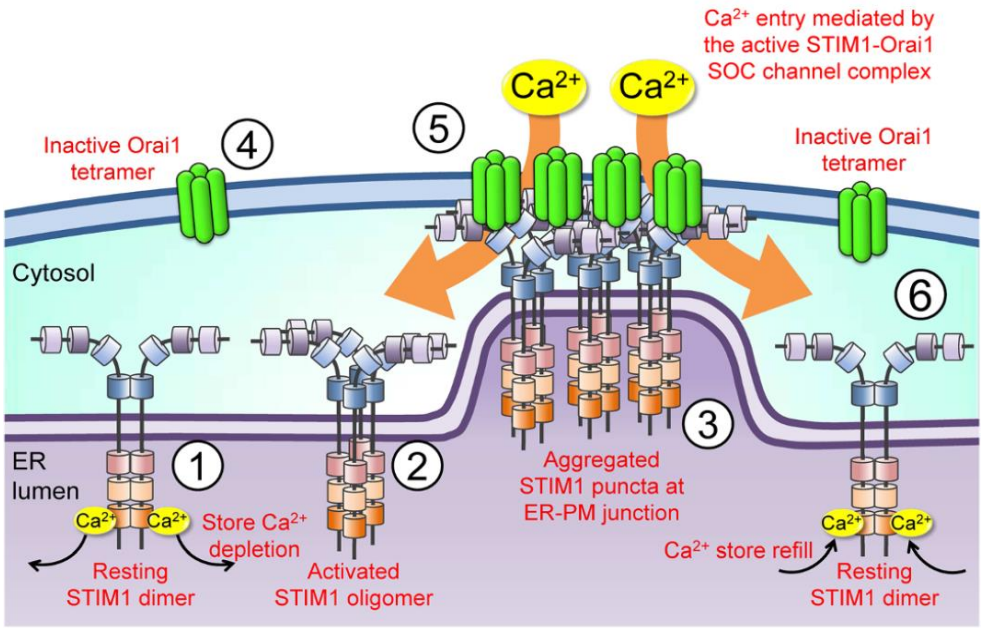

Adapted from Chen, *Journal of Biomedical Science*, 2013 (165)

Figure 47. STIM1 regulation of SOCE.

(1-2) Depletion of ER Ca^{2+} causes Ca^{2+} dissociation from STIM1 and STIM1 oligomerization. **(3)** STIM1 relocalization at ER-PM sites. **(4-5)** Orai1 goes from an inactive state to the formation of the active STIM1/Orai1 complex that opens the Orai1 channel, allowing Ca^{2+} entry. **(6)** Upon ER refilling, STIM1 binds calcium again.

STIM1-Orai1 interactions are not the only ER-PM contacts regulated by calcium. Indeed, the elevation of cytosolic calcium induced by SOCE triggers the recruitment of E-Syt1 (Extendend Synaptotagmin-1), a transmembrane protein resident in peripheral ER (137,141), at the PM. The formation of these tightly regulated contact sites can be required to facilitate lipid exchanges between the ER and the PM. Moreover, other members of the E-Syt family (E-Syt2 and E-Syt-3) that are not regulated by calcium, are also involved in contact site formation but rely on the interactions of E-Syt proteins with PI(4,5)P2 at the level of the PM (141). Interestingly, we found E-syt1 in our MS screening but its ablation, alone or in combination with the KD of E-syt2 and E-syt3, did not alter EGFR-NCE. These results suggest, once again, specificity in contact site and calcium-regulated pathways.

6. A possible role for calcium in EGFR-NCE

The mechanism of Ca^{2+} action is not known. In the literature, there are evidences for the involvement of calcium in endocytic events at the synapse (166). The problem with the analysis of calcium at synapses is that it is difficult to separate the study on endocytosis from the exocytic process of neurotransmitter release, a process regulated by calcium (166). Moreover, data on the effect of calcium in the endocytic process at synapses are discordant; indeed, calcium has been shown to be able to have a positive, a negative or no effect on endocytosis (167). It is possible that calcium signaling can have different outputs depending on the cell line under scrutiny or that calcium is differentially required in distinct endocytic pathways (168). Calcium has an established role in CME at synapses; it is able to regulate the interaction between dynamin 1 and calcineurin that act as a calcium sensor. Calcineurin is activated when it binds calcium and then dephosphorylates different proteins belonging to the synaptic endocytic machinery, among which dynamin 1, that upon dephosphorylation can localize at the PM and regulate endocytosis (169,170). Given this direct role of calcium in the activation of dynamin 1 in neurons, one possibility could be that in EGFR-NCE the EGF-induced calcium may be required for the regulation of dynamin 2 function, although no evidence for this is present in the literature.

Another hypothesis is that calcium may be critical for rearrangements of the actin cortex cytoskeleton that is required to facilitate the fission of endocytic intermediates from the PM. Indeed, actin appears to be required in different NCE pathways for the fission step, in some cases together with dynamin (4,5,32,49,52). Moreover, many enzymes involved in the actin machinery appear to be regulated by calcium, first of all gelsolin, which is needed for actin polymerization, and also the actin-binding proteins myosin II and L-plastin. Other proteins are not directly regulated by calcium but are controlled by the calcium-dependent protease calpain. Among these proteins, there are talin, ezrin and WASp (Wiskott-Aldrich syndrome); the latter, in particular, is involved in the activation of the Arp2/3 complex that is

required for the polymerization of new F-actin. Close correlation between calcium signaling and actin remodeling has been described especially in T-cell activation. In this cell context, polymerization of actin appears to be necessary for the calcium release upon activation of the T-cell receptor (TCR) and, in a bidirectional control, calcium is needed for cytoskeletal remodeling (171). Actin is important in the control of the calcium cascade also because it is involved in the formation of the scaffold that is necessary for the association of the TCR with the enzyme PLCγ (172).

PLCγ plays an important role in the calcium cascade, from the scission of phosphatidylinositol 4,5-bisphosphate PLCγ produces IP3 and diacylglycerol (DAG). In EGFR-NCE, IP3 is necessary for the release of calcium from the ER and is known that PLCγ is directly phosphorylated and activated by the EGFR (173). We are currently evaluating the role of PLCγ in EGFR-NCE, by analyzing phosphorylation of PLCγ in response to increasing EGF doses, and the impact of PLCγ inhibition on the EGF-induced Ca^{2+} wave and EGFR internalization. Together, these experiments will help us define the molecular cascade that leads to the release of Ca^{2+} from the ER upon stimulation with high EGF doses. We are also planning to test if the alteration of PLCγ could have any impact on actin and, conversely, if the alteration of the actin machinery would result in an altered regulation of PLCγ.

7. Classical and new techniques to follow calcium signaling

We undertook two techniques to follow calcium kinetics: aequorin and Fura-2, AM. Aequorin can be targeted at the PM, where NCE-contact sites take place, and gives information about a population of cells; however, it has a relatively low sensitivity for calcium and requires a good level of transfection. On the other side, Fura-2, AM is a diffusible probe that does not need any transfection and does not provide information about the localization of the calcium wave, but , instead, is more sensitive compared to aequorin and provides information about the calcium kinetics at a single cell level. Considering the lower sensitivity of aequorin, it was

important for us to characterize all phenotypes observed with PM-aequorin also with Fura-2, AM. This double approach led us, for example, to conclude that a calcium movement cannot be excluded upon stimulation of cells with low dose of EGF (Figure 36b and Figure 40b). Thus suggesting that EGF is able to induce a calcium wave also at low dose, in this case, however, the release occurs more likely in the cytosol and not specifically at the PM since we were not able to score a clear calcium response with PM-aeq in cells stimulated with low dose of EGF.

Currently, we are characterizing a new, interesting calcium-probe, GCaMP6f (174) that can be targeted in different cellular compartments, like aequorin, but has higher calcium sensitivity compared to aequorin. GCaMPs have been developed for imaging of calcium peaks in neurons (165), in which calcium levels change rapidly and, thus, require an adequate probe with an accelerated off-response, broad sensitivity range of calcium and a good signal-to-noise ratio. Importantly, GCaMP6f appears to be a good tool also to follow calcium response in the context of EGFR-NCE: we confirmed the phenotypes scored with the other techniques and, in addition, this probe is able to detect the typical oscillatory behavior of calcium peaks that are not easily visible with aequorin or Fura-2, AM. We scored the formation of repeated peaks of calcium at the PM that we can describe as "*quanta*" that may be associated with specific "*quanta*" of signaling in cells stimulated with high dose of EGF. Further experiments are needed to unravel this fascinating possibility.

8. NCE cargoes

We identified CD147 as a cargo that can enter the cell together with EGFR through NCE upon EGF stimulation. Importantly, differently from EGFR, CD147 is internalized almost exclusively via NCE in this specific setting and can, thus, be used as a specific marker for NCE. Of note, the entrance of CD147 into NCE structures is unlikely to be a passive entrapment, since CD147 internalized only into EGFR-containing TIs and not into EGFR-internalizing CCPs (unpublished data). Thus, the mechanism induced by EGF stimulation might regulate its entrance specifically via NCE. For EGFR, we have shown that ubiquitination is the signal that activates NCE (22,111). Intriguingly, CD147 was previously found in the EGF-regulated Ubiproteome (175). In addition, in the literature, growing evidences indicate that trafficking of PM transporters and carriers, among which also CD147, is regulated by ubiquitination (46,176,177). Thus, we can speculate that CD147 internalization through NCE depends on EGFR-activated ubiquitination events. This scenario might be true for other PM proteins subjected to regulation by ubiquitination.

CD147 is a transmembrane glycoprotein particularly enriched in PM of tumour cells and correlates significantly with poor prognosis in breast and ovarian cancer (178,179). CD147 has different functions but is primarily involved in the induction of matrix metallo-proteinases, a feature that renders CD147 responsible for different malignant features like invasiveness and anchorage-independent growth (180). Thus, regulation of CD147 PM levels and its intracellular fate by EGFR-NCE could be relevant for tumor progression and invasion.

Additional connections between MMP-9 (metallo-proteinases 9), one of the principal MMPs induced by CD147, calcium and EGF are present in the literature. In particular, it has been proven that calcium and EGF act together in wound healing, being more effective together than alone (181). Furthermore, in the absence of MMP-9, EGF alone does not o stimulate migration, but the increase of calcium concentration reverts this phenotype (181),

suggesting an interesting correlation between EGF, calcium and MMP9, one of the main substrates controlled by the NCE-cargo CD147.

9. Different players and integration of their function in EGFR-NCE

It remains to be established whether the identified candidates are involved in EGFR-NCE. The mechanisms underlying this pathway appear relatively complex, as the list of regulators includes, apart from ER, also mitochondrial, nuclear and RNA-binding proteins.

One of the most interesting candidates is Enoyl CoA hydratase 1 (ECHS1). The enzyme ECHS1 catalyzes the second step of mitochondrial fatty acid beta-oxidation by hydration of enoyl CoA intermediates to the S-hydroxyacyl-thioesters. ECHS1 works as a homohexamer with an integrated hydratase activity and, in fractionation studies, was found associated with mitochondrial membranes (182). Considering the function of ECHS1, and the fact that EGFR-NCE relies on cholesterol/sphingolipids-enriched PM microdomains (lipid-rafts); an interesting hypothesis is that ECHS1 might regulate lipid rafts at the level of the PM, influencing EGFR-NCE. It is possible that a small percentage of the enzyme is localized or translocated at the PM, or ECHS1 may act from its mitochondrial localization in correspondence with mitochondria-PM contact sites (183).

Functional crosstalk between PM, ER and mitochondria has been reported; for example, it is known that calcium coming from the extracellular space first has to cross the ER and can then be directed into mitochondria (184). Moreover, PM-ER-mitochondrial association has been proposed to regulate SOCE (183,185). Considering these evidences, the presence of mitochondria in correspondence with ER-PM contact sites might be connected to local calcium fluxes needed for EGFR-NCE. To test this hypothesis, we will perform

localization studies using EM analysis in order to visualize possible contact sites between mitochondria and PM in correspondence with EGFR-NCE structures.

In the literature, a possible role for RNA-binding proteins in different cell functions is emerging, for example in cell signaling (186), cell spreading (187), cell adhesion and migration (188). In EGFR-NCE, RNA-binding proteins might be involved in local translation of proteins (e.g., NCE functional regulators) at sites where they act, as reported for actin (188), or may recruit RNAs (e.g., non-coding RNAs, ncRNAs) that have a structural role, acting as molecular scaffold or signaling platforms, as it was shown in DNA damage response (189,190) and in the regulation of transcription (191). An interesting link between signaling from tyrosine-kinase receptors and RNA can be represented by one of the functional regulators, KHDRBS1, also known as Sam68. This protein is tyrosine phosphorylated and it can interact with SH2-containing proteins; it was shown to interact with the SH3 domain of Grb2 and to bind to RNA; thus, it can possibly work as a docking station to recruit other signaling molecules (192). Sam68 if often found in complex with up to 40 proteins, many of which are RNA-binding proteins and, interestingly, some evidences suggest that, upon EGF stimulation, Sam68 exits from these complexes and localizes into smaller ones. This translocation appears to be linked with the ability of Sam68 to promote cell migration upon stimulus (193).

To conclude, we have described a novel modality of internalization that depends on the formation of ER-PM contact sites and possibly requires the integration of numerous cellular functions. Further studies will define if the functional regulators identified in this study are involved only in EGFR-NCE or if they are also involved in other endocytic pathways. NCE has a major role in the regulation of EGFR as it is involved in the regulation of receptor degradation. It is now important to characterize the possible alterations of NCE players in pathological conditions involving aberrant receptor signaling.

10. Future directions

10.1 EM analysis to unravel the role of NCE-functional regulators

We have extensively characterized the effect of RTN3 KD on NCE function and morphology, especially through the usage of EM. We plan to extend this analysis to other NCE regulators in TI formation and in contact site formation by using ruthenium red and HRP-KDEL staining, respectively. These experiments will allow us to understand whether other NCE regulators are acting upstream or downstream of RTN3. In particular, we will first characterize the remaining three ER-resident proteins (REEP5, PLOD1, P4HB) identified in our proteomic screening, which could have a role in the formation of ER-PM contact sites. We will then characterize the role of ECHS1, due to its mitochondrial localization, and considering the known association between mitochondria, ER and PM (114), it will be interesting to evaluate the effect of ECHS1 KD on NCE structures and even on the localization of mitochondria.

10.2 The interaction of ER proteins with EGFR

Based on the hypothetical, indirect interaction between EGFR and RTN3, we aim to identify other ER-resident proteins that may directly contact the active EGFR at the PM and work as tethering factors. To this aim, we plan to employ unbiased proteomics strategies, such as the APEX2 technique, that has been already successfully employed for ER-PM junction proteomics analysis (194). In order to enrich for ER-localized or ER-proximal proteins, we will exploit an APEX2 construct targeted at the level of the ER membrane. We will stimulate cells with high dose of EGF to induce the formation of ER-PM contact sites in correspondence with activated EGFR. Thanks to the activity of APEX2, proteins that are in close proximity with the ER will be biotinylated upon addition of biotin-phenol and will be

easily recovered by IP with beads covered with streptavidin, allowing for isolation of protein in close proximity and/or transiently interacting with EGFR. We will couple this IP with an IP against EGFR in order to specifically select what is both EGFR-bound and biotinylated. Thus, we will recover proteins involved in the formation of ER-PM contacts that are required for the NCE of EGFR.

10.3 Defining the role of RTN3 and other NCE players in EGFR signaling, degradation and biological responses

Our laboratory has previously showed that NCE plays a crucial role in EGFR downmodulation and signal extinction (63). We have already tested the effect of RTN3 silencing on EGFR degradation by WB and ^{125}I-EGF-based degradation assays in HeLa cells. Importantly, we scored a significant delay in EGFR degradation upon RTN3 KD. We now wish to extend the analysis of the effect of RTN3 KD on EGFR internalization to other cell lines in order to identify a suitable cell model, in addition to HeLa cells, to study the impact of NCE on EGFR signaling outputs. We will then assess the effects of RTN3 silencing on i) EGFR signaling, by assessing the activation of the EGFR (e.g., EGFR phosphorylation and ubiquitination) and downstream effectors (e.g., Shc, ERKs, PI3K,) by WB analysis; ii) EGF-dependent calcium signaling; and iii) EGF-dependent biological responses, such as proliferation (growth curves, colony assays in 2D-culture and in 3D-semisolid medium, i.e., soft agar assay) and/or migration (wound healing, transwell assay).

10.4 Defining the relevance of EGFR-NCE in physiology and cancer

Given the role of EGFR-NCE in signal extinction in the presence of high ligand concentration, an intriguing hypothesis is that alterations of NCE might contribute to aberrant EGFR signaling in cancer. We will screen a panel of human normal vs. cancer primary cells (lung, prostate and/or breast, available at our Institute through a collaboration with the Molecular Medicine Unit at the IEO, Milan) by performing ^{125}I-EGF internalization assays upon KD of clathrin (CME is inhibited), RTN3 (NCE is inhibited), or dynamin (CME and NCE are inhibited) to verify the existence of the NCE pathway in primary cells and its possible alteration in cancer cells. Depending on the results, analysis of EGFR degradation/signaling and EGF-dependent proliferation will be performed.

Moreover, in order to characterize possible alterations of RTN3, as the best-characterized NCE functional regulator, we plan to analyze RNA samples coming from different types of cancer. We will analyze the presence of RTN3 mutations, its splicing patterns and the levels of RTN3 expression; eventually, this analysis will be extended to other NCE regulators. We will first focus on breast and lung cancer, for which we have enormous collections of patient material and complete clinical follow-up data.

ACKNOWLEDGMENTS

I would like to thank my Ph.D. Supervisor, Professor Pier Paolo Di Fiore for the opportunity to follow this project and for his constant guidance. I would like to thank also my added Supervisor, Sara Sigismund for her everyday supervision and teaching during the years.

A special thank goes to Giusi Caldieri who worked with me on this project, for all the support, guidance, and help in many ways; a thank goes also to all the group of Sara Sigismund, actual and previous members, in particular Gilda Nappo who started the project and followed my work at the beginning.

I would like to thank our collaborators, whose work and suggestions have been fundamental for this project: Andrea Raimondi and Davide Mazza from San Raffaele Institute, Milan; Massimo Bonora and Professor Paolo Pinton from Univerisity of Ferrara, Ferrara.

I also want to thank Wessen Maruwge, for critically reading my thesis. I'm grateful to Professor Harald Stenmark at Oslo University Hospital and Dr Simona Polo at IFOM for their useful suggestions and support during the years.

MATERIALS AND METHODS

1. Solutions

1.1 Phosphate-buffered saline

NaCl	137 mM
KCl	2.7 mM
Na_2HPO_4	10 mM
KH_2PO_4	2 mM

8 g of NaCl, 0.2 g of KCl, 1.44 g of Na_2HPO_4, and 0.24 g of KH_2PO_4 are solved in 800 ml of distilled H_2O (ddH_2O). The pH is adjusted to 7.4 with HCl and volume is brought to 1 litre with ddH_2O.

1.2 Tris-HCl (1 M)

121.1 g of Tris base are dissolved in 800 ml distilled H_2O. The pH is adjusted to 7.4, 7.6 or 8.0 (depending on the case) with HCl, and ddH_2O is added to bring volume to 1 litre.

1.3 Tris-buffered saline (TBS)

NaCl	137 mM
KCl	2.7 mM
Tris HCl pH 7.4	25 mM

8 g of NaCl, 0.2 g of KCl, and 3 g of Tris base are solved in 800 ml of distilled H_2O.

The pH is adjusted to 7.4 with HCl and ddH_2O is added to bring volume to 1 litre.

1.4 10X SDS-PAGE running buffer

Glycine	192 mM
Tris HCl, pH 8.3	250 mM
SDS	1%

1.5 10X Western transfer buffer

Glycine	192 mM
Tris HCl, pH 8.3	250 mM

For 1X western transfer buffer, the 10X stock is diluted 1:10 with ddH_2O and 20% v/v methanol or ethanol is added.

1.6 10X Tris EDTA

Tris HCl, pH 7.4	100 mM
EDTA, pH 8	10 mM

1.7 50X TAE (Tris-Acetate-EDTA)

Tris base	2 M
Acetic acid	1 M
EDTA, pH 8	10 mM

The pH is adjusted to 8.5 with HCl and ddH_2O is added to 1 litre.

2. Protein buffers

2.1 1X JS buffer

HEPES, pH 7.4	50 mM
NaCl	150 mM
Glycerol	10%
Triton X-100	1%
$MgCl_2$	1.5 mM
EGTA	5 mM

200X Proteases inhibitor cocktail from Calbiochem, sodium pyrophosphate pH 7.5 20 mM, sodium fluoride 250 mM, PMSF 2 mM, and sodium orthovanadate 10 mM are added to the buffer just before use.

2.2 1X Laemmli buffer

SDS	2%
Tris HCl, pH 6.8	62.5 mM
Glycerol	10 %
Bromophenol blue	0.1 %
β-Mercaptoethanol	5 % (v/v)

3. Reagents

EGF was from PeproTech; Alexa-EGF (555 and 647) were from Molecular Probes; ^{125}I-EGF and ^{125}I-Tf from PerkinElmer. Protein-A Gold 10 nm was from Utrecht University; EM grade glutaraldehyde and paraformaldehyde employed for EM were from Electron Microscopy Sciences; ruthenium red is from Sigma. Fura-2, AM was from ThermoFisher. Ionomycin, calcium chloride, Pluronic F-68, sulfinpyrazone, coelentarazine were from Sigma. Xestospongin C was from Abcam.

3.1 Antibodies

Primary antibodies were: rabbit polyclonal anti-EGFR (in-house), directed against amino acids 1172-1186 of human EGFR, used in IB; mouse anti-EGFR 13A9 (Genentech) used to follow endocytosis in EM analyses and in super-resolution; mouse anti-CD147 (BD); rabbit and rat anti-RTN3 (in-house), directed against amino acids 1-47, common to all isoforms; anti-dynamin-1, anti-dynamin-2, (Santa Cruz); anti-HA (BABCO); anti-tubulin (Sigma); anti-clathrin heavy chain used for IB (BD). Fluorescent secondary antibodies were from Molecular Probes. Cage 550 secondary antibody for Super-resolution microscopy was from Aberrior.

3.2 RNAi oligos

Silencing oligo sequences were:

clathrin heavy chain (Riboxx): UAAAUUUCCGGGCAAAGAGCCCCC

dynamin 1 (Riboxx): UUUCACAAUGGUCUCAAAGCCCCC

dynamin 2 (Riboxx): UGAACUGCAGGAUCAUGUCCCCC

Caveolin-1 (Dharmacon): GGCCAGCUUCACCACCUUC

Cdc42 (Stealth, Invitrogen): CCUCUACUAUUGAGAAACUUGCCAA

GRAF1 (Stealth Select RNAi™ siRNA): CCACUCAUGAUGUACCAGUUUCAAA

Rac1 (Stealth, Invitrogen): CCGGUGAAUCUGGGCUUAUGGGAUA

Rac2 (Stealth, Invitrogen): ACCUGCCUUCUCAUCAGCUACACCA

Arf6 (Stealth, Invitrogen): AAGCTGCACCGCATTATCAATTT

RhoA (Stealth, Invitrogen): GAUACCGAUGUUAUACUGAUGUGUU

RTN3-2 (Stealth, Invitrogen): 5'-CCCUGAAACUCAUUAUUCGUCUCUU-3'

REEP5-4 (Riboxx): UUAAUUGAGAUGUAGGCUGCCCCC

For RTN4 KD, we used two silencing oligos (Stealth, Invitrogen):

RTN4-1: 5'-CCAGCCUAUUCCUGCUGCUUUCAUU-3'

RTN4-2: 5'-CCUAUUCCUGCUGCUUUCAUUGACA-3'

For Endophilin A1 and A2 KD, we used a single silencing oligo and a pool of four oligos (Riboxx), respectively:

Endophilin A1: 5'-AUUAUUUCCAUCACAGCCCCC-3'

Endophlin A2-pool: 5'-UUUGAAGUCAUCAUCCAGCCCCC-3'

5'-UCUUCUUGUAGUCAAAGUCCCCC-3'

5'-ACUGGAACCUUUGUGCUUGCCCCC-3'

5'-UCGAUCCCAUCCUGUUAAGCCCCC-3'

For ZFR KD, we used a pool of four oligos (Riboxx):

ZFR_1 UUUAUUUCCUGUUGACUGCCCCC

ZFR_2 AUAUGAGUAUGAAUCCUGGCCCCC

ZFR_3 ACUUUAGUGUUAGAUGUGCCCCC

ZFR_4 AUAAUACCUAACACUGUACCCCC

For ECHS1 KD, we used a pool of four oligos (Riboxx):

ECHS1_1 AUUCACUGAUUCUUUGGCCCCC

ECHS1_2 UAUCACUUUAAUCAGCAUCCCCC

ECHS1_3 UUCCUAUUAAGAUCUCCGGCCCCC

ECHS1_4 ACUUCCUUCUGUUAAUGUCCCCC

For P4HB KD, we used a pool of four oligos (Dharmacon):

P4HB_1 CCAAGAGUGUGUCUGACUA

P4HB_2 GUGACGUGUUCUCCAAAUA

P4HB_3 GAACGCACGCUGGAUGGUU

P4HB_4 UGACAUACCAUUUGGGAUC

For PLOD1 KD, we used a pool of four oligos (Dharmacon):

PLOD1_1 CUGGACGACUCACGCAUUA

PLOD1_2 GAGAACGUGCCGACUAUUG

PLOD1_3 AGAGGGAGCAGAUCAAUAU

PLOD1_4 CUUCGUCGAUCCCUAAUUG

For LRPPRC KD, we used a pool of four oligos (Dharmacon):

LRPPRC_1 UAACAUAGAUGCCGCAAUA

LRPPRC_2 GAUGAGAGAUGCCGGAAUU

LRPPRC_3 GAAAUUAGGUGCUGUGUAU

LRPPRC_4 GUACAAGGAUGGACGUUAU

For TPR KD, we used a single oligo (Dharmacon)

TPR_1 GAAGAAGUGCGUAAGAAUA

For KHDRBS1 KD, we used a single oligo (Dharmacon)

KHDRBS1_1 GAAAGAGCGAGUGCUGAUA

3.3 TaqMAN assays for Q-PCR (ThermoFisher)

Gene Symbol	TaqmMAN assay
SH3GL1	Hs04235263_g1
SH3GL2	Hs00182352_m1
RTN4	Hs01103689_m1
REEP5	Hs01075582_m1
CLTC	Hs00964480_m1

4. Cloning technique

4.1 Agarose gel electrophoresis

DNA samples were loaded on 0.8%-2% agarose gels along with DNA markers. Gels were made in TAE buffer containing Gel Red (Biotium), according to manufacturer instructions, and run at 80 V until desired separation was achieved. DNA bands were visualized under a UV lamp.

4.2 Minipreps

Clones picked from individual colonies were used to inoculate 2 ml LB (containing the appropriate antibiotic) and grown overnight at 37°C. Bacteria were transferred to Eppendorf tubes and pelleted for 5 minutes at 16,000 xg. Minipreps were performed with the Wizard Plus SV Minipreps Kit (Promega) following manufacturer instructions. The plasmids were eluted in 50 µl nuclease free H2O.

4.3 Diagnostic DNA restriction

Between 0.5 and 5 μg DNA were digested for 2 hours at 37°C with 10-20 units of restriction enzyme (New England Biolabs). For digestion, the volume was made up depending on the DNA volume to 20-50 μl with the appropriate buffer and ddH_2O.

4.4 Large scale plasmid preparation

Cells containing transfected DNA were expanded into 250 ml cultures overnight. Plasmid DNA was isolated from these cells using the Qiagen Maxi-prep kit according to manufacturer instructions.

4.5 Transformation of competent cells

An aliquot of competent cells TOP10 (Invitrogen) were thawed on ice for approximately 10 minutes prior to the addition of plasmid DNA. Cells were incubated with DNA on ice for 30 minutes and then subjected to a heat shock for 45 seconds at 42°C. Cells were returned to ice for 5 additional minutes. Then, 300 μl of SOC was added and the cells were left at 37°C for further 60 minutes before plating them onto plates with the appropriate antibiotic. Two plates for each reaction were used, one plated with 100 μl of the transformed bacterial cells and the other one with the rest. Plates were incubated overnight at 37°C.

5. Constructs and plasmids

Human RTN3A cDNA (NM_006054) was purchased from Origene (pCMV6-AC-GFP vector) and cloned by PCR in the pECFP-N1 vector (Clontech) or in the pBABE-puro vector fused to HA-tag (22). Human EGFR was subcloned from pBABE-EGFR (111), (22) in pEYFP-N1 vector (Clontech). Esyt1-GFP was a kind gift from Pietro De Camilli (Yale School of Medicine). Cerulean-17 (Cer-17) was a kind gift from Nica Borgese (CNR, Milan).

Cerulean empty vector was a gift from Dave Piston (Addgene plasmid #15214). RTN4a-GFP was a kind gift from Gia Voeltz (Addgene plasmid #61807), pAc-GFPC1-Sec61β was a gift from Tom Rapoport (Addgene plasmid #15108), STIM1-CFP was a gift from Anjana Rao (Addgene plasmid # 19755). RTN4a and STIM1 were subcloned by PCR in pECFP-N1 vector (Clontech). Sec61β was subcloned by PCR in pCDNA3-ECFP vector (Addgene), generating ECFP-Sec61β. Snap25-Aequorin was a kind gift from Pinton Lab (195).pGP-CMV-GCaMP6f was a gift from Douglas Kim (Addgene plasmid # 40755) and for the SNAP25 tagged version the sequence of Snap25-Aequorin was used as template for the PCR reaction.

All clones were sequence-verified.

The primers were designed of similar length and annealing temperature (calculated running the primers on simulated PCR reactions, using MacVector programme). The primers were designed with suitable restriction sites, or according to the manufacturer instruction when used the In-Fusion HD® PCR cloning. These primers were used in a PCR reaction together with the DNA template and the Phusion high fidelity DNA polymerase (FINNZYMES), according to manufacturer instructions. Primers are listed in the following table:

RTN3A_XhoI_F	GGCGCTAGCATGGCGGAGCCGTCGGCG
RTN3A _ XhoI_R	GGCGCTAGCGCTTCTGCCTTTTTTTTGGCG
EGFR_ XhoI _F	CGCTCGAGATGCGACCCTCCGGGACG
EGFR _ SacII_R	CGCCGCGGTGCTCCAATAAATTCACTGC
Sec61β_EcoRI_F	GCTGTACAAGGAATTCCCTGGTCCGACCCCCAGT
Sec61β_EcoRI_R	GATATCTGCAGAATTCCTACGAACGAGTGTACTTG
RTN4a_BamHI_F	CGCGGGCCCGGGATCATGGAAGACCTGGACCAG
RTN4a_BamHI _R	GGCGACCGGTGGATCTTCAGCTTTGCGCTTCAATC

Stim1_BamHI_F	CGCGGGCCCGGGATCATGGATGTATGCGTCCGTC
Stim1_BamHI _R	GGCGACCGGTGGATCCTTCTTAAGAGGCTTCTTAAA
Snap25_BglII_F	TACCGGACTCAGATCTATGGCCGAAGACGCAGAC
Snap25_BglII_R	CATGGTGGCGAGATCTATACCACTTCCCAGCATCT

The cycling parameters are summarized in the following table.

Step	Temperature	Time	# Cycles
A	98°C	30 seconds	1
B	98°C 50-65°C (calculated for each primer pair) 72°C	30 seconds 30 seconds 60 seconds	25-30
C	72°C	7 minutes	1
D	4°C	∞	1

5.1 Site directed mutagenesis

For rescue experiments, we generated a cDNA of RTN3A resistant to RNAi oligo RTN3-2 (section 3.2) by introducing 8 silent mutations by site-directed mutagenesis (oligo seq: GTTGATCATCCGCTTGTT) into the pBABE-HA-RTN3A construct.

6. Cell culture

6.1 Cell culture media

HeLa cells were grown in GlutaMAX™-Minimum Essential Medium (MEM, Gibco Invitrogen), supplemented with 10% FBS (PAA), sodium pyruvate 1 mM (Euroclone), non-essential aminoacids (Euroclone).

6.2 Transfections

- RNAi transfections

RNAi transfections were performed using LipofectAMINE RNAi MAX reagent from Invitrogen. Cells were treated according to the following scheme:

Day 1	Reverse transfection	250,000 cells in a 6-well plate 8 nM RNAi oligo 4 µl of LipofectAMINE RNAi MAX
Day 2	Forward transfection	8 nM RNAi oligo 4 µl of LipofectAMINE RNAi MAX
Day 3	-	
Day 4	Split cells	Cells plated at the proper concentration for the final assay
Day 5	Check KD Assay	

- DNA transfection with FuGENE

For immunofluorescence study, DNA transfections were performed using FuGENE 6 reagent from Roche, according to manufacturer instructions. Briefly, cells were plated at 50% confluency on gelatin-coated coverslips placed in 10-cm dishes. The day after cells were transfected with 8 µg DNA and 6 µl FuGENE 6. 24 hours after transfection cells were stimulated with Alexa555-EGF and internalization assay was performed.

- DNA transfection with calcium phosphate

For aequorin and GCaMP6f measurements, cells were plated on 13mm coverslips placed in 6 wells plates in order to obtain for the day after cells at 40-60% of confluence. After 24 hours from plating, cells were transfected with the mix obtained adding to 100 µl of HBS solution

(50 mM HEPES, 280 mM NaCl, 1.5 mM Na_2HPO4, pH to 7.0), the mix composed by 10 µl of $CaCl_2$, 6 µg of DNA to a volume of 100 µl with sterile H_2O. The reaction was left for 20 minutes at RT to allow the formation of complexes and was then added drop by drop on cells and left over night at 37 ^oC. The day after cells were washed with PBS at least four times to remove the precipitate and fresh medium was added. 48 hours post transfection cells were analyzed.

6.3 Retroviral infection

Stable population of HeLa cells expressing RTN3A (used for reconstitution experiments) were generated by infecting cells with retroviral vector. Retroviruses were produced by transfecting the Phoenix helper cell line with 5 µg of DNA. 48 hours after transfection, supernatant was collected and passed through a 0.45 µm filter. After the addition of 8 µg/ml polybrene (Hexadimethirne bromide, Sigma), the supernatant was added to HeLa cells plated on 10 cm cell culture dishes. Two cycles of infection were repeated, after which the medium was replaced by standard HeLa medium. 48 hours after infection, selection of infected cells was performed by adding puromycin at a concentration of 1.5 µg/ml.

7. Protein procedures

7.1 Cell lysis

After washing with PBS 1X, cells were lysed in JS directly on the plates using a cell-scraper and clarified by centrifugation at 16,000 xg for 10 min at 4ºC. Protein concentration was measured by the Bradford assay (Biorad), following manufacturer instructions.

7.2 SDS-Polyacrylamide gel electrophoresis (SDS-PAGE)

Gels for resolution of proteins were made from a 30%, 37,5:1 mix of acrylamide: bisacrylamide (Sigma). As polymerisation catalysts, 10% ammonium persulphate (APS) and TEMED were used.

Separating gel mix

	Gel %			
	6	**8**	**10**	**15**
Acrylamide mix (ml)	2	2.7	3.3	5
1.5M Tris HCl pH 8.8 (ml)	2.5	2.5	2.5	2.5
ddH_2O (ml)	5.3	4.6	4	2.3
10% SDS (ml)	0.1	0.1	0.1	0.1
10% APS (ml)	0.1	0.1	0.1	0.1
TEMED	0.01	0.01	0.01	0.01
TOTAL (ml)	10	10	10	10

Stacking gel mix

Acrylamide mix (ml)	1.68
1M Tris HCl pH 6.8 (ml)	1.36
ddH_2O (ml)	6.8
10% SDS (ml)	0.1
10% APS (ml)	0.1
TEMED (ml)	0.01
TOTAL (ml)	10

7.3 Western Blot (WB)

Desired amounts of proteins were loaded onto 1.5 mm thick SDS-PAGE gels for electrophoresis (Biorad). Proteins were transferred in western transfer tanks (Biorad) to nitrocellulose (Schleicher and Schnell) in 1X Western transfer buffer (supplemented with 20% methanol) at 30 V overnight or 100 V for 1 hour.

Otherwise proteins were loaded onto Criterion™ TGX™ gels (Biorad) and trasferred with Trans-Blot® Turbo™ Nitrocellulose with the Trans-Blot® Turbo™ Transfer System (Biorad).

Ponceau staining was used to reveal roughly the amount of protein transferred to the filters. Filters were blocked 1 hour (or overnight) in 5% milk in TBS supplemented with 0.1% Tween (TBS-T). After blocking, filters were incubated with the primary antibody, diluted in TBS-T 5% milk for one hour at room temperature, followed by three washes of five minutes each in TBS-T and then incubated with the appropriate horseradish peroxidase-conjugated secondary antibody diluted in TBS-T for 30 min. After the incubation with the secondary antibody, the filter was washed three times in TBS-T and the bound secondary antibody was revealed using the ECL method (Amersham).

7.4 Co-Immunoprecipitation

Lysates prepared in JS buffer were incubated in the presence of specific antibodies (about 1-2 μg/mg of lysates) for 2 hours at 4ºC with rocking. Protein G Sepharose beads (Zymed) were then added, and samples were left for an additional hour at 4ºC, rocking. Immunoprecipitates were then washed 4 times in JS buffer.

8. Quantitative real-time PCR analysis

Total RNA was extracted from HeLa cells (control and KDs, as indicated) using the RNeasy kit from Qiagen, according to the manufacturer's protocol. Single stranded cDNA synthesis was performed using the QuantiTect Reverse Transcription Kit (Qiagen) following manufacturer's instructions.

For the analysis of RTN3 isoform expression in HeLa cells, the QuantiFast SYBR Green PCR Kit (Qiagen) was used, according to manufacturer's instructions. Light cycler 480 instrument for qPCR was from Roche.

Below is the sequence of the oligos used:

RTN3(A+D+G)-for	5'-CTGTGCGGTGCACGATCT-3'
RTN3(A+D+G)-rev	5'-ACAGCTTGGATGACGGACTT-3'
RTN3B-for	5'-CTGTGCGGAGGGATTGAG-3'
RTN3B-rev	5'-GCTCCCTAACACATGGCTTT-3'
RTN3C-for	5'-ACCTCACAAGTGCACGATCT-3'
RTN3C-rev	5'-TGACAGAGAGAAGAGCCAGGA-3'
RTN3D-for	5'-TGAGAAGTACAAGGATCCAAGC-3'
RTN3D-rev	5'-AATGGTGTTTTAGTAACTGTTGCATT-3'
RTN3E-for	5'-CCTCACAAGAGGGATTGAGC-3'
RTN3E-rev	5'-TAGGCTGGCTCCCTAACACA-3'
RTN3F-for	5'-CTGTGCGGCCAGTTTCCC-3'
RTN3F-rev	5'-CTCAGTAGGTGGTTTCTGGGCTG-3'
RTN3G-for	5'-CCATTCAAACCCAGATTGATC-3'
RTN3E-rev*	5'-AATGGTGTTTTAGTAACTGTTGCATT-3'

(*same as RTN3D-rev)

RTN3all(-G)-for 5'-ACAGCCAGCTTCAAGGAGTC-3’

RTN3all(-G)-rev 5'-TGGAAAGCTTCTGAGGACAG-3’

For the analysis of KD levels by RT-qPCR, the Taqman chemistry (Thermo Fisher Scientific) was used. qPCR instrument was from Applied Biosystems. For the different genes, inventoried Taqman assays (Applied Biosystems) were employed.

9. Assays with ^{125}I-EGF and ^{125}I-Tf

9.1 Internalization assay with ^{125}I-EGF and ^{125}I-Tf

Cells were serum starved for at least 2 hours and then incubated at 37°C in the presence of ^{125}I-EGF or ^{125}I-Tf in binding buffer (MEM, BSA 0.1%, Hepes pH 7.4 20 mM). The concentration of radiolabelled EGF/Tf used in the assays was the following:

LOW DOSE EGF internalization	^{125}I-EGF: 1 ng/ml
HIGH DOSE EGF internalization	^{125}I-EGF: 1 ng/ml + unlabelled EGF: 29 ng/ml
Tf internalization	^{125}I-Tf: 1 ng/ml

After the indicated time points (2, 4, 6 min), cells were put on ice, washed three times in PBS, and then were incubated for 5 minutes at 4°C in 300 μl of acid wash solution pH 2.5 (acetic acid 0.2 M, NaCl 0.5 M). Then, the solution was removed from the cells and the radioactivity present into it was measured. This sample represents the amount of ^{125}I-EGF/Tf bound to the receptor on the cell surface. Cells were then lysed with 300 μl of a solution containing 1M

NaOH. This sample represents the amount of internalized ^{125}I-EGF/Tf. The unspecific binding was measured at each time points in the presence of an excess of non-radioactive EGF/Tf (300X and 500x respectively). After being corrected for non-specific binding, the rate of internalization was expressed as the ratio between internalized and surface-bound radioactivity. Endocytic rate constants [Ke and Ke obs, (111) were calculated from the slope of the trend-line. Results are expressed as the internalization rate constant (Ke or Ke obs) or as a % of Ke in control cells, as indicated, and are the mean of duplicate or triplicate points. Statistical analysis was performed using JMP 10.0 statistical software (SAS Institute, Inc). Student's t-test was used to calculate statistical significance among at least two biological replicas of the different conditions.

9.2 Saturation binding with ^{125}I-EGF

Cells were serum starved for at least 2 hours and then incubated in the presence of 5 ng/ml of ^{125}I-EGF in binding buffer (MEM, BSA 0.1%, Hepes pH 7.4 20 mM). To reach the final concentration of 100 ng/ml, unlabelled EGF was added to the mix. The cell were cooled on ice for 30 minutes and incubated at 4°C with mix containing ^{125}I-EGF. After six hours, cells were washed three times in PBS, and then were lysed with 300 µl of a solution containing 1M NaOH. This sample represents the amount of ^{125}I-EGF bound at the equilibrium, which is dependent on the number of EGFRs on the cell surface. The unspecific binding was measured at each time points in the presence of an excess of non-radioactive EGF (300X). After being corrected for non-specific binding, the assay provides the quantitative measurement of the number of EGFRs for each well. By counting the number of cells plated in each well, this assay allows to measure the number of surface EGFRs/cell.

9.3 EGFR recycling assay with ^{125}I-EGF

Cells were plated into 24 wells. The day after, cells were serum-starved for at least 2 hours in binding buffer and incubated for 15 minutes at 37°C with 20 ng/ml of ^{125}I-EGF: 5 ng/ml of ^{125}I-EGF + 15 ng/ml of cold EGF. Then, cells were put on ice, washed twice with cold PBS and incubated with mild acid/salt wash buffer (0.3 M Na acetate, 0.5 M NaCl pH 4.5) for 5 min and then washed 2 times with cold binding buffer. These cells (further referred to as "^{125}I-EGF-loaded cells") contained a large pool of intracellular ^{125}I-EGF and a minimal (less than 5%) surface pool of ^{125}I-EGF.

The ^{125}I-EGF-loaded cells were further incubated in binding medium with 4 ug/ml of unlabeled EGF at 37 °C for a chase time (0', 20', 40', 60', 90'), and the amount of degraded and intact ^{125}I-EGF in the medium as well as surface and intracellular labeled ligand was determined. Briefly, after each time points: i) the medium is collected, half to count directly (free total), half to perform TCA precipitation to distinguish between intact/recycled EGF (pellet) and degraded EGF (supernatant). The amount of degraded or intact ligand radioactivity in the medium/lysate was determined by precipitating with 5% trichloroacetic acid and counting supernatant and pellet. ii) Cells were washed twice with cold PBS and incubated with acid wash buffer pH 2.5 for 5 min at 4°, to determine the amount of surface-bound ^{125}I-EGF. iii) Cells were lysed in 1 N NaOH to determine the internalized amount of ^{125}I-EGF.

9.4 EGFR degradation assay with ^{125}I-EGF

Cells were plated into 24 well. The day after, cells were serum-starved for at least 2 hours in binding buffer and incubated for 15 minutes at 37°C with 20 ng/ml of ^{125}I-EGF: 5 ng/ml of ^{125}I-EGF + 15 ng/ml of cold EGF. Then, cells were put on ice, washed twice with cold PBS and incubated with mild acid/salt wash buffer (0.3 M Na acetate, 0.5 M NaCl pH 4.5) for 5

min and then washed 2 times with cold binding buffer. These cells (further referred to as "^{125}I-EGF-loaded cells") contained a large pool of intracellular ^{125}I-EGF and a minimal (less than 5%) surface pool of ^{125}I-EGF.

The ^{125}I-EGF-loaded cells were further incubated in binding medium with 4 ug/ml of unlabeled EGF at 37 °C for a chase time (0', 20', 40', 60', 90'), and the amount of degraded and intact ^{125}I-EGF in the medium as well as surface and intracellular labeled ligand was determined. Briefly, after each time points: i) the medium is collected, half to count directly (free total), half to perform TCA precipitation to distinguish between intact/recycled EGF (pellet) and degraded EGF (supernatant). The amount of degraded or intact ligand radioactivity in the medium/lysate was determined by precipitating with 5% trichloroacetic acid and counting supernatant and pellet. ii) Cells were washed twice with cold PBS and incubated with acid wash buffer pH 2.5 for 5 min at 4°, to determine the amount of surface-bound ^{125}I-EGF. iii) Cells were lysed in 1 N NaOH, half of the lysate was used to count directly (internalized total), half to perform TCA precipitation to distinguish between intact EGF (pellet) and degraded EGF (supernatant).

10. EGFR degradation

800,000 cells were plated on five 10-cm dishes. The day after cells were serum starved for 16 hours and stimulated for the indicated time points with high dose EGF. For EGFR degradation 15 µg of total cell lysate were loaded on a 7% SDS polyacrylammide gel. Western blots were performed as described in section 7.3.

11. Immunofluorescence and colocalization studies

11.1 IF-based EGF internalization assays and colocalization analysis

HeLa cells, plated on glass coverslips, were incubated at 37°C for the indicated times with high dose Alexa-conjugated EGF. Samples were then fixed in 4% paraformaldehyde. When indicated, acid wash treatment was performed before fixation, by incubating cells for 10 min at 4°C in an acidic buffer (acetic acid 0.2 M, NaCl 0.5 M) pH 2.5 followed by washes with Hepes-supplemented medium to restore pH before fixation. Cells were then permeabilized with 0.1% TritonX-100 in PBS supplemented with 1% (w/v) BSA, and labeled with primary antibodies against the protein of interest in PBS/BSA, followed by visualization by incubation with specific secondary antibodies. Images were obtained using a Leica TCS SP2 or TCS SP2 AOBS confocal microscope equipped with a 63X oil objective and processed using ImageJ.

11.2 *In vivo* internalization assays of EGFR or CD147 using antibodies

For antibody internalization assays, serum-starved HeLa cells were incubated with anti-EGFR 13A9 or CD147 antibody for 30 min at 4 °C or for 5 min at 37 °C (to avoid temperature shift), with comparable results. Cells were then stimulated with high dose Alexa-conjugated EGF at 37 °C for the indicated times. After internalization, cells were fixed and processed for IF. For CD147 internalization assays (45), non-permeabilized cells were incubated with an excess of Alexa-647 secondary antibody in PBS/BSA 1% (to saturate PM-localized CD147 antibody), followed by permeabilization and incubation with an Alexa-488 secondary antibody to label the internalized CD147 antibody (note that also residual PM-localized CD147, not-saturated by the Alexa-647 secondary antibody, is stained).

12. Super-Resolution Microscopy

HeLa cells were labeled *in vivo* for EGFR, stimulated with 100 ng/ml EGF for 2 min at 37°C, or left unstimulated. Additionally, HeLa cells stimulated with 1 ng/ml EGF for 2 min at 37°C were used to analyze cross-correlation in conditions where only CME is active. Samples were fixed in 4% paraformaldehyde, permeabilized and then labeled with anti- antibody, followed by incubation with anti-mouse Cage-550 and anti-rabbit Alexa 647 secondary antibodies.

Super-resolution localization imaging was obtained by direct stochastic optical reconstruction microscopy (dStorm) (138). Briefly, the fluorescent molecules are induced to blink on and off by reducing agents included in the imaging medium. If few molecules are fluorescent at each time, so that the diffraction limited spots corresponding to individual fluorophores are well separated, the position of each molecule can be quantified with higher accuracy than the resolution limit (196). By acquiring multiple images of the same field (tens to hundreds of thousands), and storing the position of the localized molecules at each frame it is therefore possible to obtain an image of the sample with resolution higher than the diffraction limit.

dStorm was performed on a Leica SR GSD-3D (Leica Microsystems Srl, Milan, Italy) super-resolution microscope equipped with a 150x 1.45NA objective, an Andor iXon Ultra-897 EM-CCD sensor and three solid state lasers (405 nm 100 mW, 488 nm 300 mW, and 647 nm 500 mW). The sample was mounted on the stage and the medium was substituted prior to acquisition with a mix of glucose oxidase (560 µg/ml), catalase (400 µg/ml) and cysteamine HCl (100 mM) in TN buffer with 10% glucose (w/v) pH 8.0, to induce blinking of the fluorophores (197). Alexa 647 and Cage 500 were imaged sequentially (starting from the red channels). 30,000 images were collected for each channel with 5 to 20 ms exposure times and an increasing ramp of 405 nm laser intensity with powers between 0 and 0.8 mW was used to reactivate the molecules in long-lived dark states. Only localization events occurring at the periphery of the cell were considered (within 2 µm from the PM). Furthermore, localization

events with less than 20 photons/pixel for the Alexa 647 dye and 40 photons/pixels for the Cage 500 dye were discarded. The list of the detected molecules in the two channels was used to compute the cross-correlation of the two images as described in (139): the cross-correlation curve was then fit by an exponential decay to quantify the degree of colocalization between EGFR-Cage500 and RTN3-Alexa647 and the size of the co-clusters, respectively provided by the cross-correlation amplitude C_0 and the correlation length R_c. For visualization purposes, the super-resolution images were reconstructed by rendering each of the detected molecules as a Gaussian distribution, with width equal to the localization precision of each event.

13. FRET

Cells were acquired with a Zeiss LSM 510 confocal microscope through a Plan-Apochromat 63x/1.4 Oil objective with a pixel size 0.139 □m, time acquisition between interval was 6,5 sec. ECFP and EYFP were excited through an Argon laser at 458 and 514 nm respectively, while EGF-555 was excited with a HeNe laser at 546 nm. Emissions were selected with the following band pass filters: BP 470-500 for ECFP, BP 530-600 for FRET and EYFP, BP 560-615 for EGF-555.

Sensitized emission FRET (SE-FRET) were calculated by a custom macro written for the open source FIJI software according to (198). For sensitized emission calculations, single fluorescent protein images for each channel were acquired.

In Figure 16B, SE-FRET from the whole cell was collected. Statistical analysis was by Student's t test. In Figure 16C, SE-FRET extent was collected only in the plasma membrane regions exposed to EGF-555 by obtaining a binary mask on the EGF-555 images. Binarized EGF-555 masks were filtered by structures smaller then 0.2 μM^2 to exclude endosomal EGF-555.

14. Immunoelectron Microscopy

14.1 Sample preparation

For ER labeling, cells were transfected with HRP-KDEL (142); 24 hours after transfection, cells were subjected to pre-embedding immunolabeling with anti-EGFR 13A9 antibody followed by incubation with rabbit anti-mouse, and, finally, with Protein-A Gold 10 nm (30 min incubation on ice/each step). Cells were then incubated at 37°C for 2, 5 or 8 min with 30 ng/ml EGF, as indicated. A control sample left at 37°C for 5 or 8 min without EGF was included in the experiment to control that no internalization was induced by the antibody in the absence of ligand. Cells were then washed in PBS and fixed for 1 h at room temperature in 1.2% glutaraldehyde in 66 mM sodium cacodylate buffer pH 7.2 containing 0.5 mg/ml of ruthenium red. After quick washes with 150 mM sodium cacodylate buffer, the samples were post-fixed in 1.3% osmium tetroxide in a 66 mM sodium cacodylate buffer (pH 7.2) containing 0.5-mg/ml ruthenium red for 2h at room temperature. Cells were then rinsed with 150 mM NaCacodylate, washed with distilled water and enbloc stained with 0.5% uranyl acetate in dH_20 overnight at 4°C in the dark. Finally, samples were rinsed in dH_2O, dehydrated with increasing concentrations of ethanol, embedded in Epon and cured in an oven at 60°C for 48 h.

14.2 Image acquisition and analysis

To quantify the percentage of EGFR endocytic invaginations associated with ER tubules, the PM of HRP-stained cells was scanned and when an EGFR-positive endocytic structure (clearly connected to the PM) was encountered (CCP or TI), EM micrographs of this region and of the same area on the previous and next serial sections were acquired. The three serial sections images were aligned in IMOD (3dmod Ver 4.7.9) and imported in ImageJ, where

selection lines at ≤ 20 nm from the membrane of the endocytic structure were overlaid on the three images. An endocytic structure was considered associated with an ER tubule if at least in one section an ER tubule was present inside the delimited area.

15. Measurements of intracellular Ca^{2+} concentration.

15.1 Aequorin measurements.

Cells grown on 13-mm-round glass coverslips at 50% confluence were transfected with the appropriate cytosolic (cyto)- or PM-targeted aequorin chimeras. Aequorin constructs and protocols were previously described (195). All aequorin measurements were performed in KRB buffer (135 mM NaCl, 5 mM KCl, 0.4 mM KH_2PO_4, 1 mM $MgSO_4$, 20 mM HEPES and 5.5 mM glucose, pH 7.4), supplemented with 1 mM Ca^{2+}. When EGTA treatment was performed, aequorin measurements were recorded in KRB buffer plus 100 μM EGTA. Stimulation with EGF was performed as specified in the figure legends. The experiments were terminated by lysing the cells with 0.01% Triton in a hypotonic Ca^{2+}-rich solution (10 mM $CaCl_2$ in H_2O), thus discharging the remaining aequorin pool. The light signal was collected and calibrated into [Ca^{2+}] values, as previously described (195). Extents of Ca^{2+} waves were expressed as area under the curve (AUC) and maximal value of peak in box plot graphs. Statistical analysis was performed using GraphPad Prism. Student's t-test was used to calculate statistical significance among different samples.

15.2 Fura-2, AM, measurements

Cells were grown on 24-mm coverslips and incubated at 37°C for 30 min in 1 mM Ca^{2+}/KRB supplemented with 2.5 mM Fura-2 AM, 0.02% Pluronic F-68, and 0.1 mM sulfinpyrazone. The cells were then washed and supplemented with 1 mM Ca^{2+}/KRB. Prior the acquisition

cells were washed and supplemented with 1 mM Ca^{2+}/KRB. To determine the cytosolic Ca^{2+} response, cells were placed in an open Leyden chamber on a 37°C thermostat-controlled stage and exposed to 340/380 nm wavelength light using the Olympus xcellence multiple-wavelength high-resolution fluorescence microscopy system equipped with an ORCA ER CCD camera (Hamamatsu Photonics) and an Uplan FLN 40X oil objective (Olympus). After registration of baseline ratio, cells were stimulated with Alexa555-EGF. Fluorescence data collected were expressed as emission ratios. The extent of Ca^{2+} waves was expressed as AUC in box plot graphs. Statistical analysis was performed using GraphPad Prism. One-way ANOVA was used to calculate statistical significance between different samples.

15.3 GCaMP6f measurements

Cells were grown on 24-mm coverslips, and transfected with the construct 48hr prior the acquisition of images. For the acquisition, cells were washed and supplemented with 1 mM Ca^{2+}/KRB. To determine the cytosolic Ca^{2+} response, cells were placed in an open Leyden chamber on a 37°C thermostat-controlled stage and exposed to 490/406 nm wavelength light using the Olympus xcellence multiple-wavelength high-resolution fluorescence microscopy system equipped with an ORCA ER CCD camera (Hamamatsu Photonics) and an Uplan FLN 40X oil objective (Olympus). After registration of baseline ratio, cells were stimulated with Alexa555-EGF. Fluorescence data collected were expressed as emission ratios. The extent of Ca^{2+} peaks was expressed as AUC in box plot graphs. Statistical analysis was performed using GraphPad Prism. One-way ANOVA was used to calculate statistical significance between different samples.

15.4 Xestospongin C treatment

Cells were treated with 2 µM xestospongin C for 16 h. The drug was kept for the duration of the different experimental procedures (Fura-2 AM measurements or CD147 internalization).

15.5 Calcium depletion with ionomycin

Calcium depletion was obtained by administration of 100 µM EGTA in a calcium free KRB supplemented with 1 µM ionomycin at 4°C to reduce SERCA activity. Forty-five minutes of depletion procedure was sufficient to induce complete depletion of Ca^{2+}, as previously described (146).

BIBLIOGRAPHY

1. Mayor, S., Parton, R. G., and Donaldson, J. G. (2014) *Cold Spring Harbor perspectives in biology* **6**
2. Mao, Y., and Finnemann, S. C. (2015) *Small GTPases* **6**, 89-99
3. Masters, T. A., Pontes, B., Viasnoff, V., Li, Y., and Gauthier, N. C. (2013) *Proceedings of the National Academy of Sciences of the United States of America* **110**, 11875-11880
4. Ostrowski, P. P., Grinstein, S., and Freeman, S. A. (2016) *Developmental cell* **38**, 135-146
5. Egami, Y., Taguchi, T., Maekawa, M., Arai, H., and Araki, N. (2014) *Frontiers in physiology* **5**, 374
6. Edwards, D. C., Sanders, L. C., Bokoch, G. M., and Gill, G. N. (1999) *Nature cell biology* **1**, 253-259
7. Kumari, S., Mg, S., and Mayor, S. (2010) *Cell research* **20**, 256-275
8. Swanson, J. A. (2008) *Nature reviews. Molecular cell biology* **9**, 639-649
9. Orth, J. D., Krueger, E. W., Weller, S. G., and McNiven, M. A. (2006) *Cancer research* **66**, 3603-3610
10. Robinson, M. S. (2015) *Traffic* **16**, 1210-1238
11. McMahon, H. T., and Boucrot, E. (2011) *Nature reviews. Molecular cell biology* **12**, 517-533
12. Edeling, M. A., Smith, C., and Owen, D. (2006) *Nature reviews. Molecular cell biology* **7**, 32-44
13. Kirchhausen, T., Owen, D., and Harrison, S. C. (2014) *Cold Spring Harbor perspectives in biology* **6**, a016725
14. Traub, L. M. (2009) *Nature reviews. Molecular cell biology* **10**, 583-596
15. Cocucci, E., Aguet, F., Boulant, S., and Kirchhausen, T. (2012) *Cell* **150**, 495-507
16. Lee, D. W., Wu, X., Eisenberg, E., and Greene, L. E. (2006) *Journal of cell science* **119**, 3502-3512
17. Massol, R. H., Boll, W., Griffin, A. M., and Kirchhausen, T. (2006) *Proceedings of the National Academy of Sciences of the United States of America* **103**, 10265-10270
18. Ferguson, S. M., Raimondi, A., Paradise, S., Shen, H., Mesaki, K., Ferguson, A., Destaing, O., Ko, G., Takasaki, J., Cremona, O., E, O. T., and De Camilli, P. (2009) *Developmental cell* **17**, 811-822

19. Merrifield, C. J., Feldman, M. E., Wan, L., and Almers, W. (2002) *Nature cell biology* **4**, 691-698
20. Saffarian, S., Cocucci, E., and Kirchhausen, T. (2009) *PLoS biology* **7**, e1000191
21. Owen, D. J., Collins, B. M., and Evans, P. R. (2004) *Annual review of cell and developmental biology* **20**, 153-191
22. Sigismund, S., Woelk, T., Puri, C., Maspero, E., Tacchetti, C., Transidico, P., Di Fiore, P. P., and Polo, S. (2005) *Proceedings of the National Academy of Sciences of the United States of America* **102**, 2760-2765
23. Bitsikas, V., Correa, I. R., Jr., and Nichols, B. J. (2014) *eLife* **3**, e03970
24. Johannes, L., Wunder, C., and Bassereau, P. (2014) *Cold Spring Harbor perspectives in biology* **6**
25. Simons, K., and Gerl, M. J. (2010) *Nature reviews. Molecular cell biology* **11**, 688-699
26. Thorn, H., Stenkula, K. G., Karlsson, M., Ortegren, U., Nystrom, F. H., Gustavsson, J., and Stralfors, P. (2003) *Molecular biology of the cell* **14**, 3967-3976
27. Parton, R. G., and del Pozo, M. A. (2013) *Nature reviews. Molecular cell biology* **14**, 98-112
28. Murata, M., Peranen, J., Schreiner, R., Wieland, F., Kurzchalia, T. V., and Simons, K. (1995) *Proceedings of the National Academy of Sciences of the United States of America* **92**, 10339-10343
29. Dietzen, D. J., Hastings, W. R., and Lublin, D. M. (1995) *The Journal of biological chemistry* **270**, 6838-6842
30. Kovtun, O., Tillu, V. A., Ariotti, N., Parton, R. G., and Collins, B. M. (2015) *Journal of cell science* **128**, 1269-1278
31. Sinha, B., Koster, D., Ruez, R., Gonnord, P., Bastiani, M., Abankwa, D., Stan, R. V., Butler-Browne, G., Vedie, B., Johannes, L., Morone, N., Parton, R. G., Raposo, G., Sens, P., Lamaze, C., and Nassoy, P. (2011) *Cell* **144**, 402-413
32. Echarri, A., and Del Pozo, M. A. (2015) *Journal of cell science* **128**, 2747-2758
33. Corrotte, M., Almeida, P. E., Tam, C., Castro-Gomes, T., Fernandes, M. C., Millis, B. A., Cortez, M., Miller, H., Song, W., Maugel, T. K., and Andrews, N. W. (2013) *eLife* **2**, e00926
34. Boucrot, E., Howes, M. T., Kirchhausen, T., and Parton, R. G. (2011) *Journal of cell science* **124**, 1965-1972

35. Bickel, P. E., Scherer, P. E., Schnitzer, J. E., Oh, P., Lisanti, M. P., and Lodish, H. F. (1997) *The Journal of biological chemistry* **272**, 13793-13802
36. Edgar, A. J., and Polak, J. M. (2001) *The international journal of biochemistry & cell biology* **33**, 53-64
37. Neumann-Giesen, C., Fernow, I., Amaddii, M., and Tikkanen, R. (2007) *Journal of cell science* **120**, 395-406
38. Glebov, O. O., Bright, N. A., and Nichols, B. J. (2006) *Nature cell biology* **8**, 46-54
39. Stuermer, C. A. (2011) *Journal of neurochemistry* **116**, 708-713
40. Solis, G. P., Schrock, Y., Hulsbusch, N., Wiechers, M., Plattner, H., and Stuermer, C. A. (2012) *Molecular biology of the cell* **23**, 1812-1825
41. Howes, M. T., Kirkham, M., Riches, J., Cortese, K., Walser, P. J., Simpson, F., Hill, M. M., Jones, A., Lundmark, R., Lindsay, M. R., Hernandez-Deviez, D. J., Hadzic, G., McCluskey, A., Bashir, R., Liu, L., Pilch, P., McMahon, H., Robinson, P. J., Hancock, J. F., Mayor, S., and Parton, R. G. (2010) *The Journal of cell biology* **190**, 675-691
42. Lundmark, R., Doherty, G. J., Howes, M. T., Cortese, K., Vallis, Y., Parton, R. G., and McMahon, H. T. (2008) *Current biology : CB* **18**, 1802-1808
43. Lakshminarayan, R., Wunder, C., Becken, U., Howes, M. T., Benzing, C., Arumugam, S., Sales, S., Ariotti, N., Chambon, V., Lamaze, C., Loew, D., Shevchenko, A., Gaus, K., Parton, R. G., and Johannes, L. (2014) *Nature cell biology* **16**, 595-606
44. Grant, B. D., and Donaldson, J. G. (2009) *Nature reviews. Molecular cell biology* **10**, 597-608
45. Eyster, C. A., Higginson, J. D., Huebner, R., Porat-Shliom, N., Weigert, R., Wu, W. W., Shen, R. F., and Donaldson, J. G. (2009) *Traffic* **10**, 590-599
46. Maldonado-Baez, L., Williamson, C., and Donaldson, J. G. (2013) *Experimental cell research* **319**, 2759-2769
47. Basquin, C., Trichet, M., Vihinen, H., Malarde, V., Lagache, T., Ripoll, L., Jokitalo, E., Olivo-Marin, J. C., Gautreau, A., and Sauvonnet, N. (2015) *The EMBO journal* **34**, 2147-2161
48. Grassart, A., Dujeancourt, A., Lazarow, P. B., Dautry-Varsat, A., and Sauvonnet, N. (2008) *EMBO reports* **9**, 356-362
49. Grassart, A., Meas-Yedid, V., Dufour, A., Olivo-Marin, J. C., Dautry-Varsat, A., and Sauvonnet, N. (2010) *Traffic* **11**, 1079-1091
50. Lamaze, C., Dujeancourt, A., Baba, T., Lo, C. G., Benmerah, A., and Dautry-Varsat, A. (2001) *Molecular cell* **7**, 661-671

51. Meinecke, M., Boucrot, E., Camdere, G., Hon, W. C., Mittal, R., and McMahon, H. T. (2013) *The Journal of biological chemistry* **288**, 6651-6661
52. Boucrot, E., Ferreira, A. P., Almeida-Souza, L., Debard, S., Vallis, Y., Howard, G., Bertot, L., Sauvonnet, N., and McMahon, H. T. (2015) *Nature* **517**, 460-465
53. Renard, H. F., Simunovic, M., Lemiere, J., Boucrot, E., Garcia-Castillo, M. D., Arumugam, S., Chambon, V., Lamaze, C., Wunder, C., Kenworthy, A. K., Schmidt, A. A., McMahon, H. T., Sykes, C., Bassereau, P., and Johannes, L. (2015) *Nature* **517**, 493-496
54. van der Bliek, A. M., and Meyerowitz, E. M. (1991) *Nature* **351**, 411-414
55. Boulant, S., Kural, C., Zeeh, J. C., Ubelmann, F., and Kirchhausen, T. (2011) *Nature cell biology* **13**, 1124-1131
56. Ferguson, S. M., and De Camilli, P. (2012) *Nature reviews. Molecular cell biology* **13**, 75-88
57. Kalaidzidis, I., Miaczynska, M., Brewinska-Olchowik, M., Hupalowska, A., Ferguson, C., Parton, R. G., Kalaidzidis, Y., and Zerial, M. (2015) *The Journal of cell biology* **211**, 123-144
58. Bissig, C., and Gruenberg, J. (2013) *Cold Spring Harbor perspectives in biology* **5**, a016816
59. Del Conte-Zerial, P., Brusch, L., Rink, J. C., Collinet, C., Kalaidzidis, Y., Zerial, M., and Deutsch, A. (2008) *Molecular systems biology* **4**, 206
60. Huotari, J., and Helenius, A. (2011) *The EMBO journal* **30**, 3481-3500
61. Rink, J., Ghigo, E., Kalaidzidis, Y., and Zerial, M. (2005) *Cell* **122**, 735-749
62. Hsu, V. W., Bai, M., and Li, J. (2012) *Nature reviews. Molecular cell biology* **13**, 323-328
63. Sigismund, S., Argenzio, E., Tosoni, D., Cavallaro, E., Polo, S., and Di Fiore, P. P. (2008) *Developmental cell* **15**, 209-219
64. Maxfield, F. R., and McGraw, T. E. (2004) *Nature reviews. Molecular cell biology* **5**, 121-132
65. Hurley, J. H. (2015) *The EMBO journal* **34**, 2398-2407
66. Hurley, J. H., and Hanson, P. I. (2010) *Nature reviews. Molecular cell biology* **11**, 556-566
67. Raiborg, C., and Stenmark, H. (2009) *Nature* **458**, 445-452
68. Sigismund, S., Confalonieri, S., Ciliberto, A., Polo, S., Scita, G., and Di Fiore, P. P. (2012) *Physiological reviews* **92**, 273-366

69. Puthenveedu, M. A., and von Zastrow, M. (2006) *Cell* **127**, 113-124
70. Aguet, F., Antonescu, C. N., Mettlen, M., Schmid, S. L., and Danuser, G. (2013) *Developmental cell* **26**, 279-291
71. Syrovatkina, V., Alegre, K. O., Dey, R., and Huang, X. Y. (2016) *Journal of molecular biology*
72. Flores-Otero, J., Ahn, K. H., Delgado-Peraza, F., Mackie, K., Kendall, D. A., and Yudowski, G. A. (2014) *Nature communications* **5**, 4589
73. Haugh, J. M., and Meyer, T. (2002) *Journal of cell science* **115**, 303-310
74. Palamidessi, A., Frittoli, E., Garre, M., Faretta, M., Mione, M., Testa, I., Diaspro, A., Lanzetti, L., Scita, G., and Di Fiore, P. P. (2008) *Cell* **134**, 135-147
75. Bailly, M., Wyckoff, J., Bouzahzah, B., Hammerman, R., Sylvestre, V., Cammer, M., Pestell, R., and Segall, J. E. (2000) *Molecular biology of the cell* **11**, 3873-3883
76. Martinez-Outschoorn, U. E., Sotgia, F., and Lisanti, M. P. (2015) *Nature reviews. Cancer* **15**, 225-237
77. Shimizu, H., Woodcock, S. A., Wilkin, M. B., Trubenova, B., Monk, N. A., and Baron, M. (2014) *Cell* **157**, 1160-1174
78. Yu, C. H., Rafiq, N. B., Cao, F., Zhou, Y., Krishnasamy, A., Biswas, K. H., Ravasio, A., Chen, Z., Wang, Y. H., Kawauchi, K., Jones, G. E., and Sheetz, M. P. (2015) *Nature communications* **6**, 8672
79. Barbieri, E., Di Fiore, P. P., and Sigismund, S. (2016) *Current opinion in cell biology* **39**, 21-27
80. Fortian, A., and Sorkin, A. (2014) *Journal of cell science* **127**, 432-444
81. Villasenor, R., Nonaka, H., Del Conte-Zerial, P., Kalaidzidis, Y., and Zerial, M. (2015) *eLife* **4**
82. Tsvetanova, N. G., and von Zastrow, M. (2014) *Nature chemical biology* **10**, 1061-1065
83. Yamamoto, H., Sakane, H., Michiue, T., and Kikuchi, A. (2008) *Developmental cell* **15**, 37-48
84. Di Guglielmo, G. M., Le Roy, C., Goodfellow, A. F., and Wrana, J. L. (2003) *Nature cell biology* **5**, 410-421
85. Holbro, T., and Hynes, N. E. (2004) *Annual review of pharmacology and toxicology* **44**, 195-217
86. Citri, A., and Yarden, Y. (2006) *Nature reviews. Molecular cell biology* **7**, 505-516

87. Oda, K., Matsuoka, Y., Funahashi, A., and Kitano, H. (2005) *Molecular systems biology* **1**, 2005 0010
88. Lemmon, M. A. (2009) *Experimental cell research* **315**, 638-648
89. Lammerts van Bueren, J. J., Bleeker, W. K., Brannstrom, A., von Euler, A., Jansson, M., Peipp, M., Schneider-Merck, T., Valerius, T., van de Winkel, J. G., and Parren, P. W. (2008) *Proceedings of the National Academy of Sciences of the United States of America* **105**, 6109-6114
90. Zhang, X., Gureasko, J., Shen, K., Cole, P. A., and Kuriyan, J. (2006) *Cell* **125**, 1137-1149
91. Thiel, K. W., and Carpenter, G. (2007) *Proceedings of the National Academy of Sciences of the United States of America* **104**, 19238-19243
92. Red Brewer, M., Choi, S. H., Alvarado, D., Moravcevic, K., Pozzi, A., Lemmon, M. A., and Carpenter, G. (2009) *Molecular cell* **34**, 641-651
93. Li, H., Ruano, M. J., and Villalobo, A. (2004) *FEBS letters* **559**, 175-180
94. Stateva, S. R., Salas, V., Benguria, A., Cossio, I., Anguita, E., Martin-Nieto, J., Benaim, G., and Villalobo, A. (2015) *The Biochemical journal* **472**, 195-204
95. Hynes, N. E., Horsch, K., Olayioye, M. A., and Badache, A. (2001) *Endocrine-related cancer* **8**, 151-159
96. Shilo, B. Z. (2005) *Development* **132**, 4017-4027
97. Jiang, X., Huang, F., Marusyk, A., and Sorkin, A. (2003) *Molecular biology of the cell* **14**, 858-870
98. Woelk, T., Sigismund, S., Penengo, L., and Polo, S. (2007) *Cell division* **2**, 11
99. Xu, P., Duong, D. M., Seyfried, N. T., Cheng, D., Xie, Y., Robert, J., Rush, J., Hochstrasser, M., Finley, D., and Peng, J. (2009) *Cell* **137**, 133-145
100. Pickart, C. M., and Fushman, D. (2004) *Current opinion in chemical biology* **8**, 610-616
101. Levkowitz, G., Waterman, H., Zamir, E., Kam, Z., Oved, S., Langdon, W. Y., Beguinot, L., Geiger, B., and Yarden, Y. (1998) *Genes & development* **12**, 3663-3674
102. Thien, C. B., and Langdon, W. Y. (2001) *Nature reviews. Molecular cell biology* **2**, 294-307
103. Huang, F., Kirkpatrick, D., Jiang, X., Gygi, S., and Sorkin, A. (2006) *Molecular cell* **21**, 737-748
104. Polo, S. (2012) *BMC biology* **10**, 25

105. Carpenter, G., and Cohen, S. (1990) *The Journal of biological chemistry* **265**, 7709-7712

106. Normanno, N., De Luca, A., Maiello, M. R., Mancino, M., D'Antonio, A., Macaluso, M., Caponigro, F., and Giordano, A. (2005) *Frontiers in bioscience : a journal and virtual library* **10**, 2611-2617

107. Nesterov, A., Carter, R. E., Sorkina, T., Gill, G. N., and Sorkin, A. (1999) *The EMBO journal* **18**, 2489-2499

108. Huang, F., Khvorova, A., Marshall, W., and Sorkin, A. (2004) *The Journal of biological chemistry* **279**, 16657-16661

109. Waterman, H., Katz, M., Rubin, C., Shtiegman, K., Lavi, S., Elson, A., Jovin, T., and Yarden, Y. (2002) *The EMBO journal* **21**, 303-313

110. de Melker, A. A., van der Horst, G., Calafat, J., Jansen, H., and Borst, J. (2001) *Journal of cell science* **114**, 2167-2178

111. Sigismund, S., Algisi, V., Nappo, G., Conte, A., Pascolutti, R., Cuomo, A., Bonaldi, T., Argenzio, E., Verhoef, L. G., Maspero, E., Bianchi, F., Capuani, F., Ciliberto, A., Polo, S., and Di Fiore, P. P. (2013) *The EMBO journal* **32**, 2140-2157

112. Capuani, F., Conte, A., Argenzio, E., Marchetti, L., Priami, C., Polo, S., Di Fiore, P. P., Sigismund, S., and Ciliberto, A. (2015) *Nature communications* **6**, 7999

113. Lebiedzinska, M., Szabadkai, G., Jones, A. W., Duszynski, J., and Wieckowski, M. R. (2009) *The international journal of biochemistry & cell biology* **41**, 1805-1816

114. Phillips, M. J., and Voeltz, G. K. (2016) *Nature reviews. Molecular cell biology* **17**, 69-82

115. Henne, W. M., Liou, J., and Emr, S. D. (2015) *Current opinion in cell biology* **35**, 123-130

116. Eden, E. R., Burgoyne, T., Edgar, J. R., Sorkin, A., and Futter, C. E. (2012) *Biochemical Society transactions* **40**, 464-468

117. Friedman, J. R., Dibenedetto, J. R., West, M., Rowland, A. A., and Voeltz, G. K. (2013) *Molecular biology of the cell* **24**, 1030-1040

118. Suchanek, M., Hynynen, R., Wohlfahrt, G., Lehto, M., Johansson, M., Saarinen, H., Radzikowska, A., Thiele, C., and Olkkonen, V. M. (2007) *The Biochemical journal* **405**, 473-480

119. Rocha, N., Kuijl, C., van der Kant, R., Janssen, L., Houben, D., Janssen, H., Zwart, W., and Neefjes, J. (2009) *The Journal of cell biology* **185**, 1209-1225

120. Vihervaara, T., Uronen, R. L., Wohlfahrt, G., Bjorkhem, I., Ikonen, E., and Olkkonen, V. M. (2011) *Cellular and molecular life sciences : CMLS* **68**, 537-551
121. Raiborg, C., Wenzel, E. M., Pedersen, N. M., Olsvik, H., Schink, K. O., Schultz, S. W., Vietri, M., Nisi, V., Bucci, C., Brech, A., Johansen, T., and Stenmark, H. (2015) *Nature* **520**, 234-238
122. Jongsma, M. L., Berlin, I., Wijdeven, R. H., Janssen, L., Janssen, G. M., Garstka, M. A., Janssen, H., Mensink, M., van Veelen, P. A., Spaapen, R. M., and Neefjes, J. (2016) *Cell* **166**, 152-166
123. Rowland, A. A., Chitwood, P. J., Phillips, M. J., and Voeltz, G. K. (2014) *Cell* **159**, 1027-1041
124. Dong, R., Saheki, Y., Swarup, S., Lucast, L., Harper, J. W., and De Camilli, P. (2016) *Cell* **166**, 408-423
125. Eden, E. R., White, I. J., Tsapara, A., and Futter, C. E. (2010) *Nature cell biology* **12**, 267-272
126. Eden, E. R., Sanchez-Heras, E., Tsapara, A., Sobota, A., Levine, T. P., and Futter, C. E. (2016) *Developmental cell* **37**, 473-483
127. Haj, F. G., Sabet, O., Kinkhabwala, A., Wimmer-Kleikamp, S., Roukos, V., Han, H. M., Grabenbauer, M., Bierbaum, M., Antony, C., Neel, B. G., and Bastiaens, P. I. (2012) *PloS one* **7**, e36633
128. Stefan, C. J., Manford, A. G., and Emr, S. D. (2013) *Current opinion in cell biology* **25**, 434-442
129. Du, X., Kumar, J., Ferguson, C., Schulz, T. A., Ong, Y. S., Hong, W., Prinz, W. A., Parton, R. G., Brown, A. J., and Yang, H. (2011) *The Journal of cell biology* **192**, 121-135
130. Chung, J., Torta, F., Masai, K., Lucast, L., Czapla, H., Tanner, L. B., Narayanaswamy, P., Wenk, M. R., Nakatsu, F., and De Camilli, P. (2015) *Science* **349**, 428-432
131. Morgan, A. J., Davis, L. C., Wagner, S. K., Lewis, A. M., Parrington, J., Churchill, G. C., and Galione, A. (2013) *The Journal of cell biology* **200**, 789-805
132. Rizzuto, R., Pinton, P., Carrington, W., Fay, F. S., Fogarty, K. E., Lifshitz, L. M., Tuft, R. A., and Pozzan, T. (1998) *Science* **280**, 1763-1766
133. Vermeulen, M., Hubner, N. C., and Mann, M. (2008) *Current opinion in biotechnology* **19**, 331-337
134. Yang, Y. S., and Strittmatter, S. M. (2007) *Genome biology* **8**, 234

135. Shibata, Y., Voss, C., Rist, J. M., Hu, J., Rapoport, T. A., Prinz, W. A., and Voeltz, G. K. (2008) *The Journal of biological chemistry* **283**, 18892-18904
136. Voeltz, G. K., Prinz, W. A., Shibata, Y., Rist, J. M., and Rapoport, T. A. (2006) *Cell* **124**, 573-586
137. Idevall-Hagren, O., Lu, A., Xie, B., and De Camilli, P. (2015) *The EMBO journal* **34**, 2291-2305
138. Heilemann, M., van de Linde, S., Schuttpelz, M., Kasper, R., Seefeldt, B., Mukherjee, A., Tinnefeld, P., and Sauer, M. (2008) *Angewandte Chemie* **47**, 6172-6176
139. Sengupta, P., Jovanovic-Talisman, T., Skoko, D., Renz, M., Veatch, S. L., and Lippincott-Schwartz, J. (2011) *Nature methods* **8**, 969-975
140. Ronchi, P., Colombo, S., Francolini, M., and Borgese, N. (2008) *The Journal of cell biology* **181**, 105-118
141. Giordano, F., Saheki, Y., Idevall-Hagren, O., Colombo, S. F., Pirruccello, M., Milosevic, I., Gracheva, E. O., Bagriantsev, S. N., Borgese, N., and De Camilli, P. (2013) *Cell* **153**, 1494-1509
142. Schikorski, T., Young, S. M., Jr., and Hu, Y. (2007) *Journal of neuroscience methods* **165**, 210-215
143. Cheyette, T. E., and Gross, D. J. (1991) *Cell regulation* **2**, 827-840
144. Moolenaar, W. H., Aerts, R. J., Tertoolen, L. G., and de Laat, S. W. (1986) *The Journal of biological chemistry* **261**, 279-284
145. Marsault, R., Murgia, M., Pozzan, T., and Rizzuto, R. (1997) *The EMBO journal* **16**, 1575-1581
146. Montero, M., Brini, M., Marsault, R., Alvarez, J., Sitia, R., Pozzan, T., and Rizzuto, R. (1995) *The EMBO journal* **14**, 5467-5475
147. Bennett, D. L., Cheek, T. R., Berridge, M. J., De Smedt, H., Parys, J. B., Missiaen, L., and Bootman, M. D. (1996) *The Journal of biological chemistry* **271**, 6356-6362
148. Badura, A., Sun, X. R., Giovannucci, A., Lynch, L. A., and Wang, S. S. (2014) *Neurophotonics* **1**, 025008
149. Frittoli, E., Palamidessi, A., Pizzigoni, A., Lanzetti, L., Garre, M., Troglio, F., Troilo, A., Fukuda, M., Di Fiore, P. P., Scita, G., and Confalonieri, S. (2008) *Molecular biology of the cell* **19**, 1304-1316
150. Garrett, W. S., Chen, L. M., Kroschewski, R., Ebersold, M., Turley, S., Trombetta, S., Galan, J. E., and Mellman, I. (2000) *Cell* **102**, 325-334
151. Schafer, D. A., D'Souza-Schorey, C., and Cooper, J. A. (2000) *Traffic* **1**, 892-903

152. Oertle, T., van der Haar, M. E., Bandtlow, C. E., Robeva, A., Burfeind, P., Buss, A., Huber, A. B., Simonen, M., Schnell, L., Brosamle, C., Kaupmann, K., Vallon, R., and Schwab, M. E. (2003) *The Journal of neuroscience : the official journal of the Society for Neuroscience* **23**, 5393-5406
153. Bauer, M., and Pelkmans, L. (2006) *FEBS Lett* **580**, 5559-5564
154. Lewis, J. P., Neal, W. A., Welch, E. T., Lewis, W. G., 3rd, DuBose, C. M., Jr., Wright, C. S., and Smith, L. L. (1973) *Proc Soc Exp Biol Med* **142**, 293-298
155. Vance, J. E. (1990) *J Biol Chem* **265**, 7248-7256
156. de Brito, O. M., and Scorrano, L. (2010) *EMBO J* **29**, 2715-2723
157. Helle, S. C., Kanfer, G., Kolar, K., Lang, A., Michel, A. H., and Kornmann, B. (2013) *Biochim Biophys Acta* **1833**, 2526-2541
158. Mesmin, B., Bigay, J., Moser von Filseck, J., Lacas-Gervais, S., Drin, G., and Antonny, B. (2013) *Cell* **155**, 830-843
159. Stefan, C. J., Manford, A. G., Baird, D., Yamada-Hanff, J., Mao, Y., and Emr, S. D. (2011) *Cell* **144**, 389-401
160. Du, X., Brown, A. J., and Yang, H. (2015) *Curr Opin Cell Biol* **35**, 37-42
161. Alpy, F., Rousseau, A., Schwab, Y., Legueux, F., Stoll, I., Wendling, C., Spiegelhalter, C., Kessler, P., Mathelin, C., Rio, M. C., Levine, T. P., and Tomasetto, C. (2013) *J Cell Sci* **126**, 5500-5512
162. van der Kant, R., and Neefjes, J. (2014) *J Cell Sci* **127**, 929-938
163. Elaib, Z., Saller, F., and Bobe, R. (2016) *Advances in experimental medicine and biology* **898**, 333-352
164. Jozsef, L., Tashiro, K., Kuo, A., Park, E. J., Skoura, A., Albinsson, S., Rivera-Molina, F., Harrison, K. D., Iwakiri, Y., Toomre, D., and Sessa, W. C. (2014) *J Biol Chem* **289**, 9380-9395
165. Chen, T. W., Wardill, T. J., Sun, Y., Pulver, S. R., Renninger, S. L., Baohan, A., Schreiter, E. R., Kerr, R. A., Orger, M. B., Jayaraman, V., Looger, L. L., Svoboda, K., and Kim, D. S. (2013) *Nature* **499**, 295-300
166. Yamashita, T. (2012) *Neuroscience research* **73**, 1-7
167. Leitz, J., and Kavalali, E. T. (2014) *eLife* **3**, e03658
168. Chung, C., Barylko, B., Leitz, J., Liu, X., and Kavalali, E. T. (2010) *The Journal of neuroscience : the official journal of the Society for Neuroscience* **30**, 1363-1376
169. Lai, M. M., Hong, J. J., Ruggiero, A. M., Burnett, P. E., Slepnev, V. I., De Camilli, P., and Snyder, S. H. (1999) *The Journal of biological chemistry* **274**, 25963-25966

170. Marks, B., and McMahon, H. T. (1998) *Current biology : CB* **8**, 740-749
171. Babich, A., and Burkhardt, J. K. (2013) *Immunol Rev* **256**, 80-94
172. Kumari, S., Depoil, D., Martinelli, R., Judokusumo, E., Carmona, G., Gertler, F. B., Kam, L. C., Carman, C. V., Burkhardt, J. K., Irvine, D. J., and Dustin, M. L. (2015) *eLife* **4**
173. Iwasa, H., Yu, S., Xue, J., and Driscoll, M. (2010) *Aging cell* **9**, 490-505
174. Ding, J., Luo, A. F., Hu, L., Wang, D., and Shao, F. (2014) *Science China. Life sciences* **57**, 269-274
175. Argenzio, E., Bange, T., Oldrini, B., Bianchi, F., Peesari, R., Mari, S., Di Fiore, P. P., Mann, M., and Polo, S. (2011) *Mol Syst Biol* **7**, 462
176. Miranda, M., and Sorkin, A. (2007) *Mol Interv* **7**, 157-167
177. Acconcia, F., Sigismund, S., and Polo, S. (2009) *Exp Cell Res* **315**, 1610-1618
178. Davidson, B., Goldberg, I., Berner, A., Kristensen, G. B., and Reich, R. (2003) *Clinical & experimental metastasis* **20**, 161-169
179. Reimers, N., Zafrakas, K., Assmann, V., Egen, C., Riethdorf, L., Riethdorf, S., Berger, J., Ebel, S., Janicke, F., Sauter, G., and Pantel, K. (2004) *Clinical cancer research : an official journal of the American Association for Cancer Research* **10**, 3422-3428
180. Bai, Y., Huang, W., Ma, L. T., Jiang, J. L., and Chen, Z. N. (2014) *International journal of molecular sciences* **15**, 6356-6377
181. Morris, V. L., and Chan, B. M. (2007) *Wound Repair Regen* **15**, 907-915
182. Jackson, S., Schaefer, J., Middleton, B., and Turnbull, D. M. (1995) *Biochemical and biophysical research communications* **214**, 247-253
183. Csordas, G., Varnai, P., Golenar, T., Roy, S., Purkins, G., Schneider, T. G., Balla, T., and Hajnoczky, G. (2010) *Mol Cell* **39**, 121-132
184. Demaurex, N., Poburko, D., and Frieden, M. (2009) *Biochim Biophys Acta* **1787**, 1383-1394
185. Korzeniowski, M. K., Popovic, M. A., Szentpetery, Z., Varnai, P., Stojilkovic, S. S., and Balla, T. (2009) *J Biol Chem* **284**, 21027-21035
186. Najib, S., and Sanchez-Margalet, V. (2002) *J Cell Biochem* **86**, 99-106
187. de Hoog, C. L., Foster, L. J., and Mann, M. (2004) *Cell* **117**, 649-662
188. Katz, Z. B., Wells, A. L., Park, H. Y., Wu, B., Shenoy, S. M., and Singer, R. H. (2012) *Genes Dev* **26**, 1885-1890
189. Francia, S., Michelini, F., Saxena, A., Tang, D., de Hoon, M., Anelli, V., Mione, M., Carninci, P., and d'Adda di Fagagna, F. (2012) *Nature* **488**, 231-235

190. Sharma, V., and Misteli, T. (2013) *FEBS Lett* **587**, 1832-1839
191. Joh, R. I., Palmieri, C. M., Hill, I. T., and Motamedi, M. (2014) *Biochim Biophys Acta* **1839**, 1385-1394
192. Najib, S., Martin-Romero, C., Gonzalez-Yanes, C., and Sanchez-Margalet, V. (2005) *Cell Mol Life Sci* **62**, 36-43
193. Huot, M. E., Vogel, G., and Richard, S. (2009) *The Journal of biological chemistry* **284**, 31903-31913
194. Lam, S. S., Martell, J. D., Kamer, K. J., Deerinck, T. J., Ellisman, M. H., Mootha, V. K., and Ting, A. Y. (2015) *Nature methods* **12**, 51-54
195. Bonora, M., Giorgi, C., Bononi, A., Marchi, S., Patergnani, S., Rimessi, A., Rizzuto, R., and Pinton, P. (2013) *Nature protocols* **8**, 2105-2118
196. Thompson, R. E., Larson, D. R., and Webb, W. W. (2002) *Biophysical journal* **82**, 2775-2783
197. Dempsey, G. T., Vaughan, J. C., Chen, K. H., Bates, M., and Zhuang, X. (2011) *Nature methods* **8**, 1027-1036
198. Wouters, F. S., and Bastiaens, P. I. (2001) *Current protocols in cell biology / editorial board, Juan S. Bonifacino ... [et al.]* **Chapter 17**, Unit 17 11